Answers to Referee 1

We would like to thank dr. Chambers (Referee 1) for helpful comments and recommendations for improving the manuscript. The comments have helped making the manuscript much more transparent and easier to read. We have carefully examined the comments, modified the manuscript, and extended the modifications to answer all open questions. The uncertainties of the method and weaknesses of the manuscript were carefully investigated, and discussion will be provided point by point to answer the concerns raised by dr. Chambers. The main considerations are grouped in the following points:

1. Site characteristics

- *"The greater measurement height at AJ would reduce observed radon concentrations cf. LJ (particularly at night), and the sloping terrain would contribute to frequent katabatic flow, which deepens the nocturnal boundary layer (further reducing concentrations), and reduces radon build up within the stable nocturnal boundary layer (SNBL) (since, the ultimate source. air for the katabatic flow is the lower troposphere, where radon concentrations can be very low)."*
- *"Furthermore, while the radon source function near LJ would likely be uniform on spatial scales that influenced the model, this is not the case for AJ. The Adriatic coast lies ~20km SW of AJ (beyond which the radon flux effectively drops to zero). Mountain peaks of >1000m lie ~10 km N-NE of the site; at night under low to moderate wind speeds (as selected for this study), air would often be drawn from the lower troposphere, within which radon concentrations can also be very low."*

2. Measurement heights

- *"Much well-supported literature (including Karstens et al. 2015; ACP, 15, 12845-12865, 10.5194/acp-15-12845-2015), indicates that radon fluxes near Ajdovščina (AJ) are higher than near Ljubljana (LJ); by at least a factor of two. However, average radon (and its diurnal amplitude) reported in this study are higher at LJ than at AJ (Fig.4). This is likely attributable to: (i) a difference in radon sampling height (1m at LJ and 3m at AJ), (ii) the fact that the AJ radon observations were made on sloping ground, and (iii) the relative proximity of AJ to the coast (_20 km SW) and significant mountain peaks (_10 km N – NE)."*
- *"Two assumptions of the box model employed in this study are: (i) a well-mixed SNBL, and (ii) a uniform radon source function within the region that could influence the model. In reality, concentration profiles within the SNBL exhibit strong gradients. Consequently, making a direct comparative analysis between sites where concentrations are recorded at different heights from the surface (without correcting for this) could introduce significant biases."*
- *"In addition to the differences in radon sampling, BC observations at LJ and AJ were made at 4 and 20m a.g.l., respectively, at the primary sites. As mentioned above, at night under stable conditions, irrespective of potential differences in BC source strengths between the sites, or the flushing effect of katabatic flow at AJ, a significant gradient in BC concentrations would be expected in the SNBL between 4 and 20m agl. Even if both sites were on level ground, it would be necessary to estimate and correct for the separate sampling height differences between the sites before attempting a direct comparative analysis (at least at times when the ABL wasn't well mixed)."*

3. Selection of the suitable radon exhalation rate for the investigated region

- *"On page 12 the authors outline the approach used to estimate the seasonality of radon fluxes at LJ and AJ. Contrary to existing literature, derived radon fluxes were found to be higher at LJ than at AJ. Furthermore, the reported seasonal variability of radon flux at LJ was from 70 - 150 mBq/m2/s, compared with existing literature estimates of 15 - 25 mBq/m2/s, yet the quoted uncertainty of the adopted flux estimation technique was ~15 mBq/m2/s. Clearly, the derived radon fluxes are not appropriate for use in this study, and I would urge the authors to further investigate the cause of this discrepancy in flux estimates. Radon fluxes were estimated by regressing mixing depths from the box model (using a range of assumed fluxes), against mixing depths from the NOAA-ARL GDAS database. More information about the data selection criteria for these regressions is warranted here (including an example regression plot). Even if only using fair-weather data it would not be appropriate to make these regressions using values across the whole diurnal cycle since (i) the radon / box-model mixing height estimates are most poorly defined for the 3-5 hours in the mid-afternoon when the GDAS data is most*

representative of "reality", and (ii) nocturnal mixing depths in the GDAS database are worst at night under stable conditions, when the radon / box-model method works best (in fact, the nocturnal GDAS data has a minimum reported value of 250m a.g.l. for nocturnal mixing under stable conditions; which is around a factor of 2 higher than corresponding nocturnal mixing depths predicted by the radon / box-model method). With this in mind, perhaps the mixing depth transition periods (e.g. between 7am and noon) would be best to use (if the resolution of the GDAS record was adequate)?"

- *"The authors have sought to evaluate the fidelity of the radon / box-model's mixing depth estimates in two ways: firstly, using lidar observations (Fig. 9a), where results are very encouraging (for the chosen example) – although the comparison period ends around noon (near the time that the problematic afternoon period referred to above begins); and secondly, with vertical BC profiles recovered by drone. However, the chosen method to retrieve mixing depth estimates from the drone profiles appears to give inconsistent results. A visual inspection of Fig. S3 (a) indicates a well-mixed layer that terminates somewhere between 250 – 300m agl, yet the profile analysis method. returns a value of 412m agl. A visual inspection of Fig. S3b suggests an inversion height roughly 250m agl., whereas the chosen analysis method returns an estimate of 181 m agl. Furthermore, the reported uncertainty for these profile-derived mixing depths is ~1-3m, which is clearly unrealistic. If other parameters were retrieved from the drone (e.g. temperature, humidity or wind speed), these might help to improve the accuracy of the estimates."*

4. Model uncertainties in the mid-afternoon

- *"When the authors report whole (24-h) diurnal cycles of effective mixing depths based on the radon / box-model approach, further discussion regarding the uncertainty of the mid-afternoon values is warranted. In my opinion, neither of the cited papers (Allegrini et al. 1994 or Vecchi et al. 2018) provide robust evidence for the efficacy of this mixing depth calculation approach under convective afternoon conditions. As noted by Williams et al. (2016), several hours after the onset of morning convection a number of the necessary assumptions for the box model approach are no longer valid, until convective mixing begins to decay again in the late afternoon. Typically, for 3-5 hours in the mid-afternoon hourly ΔRn values that form the denominator of equations 9, 11 & 12 approach zero (absolute radon concentrations at this time were also often near the instrument's detection limit). In the mid-afternoon of convective days it is not clear that mixing-related influences on ΔRn dominate over advective influences, and depending on the meteorological conditions of the prior several days, radon concentrations in the lower troposphere (that can be entrained to the ABL once the residual layer has been eroded) can vary by 2 orders of magnitude. Applying a low-pass filter to the radon record (with a 4 – 12 hour cut-off; as done in this study and Vecchi et al. 2018) may improve the stability of the box model, but the actual ABL mixing characteristics at this time on a day to day basis are not correctly represented (since the variability being removed by the filtering process is a mixture of instrumental noise and several competing real physical influences). The largest BC ETR fluxes (with the largest uncertainties), are reported at these times (e.g. 2-4pm) for both workdays and Sundays – despite peak Sunday traffic not occurring at this time. Caution should be used when interpreting values at these times as they could bias daily averages.*

5. Scope of the investigation

- *"Given the measurement complexities at the AJ site, and frequent failure of measurement conditions to satisfy necessary assumptions for application of the box model, if a more accurate estimate of the local radon flux can be made the authors might consider restricting the scope of their analysis of source apportioned BC emission rates to the Ljubljana region? There would still be sufficient interest and novelty in the results of such a study to warrant publication."*

We are aware, that further discussion on the uncertainties of the model and subsequent influences on the results is needed to properly present the results of this study. Therefore, a completely new section about the uncertainties has been added to the manuscript.

Author's response

The points described above will be addressed one by one and proposed changes to the Manuscript and Supplement will be provided under each point.

1. Site characteristics

The areas under investigation differ from the point of view of geomorphology and geology, as well as population density and main economic characteristics, the later affecting the pollution source density and activity. This is also the main reason for the selection of these two regions. As pointed out by dr. Chambers, the natural characteristics of Vipava valley may limit the application of the proposed method to shorter time periods, when model assumptions sufficiently satisfy the natural conditions at the site.

In this regard we investigated in detail characteristics of the wind field in Vipava valley and its effect on Rn concentration, to restrict model results only to the periods which meet the criteria of uniform radon exhalation rate. As noted by dr. Chambers, katabatic flow from the mountain ridge and winds from the Adriatic Sea may reduce Rn concentration in the valley.

Fig. 1 shows the wind characteristics of the Vipava valley as measured at the university building. In our reexamination and reanalysis of the data, for the reason of representativeness, we have used the meteorological data from the location of the BC measurements. At this point we have to apologize for the wrong statement in the first version of the manuscript, since wind measurements from Slovenian Environment Agency network were included, instead of wind data from the location of BC measurements.

Pronounced strong winds from NE can be observed on Fig. 1b, which corresponds to bora wind events – downslope wind blowing from Trnovo plateau towards the valley. Due to extreme conditions, which do not allow a buildup of local pollutant emissions, these events were excluded from the analyses. In the periods of weak to mild wind (below 2 m/s, Fig. 1 c) the wind flow follows the geomorphology of the valley: WNW-ESE. Winds in the direction from the Adriatic Sea (SW) are very rear, but it is true, that in rear situations, when SW wind with speed higher than 1.5 m/s is present, Rn concentration in the afternoon decreases to 2 – 3 Bq/m^3 compared to ~ 5 Bq/m^3 for airflow from other directions (Fig. 1d). The Rn diurnal profile is similar in other wind directions and it only shows slight dependence on wind direction when the speed exceeds 1.5 m/s. The most pronounced change in Rn concentration is present with wind direction from NE (when wind speed exceeds 1.5 m/s), e.g. from the mountain ridge. However, the radon concentration does not decrease in these situations, but is instead higher (~ 10 Bq/m^3) than from other directions, probably due to higher radon source over the carbonate rocks of the Trnovo plateau. Higher Rn concentration would in turn decrease calculated MLH, eventually resulting in an underestimation of black carbon emission rates. No significant dependence of radon concentration on wind direction can be seen for pre-dawn period with low wind speed conditions.

Based on these observations, we have decided to limit the analyses at AJ location to the cases with average daily wind speed lower than 2 m/s (instead of previous 2.7 m/s), which accounts for around 60% of the measured dataset. Although at the higher end of wind distribution, we can expect some influence on the model results, periods with optimal atmospheric conditions can in our opinion still provide important information about black carbon emission rates.

Fig. 4 in the manuscript and Fig. S4 and S5 of the Supplement will be corrected accordingly.

a)

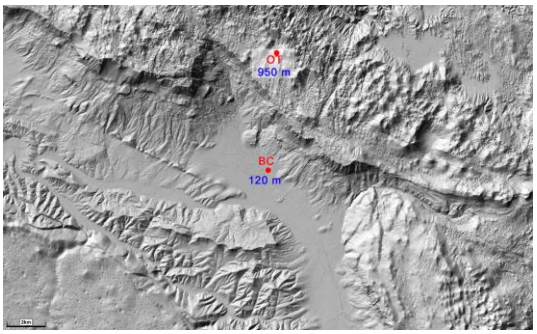

b)

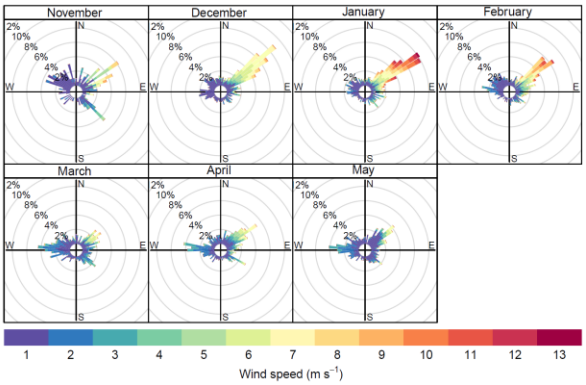

c)

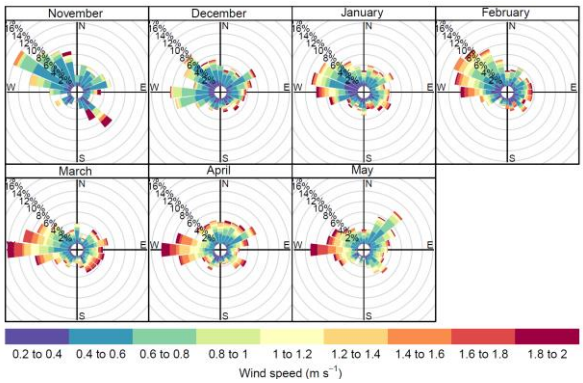

d)

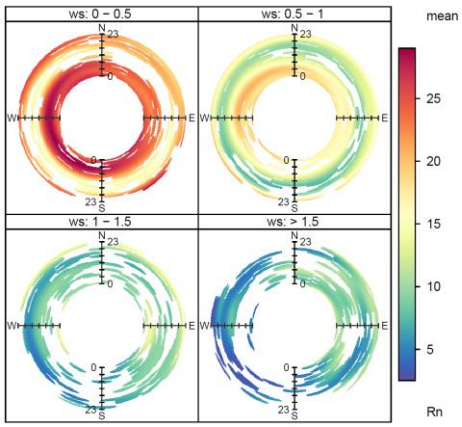

Figure 1: Vipava valley location: a) Digital elevation model of the Vipava valley with marked measurement sites, b) monthly wind rose, c) monthly wind rose for a subset of wind speed below 2 m/s, d) polar annulus plot shows how Rn concentration (color code in Bq/m^3) vary by wind direction and hour of day .

2. Measurement heights and influence on the estimated radon exhalation rate

We thank dr. Chambers for expressing the concern regarding measurement height and its influence on measured radon concentration and bias introduced by direct comparison of both sites. We are aware that this difference was not clearly presented and commented on the manuscript. Therefore, further clarification is necessary.
As explained by dr. Chambers, radon concentration profiles in the stable nocturnal boundary layer (SNBL) exhibit strong gradients. As shown for example by Ochmann (2005), measurements become characteristic for larger area with increasing height from the ground. The daily amplitude of radon concentration will thus be higher when measurements are conducted closer to the ground, especially in the SNBL conditions, which also affects an hourly increase of radon concentration (dC_{Rn}) in SNBL conditions
If we consider the case of stable atmospheric layer with known h_i, radon concentration measurements at different height above ground result in a different radon exhalation rate (E_{Rn}) estimate (Eq. 9 in the manuscript).

$$h_i = \frac{E_{Rn}\Delta T_{Rn}}{\mathrm{d}C_{Rn}}$$

This actually means, that measured or modelled values (from existing databases) of radon exhalation rate has to be evaluated/calibrated based on the radon measurement height. The radon exhalation rate estimated in this study actually represents an effective E_{Rn}, rather than real exhalation rate ($E_{Rn\text{-}0}$) for the area under consideration.

$$E_{Rn} = E_{Rn-0} \times s,$$

where *s* represents a scaling factor depending on the measurement height. This explanation was already introduced by Griffiths et al. (2013) in the study where mixing layer height from a radon model was compared with lidar derived mixing layer height. The scaling factor and thus the effective E_{Rn} will be higher when measurements are performed closer to the ground. In the mentioned study, the average scaling factor was 1.87 for measurements at 2 m a.g.l. Although a known issue, it seems to be neglected in later publications (e.g. Williams et al., 2016; Vecchi et al., 2018).
As explained in the section 2.5 (Page 12), different measures of the mixing layer height were used for the estimation of E_{Rn}. This paragraph was updated in order to clarify the difference between the effective and real E_{Rn} and explain the calibration procedure and how the effective exhalation rate is used in our model.

BC sampling height:

As mentioned in the manuscript and noted by dr. Chambers, black carbon measurements were conducted at different heights. Unfortunately, there was a mistake in the original submission in the sampling height at AJ location. After repeated measurements, we confirmed, that the sampling height was 12 m above ground, rather than 20 m. Despite this, stratification of SNBL can play a role in measured black carbon concentration, especially when comparing traffic and biomass burning BC sources, since their emissions have different characteristics. BC_{TR} is emitted from the sources at the ground surface, whereas biomass burning sources are usually higher, at the height of the chimneys. Due to dispersion and dilution processes, the concentration gradient flattens with time. This means that in the case of traffic related BC, with sources mostly active during the day, there would be enough time for the dispersion of BC_{TR} before stratification of SNBL. However, the morning emissions before the break of SNBL could be slightly underestimated in AJ, where sampling was performed at 12 m above ground. On the other hand, biomass burning BC is emitted higher above ground. For Ljubljana basin it was shown that BC_{BB} is homogeneously distributed within the city (Ogrin et al., 2016). At AJ location, with numerous biomass burning sources over smaller area, the concentration profile could be more significant, especially in stable atmospheric conditions, which could lead to increased BC_{BB} measured on the level of emissions. This could lead to slight overestimation of BC_{BB} emission rate in the afternoon – early evening, before the emission plume is dispersed.
We thank dr. Chambers to pointing out this difference, which was not discussed in the submitted version of the manuscript. Discussion regarding the influence of BC measurement height is added to the section at the end of the manuscript: 5.3 Uncertainty estimation.

3. Selection of the suitable radon exhalation rate for the investigated region

Dr. Chambers pointed out the unsuitable radon exhalation rate estimates used for both investigated locations. In this regard, we would like to point out two things:

1. Larger effective E_{Rn} estimated for LJ than for AJ locations is partially explained by the difference in measurement heights, which affect the E_{Rn} values (scaling factor mentioned above). The scaling factor reported by Griffiths et al. (2013) was 1.87 for 2 m a.g.l.
2. Modelled values of radon exhalation rate on the European scale, as published in Karstens et al. (2015) and Lopez-Coto (2013) are lacking the spatial resolution to be used as a reliable radon source term in the investigated area. Due to complex geology, the resolution may be too low to distinguish between local features of radon fluxes, which mainly follow the geological units (see the study of radon emanation of Slovenian soils by Kardos et al. (2015)). Flysch sedimentary rocks and carbonate rocks, which are completely different from the point of view of radon exhalation, are not clearly distinguished on the European scale, since flysch rocks follow the course of the valley, whereas in NE-SW direction, the lithology varies with spatial resolution below 3 km.
   As reported by Karstens et al. (2015), the radon exhalation varies in the range from 70 – 140 Bq $m^{-2}h^{-1}$ and 160 – 180 Bq $m^{-2}h^{-1}$ for AJ in winter and summer, respectively. The range of E_{Rn} in LJ area is 40 – 90 Bq $m^{-2}h^{-1}$ and 90 – 130 Bq $m^{-2}h^{-1}$ for winter and summer, respectively. Although the values reported for the region of Vipava valley are larger than for the central part of Slovenia, the flysch and carbonate bedrock is not reported separately. Therefore, caution is necessary when using modelled values of E_{Rn} on the European level to interpret local characteristics of investigated area and for the case of complex geological settings encountered in the Vipava valley, this approach would not be appropriate.

It still seems that after calibrating the radon model, the estimated radon exhalation rate (with scaling factor included) is too high for both sites. If a an approximate scaling factor of 2 would be considered for LJ location, the real E_{Rn-0} would be in the range from 125 – 275 Bq/m^2h, which is approx. by a factor of 2 higher than the expected range of E_{Rn-0} for Ljubljana area. For AJ location, with lower scaling factor – approx. 1.5 (due to measurements performed at 4 m height), E_{Rn-0} would be in the 130 – 270 Bq/m^2h range. Therefore, we investigated in detail all the variables, which may lead to these results. By applying different approximations to the radon box model, the estimated radon exhalation rate was lowered to more realistic values. Details of the box model and changes applied are presented in the following section.

4. Model assumptions and uncertainties in the mid-afternoon

After investigating the reason for high radon exhalation rate estimates, the following observation was found: as explained in the manuscript (page 12, lines 2-10) and pointed out by dr. Chambers, due to unstable model results with high uncertainty of the effective MLH in the mid-afternoon, the Rn concentration in the residual layer was set to zero (***Approach A***) in the submitted version of the manuscript. With this estimation, the effective MLH followed flatter curve during the morning transition from SNBL to daytime boundary layer (Fig. 2). When compared with MLH obtained from other measurements (NOAA, BC concentration profile, lidar), the best estimate of E_{Rn} was higher than the expected range.
We have reconsidered the approximation of Rn concentration in the residual layer in order to obtain more realistic daily evolution of MLH. In the published studies of radon box model approach (e.g.Williams et al., 2016; Vecchi et al., 2018), Rn is considered to be stable in the boundary layer (***Approach B***), affected only by the rate of its radioactive decay. The calculated MLH, however, results in strong overestimation of the mid-afternoon MLH, when PBL is fully developed.
Since Rn concentration in the residual layer actually decreases with height (Griffiths et al., 2011), a linear decrease of Rn concentration in the residual layer was finally used in the model (***Approach C***). This approximation resulted in less uncertain MLH results in the mid-afternoon.

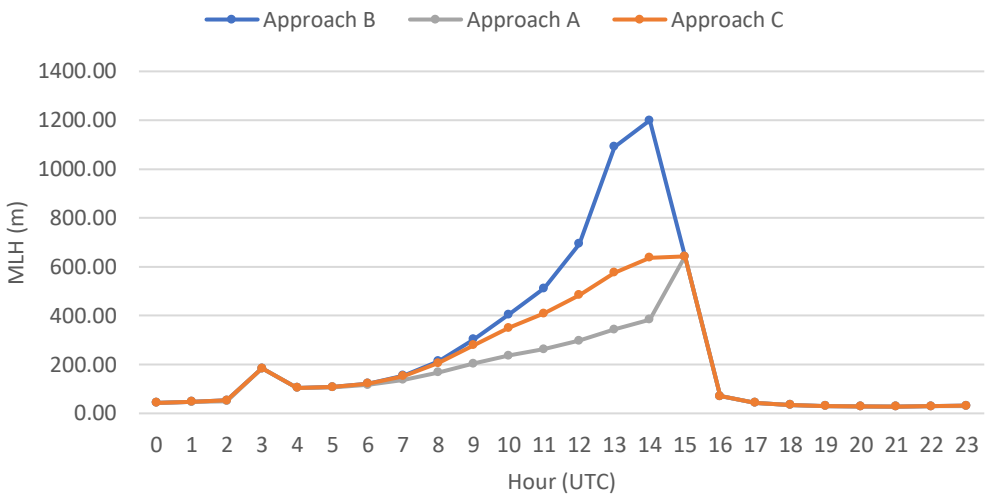

Figure 2: An example of the effective MLH evolution for different approximation of Rn concentration in the residual layer. Approach C was used in the model. Spring average diurnal profile of C_{Rn} in Ljubljana was used for comparison. E_{Rn} was fixed and does not match the values finally used in the manuscript.

The effective MLH calculated using the three different approaches mentioned above, were compared for the selected day of lidar measurements at AJ location (Fig. 3). When compared with lidar backscattered signal, daily evolution of the MLH by Approach B (constant Rn concentration in residual layer) gives too steep increase of MLH from the morning towards noon.

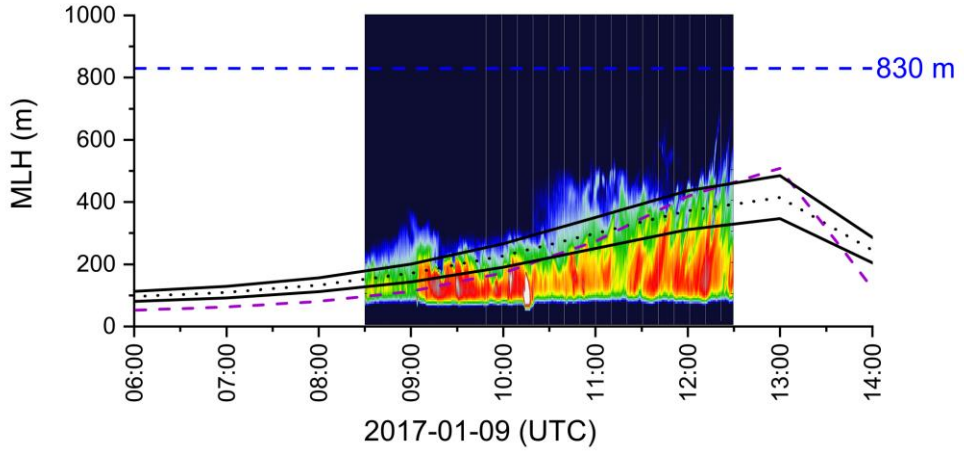

Figure 3: Comparison of effective MLH calculated using the Approach A (black dotted line), B (violet dashed line) and C (black solid line, min and max). Due to low Rn concentration in the residual layer from the previous day, the Approach A and C gives similar results in this case.

After calibrating the radon model for the best estimate of the effective E_{Rn}, lower E_{Rn} was obtained with Approach C than with the Approach A, especially for the LJ location. E_{Rn} estimates were in the range from 200 – 300 Bq m^{-2}h^{-1} and 200 to 350 Bq m^{-2}h^{-1} for LJ and AJ location, respectively. Considering that the scaling factor for 1 m a.g.l. in LJ can be around 2 or even higher (compared to 1.87 obtained for 2m a.g.l. measurements presented by Griffiths et al. (2013)), the $E_{Rn\text{-}0}$ would be in the 100 – 150 Bq m^{-2}h^{-1} range, which is similar to the range reported by Karstens et al. (2015). In the case of AJ, the expected range of $E_{Rn\text{-}0}$ would be from 130 – 230 Bq m^{-2}h^{-1} (in the case of approximate scaling factor of 1.5). In order to evaluate the bias introduced by the choice of E_{Rn}, results of BC emission rates were calculated for the 100 Bq m^{-2}h^{-1} range of E_{Rn} values (min – max) indicated in the Table 2.

Table 2 of the main text is updated accordingly.

By using the corrected radon model (Approach C) and the best estimate of radon exhalation rate obtained using calibration described above, the results slightly differ from the first version of the manuscript. All the figures and tables with model results, as well as discussion were updated. The most important changes are presented below:

Determination of MLH based on BC concentration vertical profiles

The uncertainty of MLH_{BC} (MLH derived from BC vertical profiles) estimates reported in the Table S2 is actually not the uncertainty of the MLH, but a standard error of the fitting parameter. Uncertainty of MLH_{BC} is estimated to be around 50 m and this will be explicitly stated in the section 2 (Supplement), as marked below.

Uncertainty of the mid-afternoon estimates of the radon mode

We agree that it is necessary to point out the uncertainty of the model, especially during the mid-afternoon conditions of convective days. The FFT filter with the cut-off frequency of 0.25 h^{-1} can introduce some uncertainty due to eliminating real variation of Rn concentration beside the instrumental noise. However, the instrumental noise causes very unstable model results, since shifting between the two modes of PBL evolution (growing and shrinking) is observed during the whole day. Since running window averaging affects the daily amplitude of radon signal, we decided to use the FFT filter, which can decrease the instrumental noise, especially in the mid-afternoon when C_{Rn} reaches the lower limit of detection.
Due to the uncertainty of the mid-afternoon results of BC emission rates, the calculation of daily averages was corrected. Instead of excluding mid-afternoon results, which can affect especially traffic related BC emissions, the weighted average was applied, introducing lower weight (50%) for the mid-afternoon E_{BC}. This approach would still account for the afternoon emissions, but with lower impact to avoid positive bias of results.

An additional section was added to the end of the manuscript (Page 20), expanding the discussion of the model uncertainty estimation.

5. Scope of investigation

After close examination of site characteristics, including the wind field and its effect on the radon concentration, we constrained the criteria for AJ location to average daily wind speed below 2 m/s (instead of 2.7 m/s), which excludes 40% of data with the strongest wind.
We have shown, that the radon concentration diurnal profile does not depend on the wind direction for wind speed up to 1.5 m/s, which is enough to obtain reliable results for days of stable atmospheric conditions. Most important, despite of the relative proximity of the Adriatic coast, the air flow from the SW is not commonly observed. For the dataset when valid conditions of the model are met, the strongest wind speeds were present in the mid-afternoon from the west, in direction of the Vipava valley, for which radon exhalation rate is expected to be spatially homogeneous.
Although the radon-box model has a higher uncertainty at the AJ location and the number of days, when conditions meet the criteria for the box-model are limited, we believe that the results of black carbon emission rates and the discussion regarding the uncertainty of the radon-box model approach are valuable and can serve as an important example for the future studies conducted in complex terrain.

Answers to the Referee 2

We thank the anonymous Referee 2 for positive review of the manuscript. The Referee 2 especially recommended to rewrite and shorten the Introduction and a part of Methodology section. To address the raised issues, we will answer the comments one by one and provide the changes made in the text. Due to major revision of the manuscript proposed by Referee 1, we will implement the changes to the new version of the manuscript.

1. **The introduction section is unusually long with full of irrelevant information. I would suggest the authors modify the introduction section and re-write. Instead of describing the general impacts and roles of BC in the atmosphere (which are widely available in the literature), focus your description on the existing emission estimates, their problems, and the need for the methods which have been described in the manuscript. Two pages would be more than sufficient for the introduction.**

Thank you for this comment. We agree that by rewriting the Introduction section we can draw reader's attention to the importance of the presented method. In this regard, we have shortened the:

- introduction to black carbon (BC)
- information on worldwide BC emission inventories
- information about the existing approaches for mixing layer height (MLH) determination
- introduction to radon characteristics

Based on the comments of Referee 1, the information of modelled values of radon exhalation rate were included in the Introduction section (Pages 2 – 5).

2. **Section 2.1 is also full of unnecessary information. Page 6, line 13-31: please reduce the content. There is no need to describe the population, growth, and implementation of various plans by the municipality. Please merge the 'measurement locations' and 'geological setting' together.**

As proposed by the Referee 2, the paragraph "Measurement locations" and "Geological setting" were merged and the section was shortened. However, from the point of view of interpretation of obtained results, we think it is important to provide an information regarding population density and characteristics of BC sources for both locations. When implementing abatement measures, such as traffic restrictions, the emission rate is the quantity which quantitatively demonstrates the efficiency of the measures taken.

The section "2.1 Measurement locations" was corrected accordingly.

3. **Page 8, line 3-30, already available in the literature, not needed specifically. Just cite the literature and remove the theoretical information.**

We agree to remove the theoretical information about BC source apportionment from the main text, since this allows to keep the focus of the paper on the application of radon box model and results of BC emission rates (E_{BC}). However, the parameters used for source apportionment may significantly influence the results of E_{BC}. Therefore we decided to shorten the text and move it to the Supplement.

The section "2.2 Black carbon measurements and source apportionment" on Page 8, lines 3 – 30 was corrected.

4. **Page 9, line 12: Please add the full form of FFT in the list of abbreviations in Table 1.**

Table 1 was updated with adding the FFT to the list of abbreviations.

5. **Section 2.4: It is recommended to provide a scatterplot of modelled-MLH with GDAS also in supplementary file.**

Since the same comment was also given by Referee 1, we have improved the description of methodology used for MLH comparison and the results, including the scatterplot, were added to the Supplement. A more detailed reply is provided in the Answers to Referee 1.

6. **Page 14, line 23: Authors mention that the Average Radon activity concentration was similar at both measurement locations, i.e., 15±11 Bqm^{-3} and 14±10 Bqm^{-3}. At the same time, the authors also mentioned that it was slightly lower in the spring 13±9 Bqm^{-3} and 12±8 Bqm^{-3}. Consider the standard deviations in the data, I do not see any difference in the data. Authors should check whether these differences are statistically significant or not and add a line on it.**

We agree with the observation pointed out by the Referee 2. There is in fact no significant difference in the seasonal averages of radon concentration measured at both locations. The text was corrected accordingly.

7. **Page 15, line 14: Despite significantly higher……25% higher in LJ than in AJ. What is meant by only 25% higher? And how population is a factor here? It looks highly ambiguous statement. The authors should consider removing it.**

The statement was intended to point out the difference between BC concentration at both locations, based on the assumed stronger BC emissions in the area of denser population (Ljubljana) and subsequent traffic density. Since the average BC concentrations are discussed further on in the same section, this statement was removed.

8. **Figure 1 should be modified significantly. The background map items are almost invisible.**

Thank you for this observation. Fig. 1 was modified for clear visibility of all important items.

The determination of highly time resolved and source separated black carbon emission rates using radon as a tracer of atmospheric dynamics

Asta Gregorič[1,2], Luka Drinovec[1,2,3], Irena Ježek[1], Janja Vaupotič[4], Matevž Lenarčič[5], Domen Grauf[5], Longlong Wang[2], Maruška Mole[2,6], Samo Stanič[2], Griša Močnik[1,2,3]

[1]Aerosol d.o.o., Ljubljana, SI-1000, Slovenia
[2]Centre for Atmospheric Research, University of Nova Gorica, Nova Gorica, SI-5000, Slovenia
[3]Department of Condensed Matter Physics, ~~Jozef~~ Jožef Stefan Institute, Ljubljana, SI-1000, Slovenia
[4]Department of Environmental Sciences, ~~Jozef~~ Jožef Stefan Institute, Ljubljana, SI-1000, Slovenia
[5]Aerovizija d.o.o., Ljubljana, SI-1000, Slovenia
[6]Quasar Science Resources S.L., Madrid, ES-28232, Spain

Correspondence to: Asta Gregorič (asta.gregoric@aerosol.eu)

Abstract. We present a new method for the determination of the source specific black carbon emission rates. The methodology was applied in two different environments: an urban location in Ljubljana and a rural one in the Vipava valley (Slovenia, Europe), which differ in pollution sources and topography. The atmospheric dynamics was quantified using the atmospheric radon (^{222}Rn) concentration to determine the mixing layer height for periods of thermally driven planetary boundary layer evolution. The black carbon emission rate was determined using an improved box model taking into account boundary layer depth and a horizontal advection term, describing the temporal and spatial exponential decay of black carbon concentration. The rural Vipava valley is impacted by a significantly higher contribution to black carbon concentration from biomass burning during winter (60 ~~2~~%) in comparison to Ljubljana (~~31~~27 %). ~~Results of the calculated~~Daily averaged black carbon emission rates in Ljubljana were ~~in the range from 280 to 300~~ 210 ± 110 μg $m^{-2}h^{-1}$ and 260 ± 110 μg $m^{-2}h^{-1}$ in spring and winter, respectively.~~.~~ Overall black carbon emission rate in Vipava valley were only ~~25%~~slightly lower compared to Ljubljana~~: and were in the range from 210 to 240~~ 150 ± 60 μg $m^{-2}h^{-1}$ and 250 ± 160 μg $m^{-2}h^{-1}$ in spring and winter, respectively~~. As expected, black carbon emissions from traffic prevail in Ljubljana and account for 80% of emissions during winter; the traffic contribution in the Vipava valley was only 42%.~~ Different daily dynamics of biomass burning and traffic emissions was responsible for slightly higher contribution of biomass burning to measured black carbon concentration, compared to the fraction of its emission rate. Coupling the high time resolution measurements of black carbon concentration with atmospheric radon concentration measurements can provide a useful tool for direct, highly time resolved measurements of the intensity of emission sources. Source specific emission rates can be used to assess the efficiency of pollution mitigation measures over longer time periods, thereby avoiding the influence of variable meteorology.

1. Introduction

Black carbon (BC), ~~is~~ an important component of fine particulate matter in the atmosphere~~ and its most strongly light absorbing fraction, . It is produced by incomplete combustion of various carbonaceous fuels, mainly fossil fuel and biomass. Due to its strong absorption of shortwave solar radiation, subsequent heating of the atmosphere and rapid adjustment effects on clouds and snow, it~~ significantly contributes to the climate forcing by aerosols (Pöschl, 2005; Bond et al., 2013; IPCC, 2013) and is ~~. Variety of other aerosols and precursor gases are emitted together with BC, which, after the internal mixing and aging in the atmosphere, alter BC optical properties (e.g. Cui et al., 2016; Pokhrel et al., 2017) and its atmospheric removal~~

~~rate due to changes of hygroscopic properties of BC-containing particles (e.g. Zhang et al., 2015). In addition, BC is~~ an important air pollutant, ~~decreasing local air quality and is~~ associated with undesirable health outcomes (Janssen et al., 2011; WHO, 2012).

Since BC is a chemically inert primary pollutant, it ~~is~~ can be used as a good measured indicator of emissions and can provide valuable information to authorities in the implementation and evaluation of air quality action plans, by indicating the strength of different emissions sources (e.g. Reche et al., 2011; Titos et al., 2015). On the other hand, emission inventories provide an important information for climate models by providing data about the changing pattern of BC emissions, its major sources and historical evolution. From the perspective of short-term local air quality prediction, improving local diurnal and seasonal pattern of BC emissions would greatly benefit the model prediction performance. Although ~~A~~atmospheric chemical transport models based on the fundamental description of atmospheric physical processes can improve the knowledge about temporal evolution of BC emissions at the modelled area, ~~but~~ they require comprehensive input data of atmospheric processes (Seinfeld and Pandis, 2016).

Bottom-up emission inventories rely on the information on the amount of used fuel combined with fuel-specific emission factors (e.g. Bond et al., 2007; Bond et al., 2013; Klimont et al., 2017). Although current emission inventories agree quite well on the main emission sources and regions, there exist significant uncertainties in the emission factors and activity data, used for emission calculation, with recent observationally constrained estimations much higher than the ones traditionally used (Sun et al., 2019). In contrast to bottom-up emission inventories, top-down constrained methods (such as inverse modelling) focus at minimising the difference between simulated pollutant concentration, based on estimated emission flux, and measured pollutant concentration (Brioude et al., 2013; Wang et al., 2016b; Guerrette and Henze, 2017). These methods can provide spatially and temporally better resolved assessment of pollutant emissions, including BC, but are influenced by different sources of uncertainty, mainly from the insufficient evaluation of long-range transport of polluted air-masses.

~~Based on bottom-up constructed emission inventories, BC emissions from energy related combustion have been increasing gradually from the beginning of industrial era from about 1 Tg in 1850 to 4.4 Tg in 2000 (Bond et al., 2007) and were dominated by contributions from different fuel types during technological evolution. Contribution from coal dominated until 1975, followed by biofuel and diesel fuelled engines more recently. Considering also open biomass burning, which accounts for 40 % of global BC emission, the total emissions in 2000 are estimated at about 7.5 Tg (Bond et al., 2013). According to the study of Klimont et al. (2017), where additional emission sources were considered, global BC anthropogenic emissions were estimated at about 6.6 and 7.2 Tg in 2000 and 2010, respectively, with a contribution of 0.7 Tg from Europe and Russia in 2010. Reduction of BC emission factors by implementation of cleaner technology partly offset the rapidly increasing energy consumption since 1950, resulting in slower growth of particulate matter emissions in comparison to CO_2. Although current emission inventories agree quite well on the main emission sources and regions, there exist significant uncertainties in the emission factors and activity data, used for emission calculation, with recent observationally constrained estimations much higher than the ones traditionally used (Sun et al., 2019). In contrast to bottom-up emission inventories, top-down constrained methods (such as inverse modelling) focus at minimising the difference between simulated pollutant concentration, based on estimated emission flux, and measured pollutant concentration (Brioude et al., 2013; Wang et al., 2016b; Guerrette and Henze, 2017). These methods can provide spatially and temporally better resolved assessment of pollutant emissions, including BC, but are influenced by different sources of uncertainty, mainly from the insufficient evaluation of long-range transport of polluted air-masses.~~

According to the European Union emission inventory report (LRTAP, 2018), 0.2 Tg of BC were emitted in 2016 in the EU-28 region, with the dominant energy-related emissions from on-road and non-road diesel engines accounting for about 70 % of all anthropogenic BC emissions (Bond et al., 2013). Recently updated United States black carbon emission inventory (Sun et al., 2019) pointed out decreasing trend of BC emissions from 1960 to 2000, dominated by vehicle, industrial and residential sectors. Traffic related BC emission is dominating primary particulate matter (PM) emission especially in major cities (e.g.

Pakkanen et al., 2000; Klimont et al., 2017). Recently, biomass combustion for residential heating has been promoted under the label of renewable fuel and additionally increased due to economic crises and increase of other fuel prices (Crilley et al., 2015; Denier van der Gon et al., 2015; Hovorka et al., 2015; Athanasopoulou et al., 2017). Although several studies report significant role of wood burning emissions on BC concentrations in Alpine valleys (Sandradewi et al., 2008b; Favez et al., 2010; Herich et al., 2014) and Scandinavian rural areas (Ricard et al., 2002; Aurela et al., 2011), increase in contribution of wood smoke to fine PM was noticed also in several large urban areas (Favez et al., 2009; Crippa et al., 2013; Fuller et al., 2014; Denier van der Gon et al., 2015; Hovorka et al., 2015; Helin et al., 2018; Zhang et al., 2019). Notable contribution of wood smoke was observed also in Slovenian urban (Ogrin et al., 2016) and rural areas (Wang et al., 2019), responsible for air quality deterioration especially in geographically constrained areas such as valleys and basins.

To assess the efficiency of abatement measures aiming to improve air quality, concentration of pollutants is usually measured before and after the measures are implemented, in order to quantitatively determine the reduction of pollutant concentration. However, this approach can be biased due to changes of micrometeorology of planetary boundary layer (PBL) which ~~Besides the intensity of pollutant emission, micrometeorology of the planetary boundary layer (PBL)~~ plays an important role in controlling time evolution of pollutant concentration. Therefore, assessment of BC emission rate requires decoupling of meteorologically driven variation from the dynamics of the sources. On diurnal timescales, atmospheric stability/dynamics plays a key role on the variability of primary inert pollutants (e.g. Quan et al., 2013; McGrath-Spangler et al., 2015; Tang et al., 2016), such as BC, and is affected by them (e.g. Ferrero et al., 2014). The evolution of the planetary boundary layer (PBL), ~~is~~ the lowest part of the troposphere, ~~which is directly affected by the presence of the Earth's surface. Soon after sunrise~~is driven~~, convectively driven~~ by convective heat transfer from the ground surface and by mechanical mixing (due to wind shear and surface roughness), which are ~~is~~ responsible for the formation of the turbulent mixing layer (ML). ~~,~~ML ~~which~~ grows by entraining the air from above and reaches its maximum depth in the late afternoon. ~~Thus, the mixing layer height (MLH) strongly depends on the intensity of solar radiation reaching the ground. Entrainment of air from above takes place in a stable layer at the top of the ML, the so-called entrainment zone.~~ The residual layer is formed after the decay of turbulence shortly before sunset, with its bottom portion transformed into a stable nocturnal boundary layer (SNBL) during the night. SNBL is characterized by stable stratification with low mixing. ~~The bottom 10 % of the boundary layer, either ML or SNBL, represents the surface layer, where turbulent fluxes and stress vary by less than 10 % of their magnitude (Stull, 1988). Anthropogenic air pollutants are generally emitted from the surface and trapped within the PBL, where their concentrations are controlled by the turbulent mixing. Therefore, on diurnal timescales, atmospheric stability/dynamics (tendency of the atmosphere to resist or enhance the initial displacement of air parcels) plays a key role on the variability of primary inert pollutants, such as BC, and is affected by them (e.g. Ferrero et al., 2014).~~

Different approaches exist for MLH determination ~~are reflected in different definitions found in literature~~ (Seibert et al., 2000). ~~One of generally adopted definitions relies on the vertical extent of dispersion of pollutants, which are released from the surface within 1-hour time period. However, since slope winds may influence vertical pollutant transport, this definition may be ambiguous at complex terrains such as Alpine valleys (Leukauf et al., 2016). MLH can be determined by indirect methods based on remote sensing using lidars (Caicedo et al., 2016; de Bruine et al., 2017) or radiosounding measurements, by applying different measures, such as Richardson number, Monin-Obukhov length or turbulence kinetic energy (Stull, 1988). These methods have usually low spatial and/or temporal resolution. Furthermore, interpretation of mixing in very stable conditions is challenging due to phenomena such as nocturnal jets and local flow perturbations (Williams et al., 2013), leading to non-reliable representation of stable atmospheric conditions by numerical weather or dispersion models.~~

~~Assessment of the BC emission rate requires decoupling of meteorologically driven variation from the dynamics of the sources.~~

An alternative way to overcome the difficulty associated with the proper physical interpretation of micrometeorological properties of the ML and dispersion characteristics is the use of a tracer method. Naturally occurring noble radioactive gas

radon (^{222}Rn) has been applied in the past for different studies. Radon characteristics, its emanation from rocks and its transport in rocks, soil (e.g. Etiope and Martinelli, 2002) and atmosphere (e.g.Williams et al., 2011; Williams et al., 2013) were comprehensively studied in the past. Radon was used to study: ~~the study of~~ long-range transport of air masses (Hansen et al., 1990; Crawford et al., 2007), ~~and recently for studying~~ PBL characteristics (e.g. Griffiths et al., 2013; Williams et al., 2013; Pal et al., 2015; Salzano et al., 2016; Vecchi et al., 2018), microclimate spatial variability (Chambers et al., 2016; Podstawczyńska, 2016) and impact assessment of atmospheric stability on local air pollution (Perrino et al., 2001; Chambers et al., 2015a; Chambers et al., 2015b; Crawford et al., 2016; Wang et al., 2016a; Williams et al., 2016). Good correlation, at least for the periods of thermally driven PBL convection, was observed in previous studies comparing effective MLH derived by the box model and MLH obtained by modelling approaches based on turbulence variables (Allegrini et al., 1994; Vecchi et al., 2018; Kikaj et al., 2019) or remote sensing techniques (sodar, lidar) (e.g. Salzano et al., 2016). Kikaj et al. (2019) successfully identified persistent inversion events in the Ljubljana basin based on ^{222}Rn measurements. The emission pattern of gaseous traffic related air pollutants in Bern (Switzerland), estimated by a box-model based on radon tracer, with an included advection term, showed an excellent correlation with traffic density (Williams et al., 2016). These studies imply that radioactive tracer method gives reliable information on the effective mixing layer height and indication of atmospheric stability (e.g. Perrino et al., 2001), which can be easily implemented in the environmental monitoring networks.

~~Radon is the only gaseous element in the ^{238}U radioactive decay chain, with its only significant sources in the natural environment being rocks and soil. After emanation from rock surfaces and soil grains, it is transported by diffusion and advection to the surface by carrier gasses (Etiope and Martinelli, 2002). Once exhaled from the Earth's surface, it is subjected to the mixing within the ML, thus experiencing the same extent of dispersion as other air pollutants emitted from ground-based sources. As a noble gas with a relatively short half-life (3.82 days), it represents an ideal tracer for the study of PBL processes.~~

The strength of radon flux from the surface to the atmosphere, the so-called radon exhalation rate (E_{Rn}), depends mainly on the surface permeability and the radon potential (Karstens et al., 2015), which are controlled by geological and climatic characteristics of the area (e.g. Vaupotič et al., 2007; Vaupotič et al., 2010; Kardos et al., 2015; Karstens et al., 2015). ~~. Surface permeability is controlled by geological setting – lithological (rock type, structural characteristics (presence of fault zones) (e.g. Vaupotič et al., 2010) and soil moisture. Fault zones can act as a pathway for different gaseous species especially in the geologically active environments, leading to anomalies in E_{Rn}, whereas E_{Rn} above karst caves and fractured rocks can experience high spatial and temporal variability (Vaupotič et al., 2010; Gregorič et al., 2014). Since radon is poorly soluble in water, its only sink is the radioactive decay, which can be neglected on hourly bases.~~ As reported by Vaupotič et al. (2007) measured E_{Rn} on Slovenian territory spans over large range from few tens to several hundred mBq m^{-2} s^{-1}. Karstens et al. (2015) reported modelled radon exhalation rate on European scale, which varies in the range from 70 – 150 Bq m^{-2}h^{-1} and 160 – 180 Bq m^{-2}h^{-1} in the south-western part of Slovenia in winter and summer, respectively. The range of E_{Rn} in the central part of Slovenia is 35 – 90 Bq m^{-2}h^{-1} and 90 – 125 Bq m^{-2}h^{-1} for winter and summer, respectively. Radon exhalation rate is usually considered constant on short temporal scales in areas with homogeneous geologic characteristics (Pearson and Jones, 1965). However, exhalation of Rn is a complex process which can be assessed with different modelling approaches. Salzano et al. (2016) showed, that the error in the modelled effective MLH by considering constant radon source can be up to 10 %. Local heterogeneity of E_{Rn} due to heterogeneous soil permeability (within few meters range) is homogenised in the thin atmospheric layer (~0.5 m) close to the ground and does not represent a significant concern for measurements above this height. Due to continuous source from the surface, radon concentration profiles in the SNBL can exhibit strong gradients, resulting in higher radon concentration when measurements are conducted closer to the ground, especially in the SNBL conditions. ~~.~~On a seasonal scale, however, E_{Rn} decreases with the presence of snow cover, frozen soil or during and shortly after (on time scale of few days) rainy periods, due to reduced surface permeability, thus representing one of the main sources of uncertainty in the box model. It is also worth noting, that reliable exhalation rate measurements (used for the box model) should be conducted in a broad network in the extent of modelled area in different periods of year, so the seasonal changes in

soil permeability would also be considered. The seasonal changes of E_{Rn} were already pointed out in different studies (Karstens et al., 2015; Salzano et al., 2016; Williams et al., 2016; Chambers et al., 2019).

The aim of this paper is to determine the BC emission rate apportioned to traffic and biomass burning sources, its diurnal pattern and monthly variation for two distinct locations in Slovenia (Europe), which differ from the point of view of their natural characteristics (geology, geomorphology, meteorology) and urban environment (urban and rural background). Both sites are subjected to their own pattern of air pollution episodes which will be addressed and interpreted based on Eulerian box model. The effective mixing layer height will be reproduced for both sites based on Rn measurements, taking into account seasonally resolved E_{Rn}, then used for decoupling meteorologically driven changes of measured BC concentration from the one resulting from the source dynamics. The highly time-resolved and source apportioned BC emission rate (E_{BC}) represents an essential information for short-term forecasts of air pollution episodes, as well as for the evaluation of the efficiency of air quality abatement measures and their potential adaptation. Temporal variation of BC concentration will be highlighted from the point of view of PBL evolution.

A list of acronyms and symbols used in this paper is given in Table 1.

.

2. Method

2.1 Measurement locations

Two distinct measurement locations were selected for this study. The first one is located in the urban area of Ljubljana (LJ, capital city of Slovenia), which lies in the central part of Slovenia (Europe) (Figure 1). The second measurement location was in a small town Ajdovščina (AJ), located in the Vipava valley in the western part of Slovenia. Measurement campaigns lasted from autumn 2016 to spring 2017 (November 23, 2016 to May 20, 2017) in Vipava valley and from winter 2017 to summer 2017 (February 1, 2017 to June 8, 2017) in Ljubljana. Due to its basin location, Ljubljana is characterised by poor ventilation and frequent occurrence of persistent temperature inversions (Kikaj et al., 2019), which constrains pollutants emitted from surface sources within the limited air volume inside the basin. During stable atmospheric conditions, especially in the SNBL, a thin layer of drainage winds (colder air, adjacent to the ground, flowing downhill under the influence of gravity) and a flow of air from the edge of the city towards the centre (formed due to the heat island) governs air circulation within the Ljubljana basin (Stull, 1988; Ogrin et al., 2016). ~~During the measurement campaign, around 10 cm of snow cover was present from January 14 to February 2, 2017.~~Ljubljana is characterised by temperate continental climate, with a significant seasonal temperature cycle.

The population of the wider Ljubljana basin is around 500,000, of which 287,000 live in the urban municipality of Ljubljana. Much more than 100,000 daily commuters from other municipalities represent additional traffic flow on working days~~.~~ (Ogrin et al., 2016). ~~Rapid growth of automobile use is observed in the last few decades, leading to daily traffic jams inside the city and its surroundings. In the recent years, the local municipality has implemented different measures of sustainable mobility in order to improve the air quality. In particular, the traffic restriction in the major road in the city centre has led to 70% decrease of local BC concentrations (Titos et al., 2015).~~ Besides traffic-related air pollution, emissions from combustion of biomass fuel for residential heating are a significant source of particulate concentrations in the whole country (Gjerek et al., 2018), not only in rural areas, but in Ljubljana as well. Although district heating is provided in several areas of the city, the use of wood boilers and fireplaces is a common practice.

The population of the second area of interest, including surrounding villages is relatively small, with ~~about 19,000 residents living in the municipality of Ajdovščina, of which~~ about 7,000 residents ~~live~~living in the town of Ajdovščina. The Vipava valley is confined to the north by the steep ridge, which rises up to about 1000 m a.s.l., and to the south by the Karst plateau with an average altitude of about 300 m. Due to the complex topography, the valley usually experiences two extreme cases of atmospheric stability conditions. On one side, stable atmospheric conditions can last for several days, leading to the formation of strong vertical aerosol gradients, which are followed by frequent occurrences of strong downslope Bora wind (Mole et al., 2017; Wang et al., 2019). A highway connecting the central part of Slovenia with Italy runs through the valley on the southern border of the town, around 800 m away from our measurement site. The Mediterranean climate of this area is responsible for mild winters and warm summer season, with residential heating mainly limited to the cold season, from November to February, with biomass fuel being the primary source of energy.

~~**Geological setting**~~

From geological point of view, the city of Ljubljana lies in the neotectonic basin with extensive and thick accumulations of Quaternary glaciofluvial sediments on the northern and central parts (gravel and conglomerate), whereas the south-western part of Ljubljana basin is filled with lacustrine and paludal sediments (Janža et al., 2017). The maximum thickness of sediments is around 170 m. Non-consolidated Quaternary sediments are permeable enough to allow spatially and temporally homogeneous Rn exhalation rate.

The geological structure of the broader area of Vipava valley results from Tertiary thrust of Cretaceous limestone, which forms the steep north-eastern ridge of the valley, on the Eocene flysch rocks, forming the valley floor. Flysch rocks consist of

alternating layers of marlstone and carbonatic sandstone. Due to physical weathering of the limestone, a large amount of limestone scree material has been formed and deposited on the underlying flysch rocks on the slopes of the north-eastern ridge. Valley floor is covered by clayey weathered residual of flysch rocks with fine flysch scree (Jež, 2007). Spatially homogeneous Rn exhalation rates can be expected along the valley.

2.2 Black carbon measurements and source apportionment

Measurements of black carbon concentration were conducted at two sites at each location, Ljubljana and Vipava valley, one at the urban background and the other one at the higher altitude (Figure 1), in order to provide an insight into the extent of the vertical aerosol mixing. Periods during which similar BC concentrations were measured at both sites indicate time periods when MLH reached or exceeded altitude difference between both sites. Although this kind of measurement composition certainly indicates periods of stable PBL conditions, detection of the exact time of MLH reaching the upper site is more uncertain due to diffusion mixing (in the case of Ljubljana) or local slope winds (Leukauf et al., 2016) (Vipava valley) and therefore it does not provide undisturbed MLH evolution characteristic for the whole valley/basin.

The urban background site of the Slovenian Environment~~al~~ Agency (ARSO) was used for BC measurements in the city of Ljubljana (295 m a.s.l.), while measurements at the Golovec Astronomical and Geophysical Observatory (GOL), 100 m above Ljubljana city (395 m a.s.l.) were used as the hill site. The inlet at ARSO was about 4 m above the ground, while the inlet at GOL was about 2.5 m above ground. Measurements in the Vipava valley were conducted about ~~20~~ 12 m above ground level (120 m a.s.l) on the roof of the building of University of Nova Gorica, located in the town of Ajdovščina (AJ). About 830 m higher (950 m a.s.l.), on the north-eastern ridge of the valley, the second measurement site was installed at the Otlica Meteorological observatory (OT) of the same university.

Aerosol light absorption and corresponding mass equivalent black carbon concentration (BC) was measured at 7 different wavelengths (370 – 950 nm) using the Aethalometer model AE33 (Magee Scientific / Aerosol d.o.o.), with "dual spot" technique used for real-time loading effect compensation (Drinovec et al., 2015). Flow rate was set to 5 l/min and the measurement time resolution to 1 minute. TFE-coated glass fibre filter was used with multiple scattering parameter (C) set to 1.57. The mass absorption cross section σ_{air} of 7.77 $m^2\ g^{-1}$ was used to convert the optical measurement at 880 nm to BC mass concentration.

Aethalometer measurements at different wavelengths provide an insight in the chemical composition of light absorbing particles. The so called Aethalometer model (Sandradewi et al., 2008a) was used to apportion BC to traffic (BC_{TR}) and biomass burning (BC_{BB}) sources. The model uses an a priori assumed pair of absorption Ångström exponents (AAE) for traffic (AAE_{TR}) and biomass burning (AAE_{BB}) to determine the contribution of both sources. AAE_{TR}/AAE_{BB} were set to 1.0 and 2.0 for, respectively. ~~A narrow range of AAE_{TR} (0.8 – 1.1) values is reported in the literature, whereas larger AAE_{BB} values (from about 1.5 up to 3.5) in the wider range are characteristic for biomass burning sources (Kirchstetter, 2004; Saleh et al., 2013; Garg et al., 2016; Zotter et al., 2017). Higher values of AAE_{BB} result from enhanced light absorption in the near-UV and blue part of the spectrum caused by organic carbon species, present in biomass-smoke. Source specific AAE can be independently determined using auxiliary measurements of OC/EC, and ^{14}C (Sandradewi et al., 2008a; Zotter et al., 2017), or biomass burning tracers like levoglucosan (Favez et al., 2010; Herich et al., 2014; Hellén et al., 2017; Helin et al., 2018). Since independent measurements allowing the determination of the AAE pair representative for our measurement locations were not available, the most suitable AAE pair was estimated according to the commonly used AAE values published in the literature, by considering overall distribution of AAE (Figure S1) for each measurement location and the corresponding diurnal variation of traffic (BC_{TR}) and biomass burning related BC (BC_{BB}) (Figure S2). AAE was calculated using the Eq. 1 for 470 nm and 950 nm wavelengths, where b_{abs} stands for the absorption coefficient at 470 nm and 950 nm.~~

$$AAE = \frac{\ln\left(\frac{b_{abs(470)}}{b_{abs(950)}}\right)}{\ln(950/470)} \quad (1)$$

By taking into account equations provided by Sandradewi et al. (2008a), the BC_{BB} and BC_{TR} were finally calculated using the Eq. 2 and 3, respectively.

$$BC_{BB} = \frac{\frac{b_{abs(470)}}{b_{abs(950)}} - \left(\frac{950}{470}\right)^{AAE_{TR}}}{\left(\frac{950}{470}\right)^{AAE_{BB}} - \left(\frac{950}{470}\right)^{AAE_{TR}}} \times BC \quad (2)$$

$$BC_{TR} = BC - BC_{BB} \quad (3)$$

AAE_{TR} / AAE_{BB} pair of 1.0 and 2.0, respectively, was chosen for both measurement locations. Further discussion on the choice of AAE pair used for source apportionment is provided in the Section 1 of the Supplement.

2.3 Radon measurements

Radon measurements were conducted at both measurement locations, in the city of Ljubljana on the floor of the basin and on the floor of Vipava valley, close to the town of Ajdovščina. Measurements cover longer period than BC measurements: from November 11, 2016 to May 31, 2017 in Vipava valley (with about one-month gap in March 2017 due to instrument malfunction) and from December 14, 2016 to June 8, 2017 in Ljubljana. At both measurement sites, instruments were installed outdoors under a roof of single-family house (to shelter instruments from environmental effects, but otherwise open), surrounded by unperturbed natural soil ground. Both sites were selected in the area that is subjected to the same boundary layer characteristics as aerosol measurements. Instruments were installed 1 m and 3 m above ground in Ljubljana and Vipava valley, respectively. Radon activity concentration (C_{Rn}) was measured using AlphaGUARD PQ2000 PRO (Bertin Instruments) radon monitor. In the instrument, the measured gas diffuses through a large-surface glass fibre filter into the ionization chamber. The instrumental lower limit of detection is 2 – 3 Bq m^{-3} at 1-hour time resolution. In order to decrease noise, radon measurements were smoothed by applying an FFT filter with cut-off frequency of 0.25 h^{-1}. Comparison of smoothed and raw Rn measurements is shown in Figure S6. Due to sampling in diffusion mode, 1 hour time lag was considered when combining C_{Rn} data with other measurements.

2.4 Meteorological parameters and supporting information

Meteorological parameters, such as air temperature (*T*), wind speed and direction (*ws*, *wd*), amount of precipitation and snow cover were provided by the Slovenian Environment Agency (ARSO) for the Ljubljana measuring location. In the Vipava valley, all meteorological parameters are measured at the meteorological station situated at the valley floor close to the town of Ajdovščina, whereas wind data were collected at the rooftop of the University of Nova Gorica building in Ajdovščina as a part of research conducted at the Centre for Atmospheric Research (Mole et al., 2017).

MLH dataset, obtained from the NOAA Air Resources Laboratory (NOAA-ARL) Global Data Assimilation System (GDAS) database (Rolph et al., 2017), was considered as supplementary information for comparison with the effective MLH values derived from the box model. Archived dataset has spatial resolution of 1° and temporal resolution of 3 hours. Although spatial resolution is not fine enough to capture local micrometeorological characteristics, it gives an estimation on the wider area PBL stability and effective mixing height.

Traffic counts data for Ljubljana were provided by the Municipality of Ljubljana for the whole period of measurements for several different locations within the city.

Two complementary methods were used for detection of MLH and comparison with MLH derived by the box model. Scanning mobile Mie-scattering lidar is used at the University of Nova Gorica for studies of Bora wind (Mole et al., 2017), aerosol properties and PBL characteristics (Wang et al., 2019) in the Vipava valley. Detailed lidar configuration and performance is provided by He et al. (2010). In our study, MLH was estimated based on the retrieval of range-corrected lidar signal in selected periods. On the other hand, vertical BC concentration profiles were measured over the Ljubljana basin by ultralight aircraft on selected days from February to May 2017. A lighter modified version of Aethalometer AE33 with an isokinetic sampling inlet was used for BC vertical profile measurements. Measurements provided useful information about aerosol vertical dispersion characteristics and MLH estimation (Ferrero et al., 2011). Further details about analyses approach is provided in the Supplement (Section 2).

2.5 Radon-based MLH modelling

The box model approach introduced in previous studies (Sesana et al., 2003; Griffiths et al., 2013; Salzano et al., 2016; Williams et al., 2016; Vecchi et al., 2018) employs the Eulerian approach, including a constant radon source (E_{Rn}) and vertical entrainment of air mases from the residual layer. Salzano et al. (2016) improved the model performance by considering the variability in the soil radon exhalation rate, where the authors showed up to 10 % difference in modelled MLH compared to the model using constant Rn source. In this paper we applied the approach introduced by Williams et al. (2016), where an inclusion of a simplified horizontal advection term allows the quantification of local emissions of air pollutants.

Considering a vertically well mixed box (box dimension discussed in detail in Sec. 2.6.1) with species concentration C_s, the mass of species "*s*" in a column of air within the effective MLH (h) over one m^2 at time t_i depends mainly on the emissions (E_s) from the surface and the remaining mass of species from the previous time period (t_{i-1}). When ML is growing (c_s^+), there is an additional encroachment of species, which remained in the residual layer from the previous day, while in the case when this layer is shrinking (c_s^-), a part of mass is considered to be removed from the mixing layer (Eq. 14).

$$C_{s_i}h_i = E_s\Delta T_s + C_{s_{i-1}}h_{i-1}e^{-\lambda'_s \mathrm{d}t} + c^{\pm}_{s_{i-1}}(h_i - h_{i-1})e^{-\lambda'_s \mathrm{d}t} \quad (14)$$

The term ΔT_s (Eq. 25) includes correction due to decay of species in time period $\mathrm{d}t = t_i - t_{i-1}$, which is characterized by decay constant λ'_s. If decay rate is very slow, decay of species within dt becomes negligible, thus $\Delta T_s \rightarrow \mathrm{d}t$.

$$\Delta T_s = \frac{1-e^{-\lambda'_s \mathrm{d}t}}{\lambda'_s} \quad (52)$$

Decay constant λ'_s $[h^{-1}]$ takes into account temporal decay and horizontal advection. The temporal decay constant λ_s $[h^{-1}]$ accounts for internal sinks due to chemical reactions, dry and wet deposition or radioactive decay. Horizontal advection assumes exponential decrease of species concentration downstream (Eq. 36) and is characterized by spatial decay constant γ_s $[m^{-1}]$:

$$\lambda'_s = \lambda_s + U\gamma_s \quad (63)$$

where U represents layer averaged wind speed. A small uncertainty is introduced to the model, since wind data were available only from standard meteorological measurements at the height of 2 m above the surface.

Three different cases can be parameterized during a course of a day:

1. During stable conditions, when $h_i = h_{i-1}$, Eq. 14 is reduced to Eq. 47:

$$C_{s_i} - C_{s_{i-1}}e^{-\lambda'_s \mathrm{d}t} = \frac{E\Delta T_s}{h_i} \quad (74)$$

2. After the sunrise when PBL starts to grow ($h_i > h_{i-1}$), a volume of air mass from the residual layer is incorporated into the expanding ML and the term $c_s^{\pm}$ from the last part of Eq. 4 is modelled as c_s^+ (Eq. 58):

$$c_{s_{i-1}}^+ = c_s^0 e^{-\lambda_s'(t_{i-1}-t_0)} \quad (85)$$

where c_s^0 is species concentration from the previous day at time t_0, just before the afternoon transition to SNBL. c_s^+ represents the concentration of species in the residual layer.

3. When PBL is shrinking ($h_i < h_{i-1}$) a volume of air is decoupled from ML and forms the residual layer. $c_s^{\pm}$ of Eq. 14 is set to $c_{s_{i-1}}^- = C_{s_{i-1}}$.

The first phase of modelling is focused to the quantification of the effective MLH based on atmospheric Rn concentration measurements. Rn data with 1 hour time resolution were first smoothed by applying FFT filter with cut-off frequency of 0.25 h^{-1} in order to decrease noise level, since small changes of Rn concentration can cause unexpected fluctuation in the calculated MLH. Assuming constant, spatially homogeneous radon source, which extends beyond the limits of our modelled area, spatial decay constant in Eq. 36 can be approximated to zero ($\gamma_{Rn} = 0$) and decay constant λ_{Rn}' is equal to radon radioactive decay constant: $\lambda_{Rn} = 0.0076\ h^{-1}$. Radioactive decay accounts for less than 1 % of C_{Rn} decrease during the course of one hour.

For stable atmospheric conditions, when $h_i = h_{i-1}$, Eq. 14 is simplified to

$$h_i = \frac{E_{Rn}\Delta T_{Rn}}{\mathrm{d}C_{Rn}} \quad (96)$$

where $\mathrm{d}C_{Rn}$ represents difference in radon concentration measured in the time period d*t*:

$$\mathrm{d}C_{Rn} = C_{Rn_i} - C_{Rn_{i-1}} e^{-\lambda_{Rn}\mathrm{d}t} \quad (107)$$

Condition of expanding or shrinking ML is tested by comparing difference of concentration with emission of Rn to the ML with MLH $= h_{i-1}$ in the same time period. In the case of expanding ML, change of Rn concentration is smaller than expected for stable MLH: $dC_{Rn} < E_{Rn}\Delta T_{Rn}/h_{i-1}$ (Eq. 811), whereas in the case of shrinking ML, concentration increases faster than it would be expected for stable MLH: $dC_{Rn} > E_{Rn}\Delta T_{Rn}/h_{i-1}$ (Eq. 912). Effective MLH is then calculated for the two separate conditions as:

$$h_i = \frac{E_{Rn}\Delta T_{Rn} + h_{i-1}\left(C_{Rn_{i-1}} - C_{Rn_{i-1}}^+\right)e^{-\lambda_{Rn}\mathrm{d}t}}{C_{Rn_i} - C_{Rn_{i-1}}^+ e^{-\lambda_{Rn}\mathrm{d}t}} \quad (118)$$

$$h_i = \frac{E\Delta T_{Rn}}{C_{Rn_i} - C_{Rn_{i-1}} e^{-\lambda_{Rn}\mathrm{d}t}} \quad (129)$$

where~~Where~~ $C_{Rn_{i-1}}^+$ ~~-~~represents radon concentration remaining after decay in the residual layer from the previous afternoon. An approximation of linear decrease of $C_{Rn_{i-1}}^+$ with height was considered (Williams et al., 2011), reaching radon concentration of zero at the top of the previous day's residual layer.

When MLH reaches its full extent in the late afternoon, it can extend above the previous day's residual layer, thus incorporating Rn "free" air into the ML. ~~In these conditions C_{Rn} reaches its lowest daily concentration, which can be similar or even lower than concentration from the previous day's residual layer (C_{Rn}^+). In such conditions, calculation following Eq. 11 becomes unstable with high uncertainty, leading to significant overestimation of the effective MLH. Since incorporation of residual layer into the Eq. 11 resulted in most cases in non meaningful determination of MLH in the couple of hours preceding the afternoon transition to SNBL, residual layer Rn concentration was set to zero ($C_{Rn_{i-1}}^+ = 0$).~~

2.5.1 Determination of radon exhalation rate - E_{Rn}

The ~~results of~~ MLH values, determined by the box model, strongly depend on the correct estimation of radon exhalation rate. As discussed in previous sections, E_{Rn} is affected by seasonal meteorological changes mostly by varying soil humidity and permeability. Since continuous monitoring of E_{Rn} is usually not available, the box model has to be calibrated to ~~any~~ the available information of MLH. Due to vertical gradients in radon concentration, which are present especially during the SNBL conditions, the height of radon measurements above ground level can play an important role in its observed daily variation, potentially biasing the results of the modelled MLH, if the measurement height is not taken into account. As introduced by Griffiths et al. (2013), the actual radon exhalation rate ($E_{Rn\text{-}0}$) has to be calibrated based on the radon measurement height. Therefore, the radon exhalation rate estimated in this study represents an effective E_{Rn}, rather than actual $E_{Rn\text{-}0}$ for the area under consideration (Eq. 10):

$$E_{Rn} = E_{Rn-0} \times s \quad (10)$$

where s represents a scaling factor which depends on the measurement height. Lower measurement height results in larger s. We use this effective exhalation rate, representing a wider region, in our model.

The calibration of the radon box model in terms of selection of appropriate E_{Rn} was performed by combining three different approaches.

1. Comparison of the radon derived MLH (MLH_{Rn}) (for E_{Rn} in the range from 50 – 400 Bq $m^{-2}h^{-1}$) based on Eqs. 6, 8, 9, with modeled values of MLH, obtained from the Air Resources Laboratory (NOAA-ARL) Global Data Assimilation System (GDAS) database. The approach is explained in detail in the Supplement Section 5.1. 100 Bq $m^{-2}h^{-1}$ acceptable range was used.
2. MLH determined in the first step was compared to black carbon measurements at different elevations. When MLH exceeds the elevation of the higher BC measurement site (hill), BC concentration is expected to be similar at both measurement sites (city and hill), whereas in the period when MLH is below the hill measurement site, a strong gradient in BC concentration is observed.
3. In the third step, radon derived MLH_{Rn} for selected days was compared to the MLH determined from vertical profiles (MLH_{BC}) of BC measured with an aircraft over the Ljubljana basin (Supplement Section 2) or with lidar-derived MLH in the Vipava valley.

The results of the first approach were used as the first estimate of the E_{Rn}. In the case of high uncertainty (low number of data points, wide confidence interval level, unrealistic values of E_{Rn} estimate), the second approach was used to confirm the previously obtained E_{Rn} estimates or to obtain a suitable range of E_{Rn}. For the months, when the BC vertical profiles or lidar-derived MLH were available, the third approach was used to estimate the E_{Rn}. Graphical presentation of above-mentioned approaches for each month is presented in the Supplement Section 5.2.

~~In our study we used the modelled MLH for the determination of E_{Rn} in the following way:~~

~~1. E_{Rn} was considered to be stable during the course of one month. In this regard, periods of specific microclimatic conditions, such as rainy and windy days were removed from the analyses.~~

~~2. Modeled MLH was obtained from the Air Resources Laboratory (NOAA ARL) Global Data Assimilation System (GDAS) database, noting the limited spatial and time resolution of the model.~~

~~3. MLH was calculated using Eqs. 9, 11, 12 for different values of radon exhalation rates in the range from 50 to 600 Bq $m^{-2}h^{-1}$ (Rn-model).~~

~~4. GDAS-modeled-MLH was correlated with Rn-model derived one for each choice of exhalation rate at the GDAS time resolution. Correlation slopes are presented in Figure 2. We obtained the monthly average exhalation rate at unity correlation slope.~~

This method allowed us to obtain average monthly exhalation rate (Table 2) using the data from the meteorological model (GDAS), even though the model spatial and time resolution is low. We interpret this effective exhalation rate to be representative of the investigated regions for the purpose of using it in our model. ~~The uncertainty of E_{Rn} is assessed from the slope error and was estimated to be 50 Bq m^{-2} h^{-1}. The obtained exhalation rates were validated by comparing Rn model MLH to MLH determined from vertical profiles of BC measured with an aircraft (Supplement Section 2) and show good agreement at the time of the airplane flights.~~

2.6 Black carbon emission rate modelling

The second part of modelling uses the box model (Eq. 14), where measured BC concentrations, apportioned to sources, are inverted, taking into account effective MLH determined during the first step, to calculate hourly resolved BC emission rate (E_{BC}).

1-minute dataset of source apportioned BC concentration was first averaged to 1-hour time base in order to correspond to the determined MLH values. BC emission rates were calculated separately for traffic (E_{TR}) and biomass burning emissions (E_{BB}), using Eq. 1~~3~~ and 1~~4~~, for increasing and decreasing MLH, respectively:

$$E_{BC} = \frac{1}{\Delta T_{BC}}\left(C_{BC_i}h_i - C_{BC_{i-1}}h_{i-1}e^{-\lambda'_{BC}\mathrm{d}t} - C^{+}_{BC_{i-1}}(h_i - h_{i-1})e^{-\lambda'_{BC}\mathrm{d}t}\right) \quad (1~~3~~)$$

$$E_{BC} = \frac{h_i}{\Delta T_{BC}}\left(C_{BC_i} - C_{BC_{i-1}}e^{-\lambda'_{BC}\mathrm{d}t}\right) \quad (1~~4~~2)$$

where the index i represents the traffic (TR) or biomass burning (BB) contributions to BC concentrations, and λ'_{BC} is the decay constant calculated by Eq. 6, which accounts for temporal decay and horizontal advection. The latter is introduced due to dispersion characteristics and inhomogeneous spatial distribution of emission sources, which usually leads to decrease of species concentration downstream. In the Eulerian box model, the difference between species concentration within the modelled area and outside the box controls the spatial decrease of the concentration downstream. Based on the study presented by Williams et al. (2016), an assumption of exponential decay was considered in this study to simplify the model and overcome the fact of missing measurements at the box outer limits. The size of the modelled area and distribution of specific sources leads to source specific spatial decay constants, namely γ_{BB} for biomass burning and γ_{TR} for traffic related BC. Spatial decrease of BC concentration with distance from the source for different choice of γ is presented in Figure S1~~3~~9 a.

Since BC particles are inert, the rate of BC removal from the atmosphere is governed by wet deposition (e.g. Blanco-Alegre et al., 2019). The temporal sink was estimated based on mean life-time of soot particles in the atmosphere, which can be considered between 1 week and 10 days (Cape et al., 2012). Therefore λ_{BC} of 0.006 h^{-1} was considered in this study, corresponding to 1 week mean lifetime of BC. The same temporal sink was considered regardless of BC source.

Data analysis and graphical representation was performed using R programming language (R Core Team, 2018), with "ggplot2" (Wickham, 2009), "openair" (Carslaw and Ropkins, 2012), ~~and~~ "dplyr" and "deming" packages. If not stated otherwise, time is reported as local time (CET/CEST). Seasonal statistics was computed considering December – February as winter, March – May as spring, June – August as summer and September – November as autumn.

2.6.1 Determination of decay constants

Horizontal advection dominates over BC temporal sink, which is responsible for a small offset in modelled emission rates. A longer estimated lifetime of BC particles would result in lower modelled emission rates. Changing λ_{BC} from 0.006 h^{-1} (mean lifetime of 7 days) to 0.004 h^{-1} (mean lifetime of 10 days) would lower the average BC emission rate by approximately 15 %.

On the other hand, horizontal advection as parametrized by the estimated spatial decay constant, has much stronger influence on the calculation of BC emission rates. Since horizontal advection strongly depends on wind speed, the total decay constant (λ'_{BC}) also follows diurnal wind pattern with the highest values in the afternoon (Figure S5). When $ws \rightarrow 0$, the only process responsible for decrease of BC concentration is its temporal sink. With higher wind speed, concentration would decrease exponentially. Previous studies of BC source apportionment and distribution of BC apportioned to traffic and biomass burning sources, performed in the Ljubljana basin, have revealed a homogeneous distribution of BC_{BB}, while BC_{TR} showed a stronger dependence on the proximity of traffic sources (Ogrin et al., 2016). Therefore, γ_{BB} for the Ljubljana basin was selected based on the general area contributing to BC_{BB} concentrations and was set to 5×10^{-5} m^{-1} (Table 3) which corresponds to half-distance decay of approximately 14 km. On the other hand, a smaller contributing area was chosen for BC_{TR}, thus γ_{TR} was set to 7×10^{-5} m^{-1} (corresponding to 10 km half-distance decay). A comparison with the traffic density shows that the most suitable γ_{TR} for Ljubljana is found in the range from ~~5~~4 $\times 10^{-5}$ m^{-1} to ~~7~~9 $\times 10^{-5}$ m^{-1} (Figure S13~~9~~ b). Overestimating horizontal advection (an overestimation of the γ value) would result in an overestimation of E_{TR} (and E_{BB}), which would be especially pronounced during the periods of stronger wind speed, thus in the afternoon, which would result in an altered E_{TR} diurnal pattern. Results of sensitivity analyses of modelled E_{TR} for different γ_{TR} values, which was performed based on comparison with measured traffic density at representative location close to BC measurement site in Ljubljana, is presented in the Supplement (Section ~~6~~5).

Vipava valley is geographically constrained to smaller area, with small urban centre, widespread distribution of individual houses and highway running along the valley. Considering these characteristics, γ_{BB} and γ_{TR} were both set to 10^{-4} m^{-1} (7 km half-distance decay).

3. Results

3.1 Radon concentration and meteorological conditions

Average radon activity concentration derived from hourly measurements (Figure 2) was similar at both measurement locations, 15 ± 11 Bq m^{-3} and 14 ± 10 Bq m^{-3}, ~~measured~~ in winter and 13 ± 9 Bq m^{-3} and 12 ± 8 Bq m^{-3} in spring, in Ljubljana and Vipava valley, respectively~~. Slightly lower average C_{Rn} was characteristic for spring: 13 ± 9 Bq m^{-3} and 12 ± 8 Bq m^{-3}, respectively for both locations~~ (Table 4). These values are above annual average outdoor radon concentration of 10 Bq m^{-3} reported by UNSCEAR (2000) for the continental areas. Due to limited atmospheric mixing, higher winter concentrations are usually observed. However, decrease of atmospheric C_{Rn} by more efficient atmospheric mixing is compensated by increased radon exhalation rate in the warmer season. ~~, which complies with the seasonal variation, which usually results in higher winter concentrations due to limited atmospheric mixing~~.

Apart from the changes in radon exhalation rate from the ground, time evolution of C_{Rn} is mainly affected by atmospheric dispersion characteristics. Periods of mechanically driven mixing within the PBL, with stronger wind speeds, and periods of prevailing thermally driven mixing can be distinguished especially during winter months, which results in irregular diurnal time evolution. Typical diurnal variation is more pronounced in spring, when thermally driven atmospheric mixing prevails. Due to the limitations of the box model, this study is limited to the cases with thermally driven convective boundary layer. With this regard only days with average daily wind speeds below the 80th percentile of all values were considered and addressed further on as "normal" wind conditions. Local wind conditions are further presented in the Supplement (Section 3, Figure S4 and Figure S5). Diurnal variation of C_{Rn} in thermally driven convective mixing, presented in Figure 3, reflects daily evolution of the PBL with the lowest C_{Rn} in the middle of the day, when PBL is fully mixed. The lowest values of C_{Rn} are on average around 5 Bq m^{-3}. C_{Rn} starts to increase with the afternoon transition to the stable boundary layer and reaches highest values in the early morning. The amplitude of diurnal variation is controlled by PBL stability and duration of SNBL, resulting in the highest morning peak values in winter months, when NSBL regime lasts longer.

3.2 Black carbon concentration, diurnal and seasonal cycle

Clear seasonality of BC concentrations was observed at both urban background sites. Higher concentrations were measured in the colder season (Figure 4), resulting from weaker dispersion characteristics within the more stable PBL, as well as from stronger biomass burning sources. ~~Despite significantly higher population density in LJ, BC concentrations are only about 25 % higher in LJ than in AJ.~~

The average BC concentration in winter was 4.5 ± 5.7 and 3.4 ± 4.2 μg m^{-3} for LJ and AJ, respectively (Table 4). However, a significant micrometeorological difference between both locations has to be considered. Vipava valley is characterised by two extremes in atmospheric stability: very stable atmospheric conditions with strong pollution events can shift within few hours to the strong bora wind conditions, which disperse all atmospheric pollutants to the nearly regional background levels. In fact, during stable PBL conditions in winter, BC concentration in AJ can easily exceed concentrations in LJ, reaching average daily BC concentration of 10 – 15 μg m^{-3}. Based on the source apportionment model described in Section 2.2, there was a significantly higher contribution of biomass burning observed during winter in AJ (62 %) than in LJ (31 %), corresponding to the rural characteristics of Vipava valley area. Significantly lower BC concentrations were measured in spring, 1.5 ± 1.6 μg m^{-3} and 1.1 ± 1.2 μg m^{-3} in LJ and AJ, respectively.

BC concentrations at both hill sites were expectedly lower than that at the urban background sites. Golovec site (GOL), which is located 100 m above the city of Ljubljana is nevertheless more affected by urban emissions than Otlica site (OT), which lies about 830 m above the valley floor. BC concentrations measured at GOL were 2.2 ± 2.0, 1.1 ± 1.0 and 0.8 ± 0.5 μg m^{-3} in winter, spring and summer, respectively, which is 51 %, 42 % and 38 % lower than in the city. This indicates more intensive vertical dispersion of air pollutants (including BC) towards warmer season. Nevertheless, since vertical difference between ARSO and GOL site is only 100 m, the GOL site remains above the ML only during very stable PBL conditions.

On the other hand, the vertical difference between the AJ and OT sites in Vipava valley is much larger, resulting in significantly lower BC concentrations on the hill. BC concentrations measured at OT during autumn, winter and spring season were similar, 0.4 ± 0.5, 0.6 ± 0.8 and 0.4 ± 0.4 μg m^{-3}, respectively. Slightly higher winter concentrations can be assigned to small local contribution from a few houses which are spread on the slope around the observatory and small natural grass fire nearby the observatory on December 18, 2016, which increased BC concentrations to around 30 μg m^{-3} for several hours (Figure 4). The OT site is located above PBL most of the time during winter and therefore represents regional background BC concentrations. Towards spring, when MLH frequently reaches the OT site in the afternoon, the site is affected by polluted air masses from the valley (Figure 8c) and BC concentrations increase. The OT site can lie during the night and morning hours in either the residual layer - in the case when MLH reached the OT site in the previous afternoon; or in free atmosphere - in the case when MLH remained below OT altitude in the previous day.

BC diurnal variation presented in Figure 5 reflects different dynamics of sources and their relative contribution. In general, the main driver of BC concentrations at both sites is atmospheric stability, leading to dispersion of pollutants during the day, and subsequently lower BC concentration in the middle of day, and thus lower exposure of the population, except in the case of stable PBL conditions. Besides that, two peaks are usually observed in traffic related BC concentration (BC_{TR}), which is a combined consequence of traffic density and PBL stability. Morning traffic related peak of BC_{TR} concentration is usually stronger at both locations, since dispersion of BC in the morning hours is limited due to low MLH. Due to higher traffic density and consequently stronger BC sources in LJ, it usually takes more time for BC to decrease during the day than in AJ. The afternoon peak, on the other hand, strongly depends on daylight hours (which in general drives the PBL evolution). In winter, BC concentrations start to increase already between 16:00 and 17:00, whereas in spring and summer, much smaller increase can be observed, which is constrained to evening hours. Biomass burning BC sources are mostly limited to the colder season, when higher concentrations are measured especially in the evenings and first part of night. In contrast to LJ, AJ is affected by

increased BC_{BB} concentration also during the morning hours. During the weekends, lower BC_{TR} concentrations are observed in LJ, whereas no significant difference can be seen in AJ, leading to the assumption that meteorology plays much stronger role in Vipava valley than it does in Ljubljana (where BC sources are stronger) or it could be assumed that highway along the valley represents continuous source of BC, regardless of the week day.

3.3 Effective mixing height derived from box model

Hourly resolved MLH values were calculated based on Eq. ~~9~~6, ~~11~~ 8 and ~~12~~ 9 for the whole period, when C_{Rn} measurements were available. Although MLH results represent an intermediate model outcome and are actually not required for emission rate modelling, the results are important for understanding diurnal characteristics of PBL evolution and extent of pollutant dispersion, which allow us to compare the two locations from the point of view of micro-meteorological characteristics. They also serve as a quality control parameter of the model. Derived MLH for both locations, calculated from the specifically selected monthly values of effective radon exhalation rate (Section 2.5) are presented on Figure 6. SNBL height was in general between 100 and 200 m a.g.l. at both locations and was found to slightly increase from cold to warm season. However, the seasonal pattern of SNBL height is not as pronounced as the seasonal pattern for the thermally driven daytime MLH. In February PBL reached its highest altitude at around 15:00, with the median MLH value for LJ of 450 m. On the contrary, in June MLH reached its highest extent of ~~1550~~ 1210 m (median) at 17:00. In conditions of extremely unstable boundary layer, the maximum observed MLH extended higher than 2~~5~~000 m at both locations. The influence of MLH on BC concentration measured at the urban background site (ARSO) and on the hill (GOL) is presented on Figure 7 for selected days, when derived MLH was validated from vertical profiles of BC concentration measured by plane. The highest BC concentrations at ARSO and the highest difference between ARSO and GOL is observed during periods when MLH extends below the altitude of the hill site, 100 m a.g.l. (Figure 7a).

The ~~strongest PBL stability~~most stable PBL conditions (excluding periods of Bora wind) in the Vipava valley ~~was~~ were observed in December 2016 and February 2017, when no significant diurnal variation could be detected. During these two months median MLH values at 15:00 were 2~~4~~3~~0~~ m and ~~270~~ 330 m, respectively. The highest vertical extent of PBL was observed in April, when MLH reached ~~1340~~ 1400 m (median) at 16:00. Results of MLH values also explain the measured BC concentration in AJ and OT (Section 3.2), where comparison of BC concentration reveals the time periods, when both sites are located within the same air volume (i.e. periods when MLH overreaches OT site at 830 m a.g.l.). Especially in April and May, MLH reaches OT site in the afternoon frequently (from noon to 16:00), leading to increase of BC concentrations at OT and decrease of BC concentrations at AJ site (Figure 8 b and c). Good correlation was observed between MLH (derived from the box model) and vertically resolved lidar backscatter signal over Vipava valley in periods when conditions are met for the application of both approaches. Figure 8a represents measurements from January 9, 2017.

Results show that PBL reaches its full depth in the early afternoon, between 15:00 and 17:00, depending on the extent of daylight hours. Strong thermally driven mixing starts to diminish about 2 hours before sunset, followed by rapid transition to the SNBL conditions (Figure 6).

3.4 Black carbon emission rates

BC emission rates were determined in the second phase by inversion of BC concentrations based on the results of derived MLH values using Eq. ~~13~~ 11 and ~~14~~12. Emission rates from traffic (E_{TR}) and biomass burning (E_{BB}) sources were determined separately in order to take into account spatial characteristics and different dynamics of sources. Average daily BC emission rates in different seasons for both locations are presented in Table 5. As expected, higher BC emissions are characteristic for Ljubljana, where overall BC emission rates ranged from ~~280~~ 210 to ~~300~~ 260 $\mu g\ m^{-2}h^{-1}$ in spring and winter, respectively. ~~On~~

~~the other hand, 25%~~ Lower~~lower~~ overall BC emissions were found in Vipava valley and were in the range from ~~210~~ 150 to ~~240~~ 250 μg $m^{-2}h^{-1}$ in spring and winter, respectively. Emissions from traffic prevail~~s~~ in the city of Ljubljana ~~city~~ and account for ~~80~~ 73 % in winter time. On the other hand, biomass burning in individual houses contribute more than half (~~58~~ 60 %) of the emitted BC in Vipava valley during the heating season. In spring, however, outdoor temperature increases faster in the Mediterranean climate of Vipava valley than i~~t~~n does in Ljubljana, which means that heating season end~~s~~ much sooner in spring, resulting in only 27 % contribution of biomass burning emissions in the Vipava valley and 14 % contribution in Ljubljana~~. Similar biomass burning emission rates are thus characteristic for spring in Vipava valley and Ljubljana.~~ The fraction of source specific emission rates slightly differs from the contribution fraction of actually measured BC concentrations from both sources (Table 4) after mixing and dispersion within the PBL. Due to difference in daily dynamics of emission rate from biomass burning and traffic, the fraction of BC concentration from biomass burning is slightly higher than the fraction of its emission rate. Traffic emissions are occurring mostly during the daytime and are dispersed in the PBL more effectively than biomass burning emissions, with the sources active also during the night hours, thus having stronger impact on the concentrations. Average determined BC emission rates are about ~~two~~ an order~~s~~ of magnitude higher than Slovenian national BC emissions of 2.2 kilotons reported by the EMEP (The European Monitoring and Evaluation Programme) emission inventory for 2016, which corresponds to the average hourly emission rate of 12.4 μg $m^{-2}h^{-1}$. Difference is reasonable if we account for spatially heterogeneous emissions and the small contribution of less populated areas like forests and mountains. BC emission rates calculated in our study are nevertheless lower than reported for larger cities, as Kathmandu, where 316 μg $m^{-2}h^{-1}$ and 914 μg $m^{-2}h^{-1}$ were reported for summer and winter period, respectively, or Delhi (608 μg $m^{-2}h^{-1}$) and Mumbai (2160 μg $m^{-2}h^{-1}$) (Mues et al., 2017).

Daily average E_{TR} remains constant through the year and in general does not depend on outdoor temperature (Figure 9). ~~Slight increase of E_{TR} towards warmer days is observed in Vipava valley, which is probably a combination of several sources of uncertainty rising at the first place from the BC source apportionment model and uncertainties in the selection of radon exhalation rate combined with its daily changes, which are not accounted for in the model. Even a small difference in the BC source apportionment can lead to underestimation of E_{TR} and simultaneous overestimation of E_{BB} in winter.~~ As expected, E_{BB} is higher in colder days due to the stronger heating demand. Since wood is the most frequently used fuel for heating in individual houses in the Vipava valley, emission rate increases much faster with colder days than it does in Ljubljana, where parts of the city dominated by individual houses are connected to the district heating system powered by the local thermal power plant. At both locations, higher E_{BB} is observed when average daily temperature drops below 15 °C.

3.4.1 Hourly resolved source specific BC emission rate

Typical diurnal profile of E_{TR} averaged over the whole measurement period reflects the traffic dynamics in the city of Ljubljana and in much smaller town – Ajdovščina in the Vipava valley (Figure 10). Statistical summary of source apportioned E_{BC} is presented in Table 5. ~~To account for higher model uncertainty during the mid-afternoon, daily averages were calculated by applying 50 % weight to the E_{BC} results between 11:00 and 17:00.~~

Minimum BC emissions are observed during the night hours, between midnight and 4:00 in LJ and between 2~~3~~:00 and 4:00 in AJ. Traffic and consequently E_{TR} start to increase in the morning around 5:00 and peak during working days between 6~~7~~:00 and 8:00 with E_{TR} in LJ of 240 ± 110~~280~~ μg $m^{-2}h^{-1}$, 210 ± 160 μg $m^{-2}h^{-1}$ and ~~250~~ 200 ± 240 μg $m^{-2}h^{-1}$ (~~median values~~weighted mean) in winter, spring and summer, respectively~~in LJ~~ (Table 5). Morning peak E_{TR} during working days was similar in AJ as in LJ~~and AJ~~: 220 ± 110 μg $m^{-2}h^{-1}$, 260 ± 130 μg $m^{-2}h^{-1}$, and 170 ± 90 μg $m^{-2}h^{-1}$ in autumn, winter and spring, ~~,~~respectively. Slightly lower morning E_{TR} in warmer months at both locations is probably the result of transportation changes when warmer weather facilitates environmentally friendly mobility. ~~-~~Morning peak is not observed during Sundays, when E_{TR} during this period reaches significantly lower values: 30 ± 20 μg $m^{-2}h^{-1}$ and 60 ± 20 μg $m^{-2}h^{-1}$ in LJ in winter

and spring, respectively. Sunday morning E_{TR} in AJ~~and~~ was 90 ±20 μg $m^{-2}h^{-1}$ and ~~110~~ 70 ± 30 μg $m^{-2}h^{-1}$ in winter and spring, respectively. ~~LJ and AJ, respectively~~. The morning peak is followed by a slight decrease of E_{TR} in LJ, whereas in AJ, E_{TR} drops substantially. E_{TR} starts to increase again in the late morning and accelerates in the early afternoon ~~at around 13:00~~, peaking in the mid-afternoon (15:00 – 16:00). During this period the calculated BC emission rates are the most uncertain due to the reasons explained in detail in the Section 3.5. During the working days, maximum E_{TR} ~~was observed~~ during the afternoon traffic peak ~~(, which is~~ between 15:00 and 16:00~~)~~ was ~500 ~~(median E_{TR} of 530~~ μg $m^{-2}h^{-1}$~~)~~ in LJ and ~350 μg $m^{-2}h^{-1}$ in AJ~~, and between 15:00 and 17:00 in AJ (median E_{TR} of 410 μg $m^{-2}h^{-1}$)~~. These results are comparable to results published by Ježek et al. (2018) for traffic BC emissions in Maribor (the second largest Slovenian city), where E_{TR} during the afternoon peak in the range of 300 – 1300 μg $m^{-2}h^{-1}$ is reported for 500 m × 500 m grid cells. In the evening hours E_{TR} decreases faster in AJ than in LJ. Since traffic BC emissions continue also after PBL shifts to the NSBL conditions, which is especially true during winter in LJ, this leads to stronger evening peak of BC_{TR} concentration in LJ as compared to AJ. Sunday E_{TR} was found to increase from the morning towards the evening ~~be higher in the afternoon, from 15:00 to 21:00 in Ljubljana (up to 340 μg $m^{-2}h^{-1}$) and from 16:00 to 18:00 in Ajdovščina (up to 240 μg $m^{-2}h^{-1}$),~~ when similar E_{TR} was observed. ~~but it was nevertheless lower than during the working days.~~ The emission rates are correlated with the traffic density in Ljubljana (Figure 12~~) (Figure S8)~~, especially in the time period from midnight to 10:00, when the uncertainty of the model is expected to be the lowest.

Biomass burning BC emission rates (E_{BB}), on the other hand, show weaker diurnal dynamics than traffic BC emission rates (Figure 11). Although seasonal variation of E_{BB} is more pronounced, diurnal pattern in LJ shows slightly higher emission rates in the afternoon and evening hours. However, high uncertainty of the mid-afternoon results may be the reason for increased E_{BB} in the mid-afternoon. , with average winter ~~hourly median~~ E_{BB} increasing from ~~10~~ 60 ±70 μg $m^{-2}h^{-1}$ ~~at 4:00~~in the morning to ~~10~~90 ± 45 μg $m^{-2}h^{-1}$ between ~~15~~18:00 and ~~19~~20:00 (working days). In AJ, an additional morning increase is present in winter between ~~6~~7:00 and 8:00, with E_{BB} of ~~150~~ 200 ± 160 μg $m^{-2}h^{-1}$ (working days) followed by stronger afternoon peak of ~~420~~ 900 ±1200 μg $m^{-2}h^{-1}$ ~~at~~ between 16:00 and 17:00. ~~Although there were only 8 suitable days for model application in autumn, results show a similar diurnal pattern as in winter months.~~ In spring, ~~a~~ similar average daily ~~afternoon~~ E_{BB} was obtained in LJ (30 ± 20 ~~60~~ μg $m^{-2}h^{-1}$) and AJ (40 ± 30~~70~~ μg $m^{-2}h^{-1}$).

Traffic was found to be the main source of BC emissions in Ljubljana, where biomass burning represents 27 % of all BC emissions in winter. On the other hand, biomass burning exceeds traffic BC emissions in the Vipava valley, with 60 % contribution in the winter months.

~~It has to be pointed out, however, that higher uncertainty is expected for emission rate values in the afternoon hours, as discussed in Section 2.6.1. Horizontal advection, which is accounted for by introducing spatial decay constants to the box model, can lead to overestimation of the emission rate in the presence of stronger wind conditions. Another contribution to the uncertainty arises from Rn measurements, which especially in strongly unstable PBL, reach the instrumental lower detection limit in the early afternoon. This can lead to underestimation of MLH and consequently also underestimation of derived BC emission rate. The comparison of the E_{TR} and the traffic density in LJ shows the presence of the higher model uncertainty in the afternoon (Figure S8).~~

~~Negative hourly E_{BC} values result from BC distribution, from temporal and spatial point of view, which does not comply with the expected background evolution of BC concentration. Thus, the local BC concentration peak, measured at the urban background site, would result in a high calculated emission rate, followed by negative calculation of the emission rate. The frequency of negative values also agrees with the time period when sources are active. Higher noise is thus obtained during unstable atmospheric conditions in the presence of local BC concentration peaks. The traffic BC emission rate thus results in more noisy results than biomass burning BC emissions. Higher noise is also observed for the Vipava valley emission rate calculation, induced by stronger wind and non homogeneous distribution of biomass burning sources. Negative values were treated as valid model results, since averaging results in a more realistic estimation of the emission rate.~~

3.5 Uncertainty estimation

The uncertainty of the box model depends on different parameters and processes:

a) The results of MLH determined by the box model strongly depend on the correct ***estimation of the radon exhalation rate***. A biased effective E_{Rn} estimate would bias results of the E_{BC} in positive or negative way. Due to seasonal changes of the E_{Rn}, it has to be evaluated for each season/month separately. Since continuous monitoring of E_{Rn} is usually not available, the box model has to be calibrated to any available information on the MLH in order to get the E_{Rn}, scaled for the measurement height. In this regard it has to be pointed out that additional measurements, which can be used to determine the MLH for limited time periods, are necessary to lower the uncertainty of the E_{Rn} estimate. The uncertainty of the E_{Rn} was estimated to be 50 Bq $m^{-2}h^{-1}$ (~20 % of the mean E_{Rn} estimate for the area under investigation). To account for this, the model was evaluated for upper and lower E_{Rn} estimates which were selected 100 Bq $m^{-2}h^{-1}$ apart (Table 2).

b) Uncertain levels of the ***Rn concentration in the residual layer*** and approximation of its vertical gradient can influence the modelled daily evolution of MLH, especially towards the mid-afternoon, when the denominator in the Eq. 11 and 12 limits towards zero, making the box-model highly uncertain. The uncertainty of the Rn concentration in the residual layer is estimated to be ~50 %. However, the uncertainty of the MLH results increases with decreasing radon concentration in the mixing layer, when the resulting difference of Rn concentration between mixing and residual layer approaches zero. This uncertainty reflects in the worst-case scenario of 50 – 75 % uncertainty of the MLH calculation in the mid-afternoon of convective days. On the other hand, the residual layer Rn concentration does not influence the MLH estimates in the SNBL conditions.

c) As discussed in Section 2.6.1., ***horizontal advection***, which is accounted for by introducing spatial decay constants to the box model, can lead to an overestimation of the E_{BC}, when advection prevails over the convective mixing. This effect is again present mostly during the mid-afternoon and adds to the uncertainty of emission rates estimation. The uncertainty of BC spatial decay constant is estimated ~30 %, where a 30 % increase in the spatial decay constant results in a 30 % increase in BC emission rates at mid-afternoon in the case of Ljubljana (on average).

d) Another contribution to the uncertainty arises from Rn measurements, when radon concentration, especially in the convective PBL, reaches the ***instrumental lower detection limit*** in the early afternoon. This can lead to underestimation of the MLH and consequently also underestimation of derived BC emission rate.

Uncertainty contributions described above, lead to the conclusion, that the highest uncertainty of emission rates estimate can be expected in the mid-afternoon period during the convective days, when the overall uncertainty can reach 100 %. On the other hand, the model uncertainty is the lowest in stable atmospheric conditions, when the main sources of uncertainty come from points a) and b), resulting in ~30 % uncertainty of the BC emission rate estimates. The comparison of the traffic related emission rate E_{TR} and the traffic density in LJ shows the presence of the higher model uncertainty (overestimated emissions) in the mid-afternoon (Figure S12).

Negative hourly E_{BC} values result from the BC distribution, from temporal and spatial point of view, not complying with the expected background evolution of BC concentration. Thus, the local BC concentration peak, measured at the urban background site, would result in a high calculated emission rate, followed by a negative calculation of the emission rate. This effect (positive-negative spike due to local BC concentration peak) is usually observed in the time period when sources are active. Higher noise is thus obtained during unstable

atmospheric conditions in the presence of local BC concentration peaks. The traffic BC emission rate results in more noisy results than biomass burning BC emissions. Higher noise is also observed for the Vipava valley emission rate calculation, induced by non-homogeneous distribution of biomass burning sources. Negative values were treated as valid model results, since averaging removes these oscillations and results in a more realistic estimation of the emission rate.

Due to different BC sampling height at LJ and AJ location – 4 and 12 meters, respectively, some uncertainty of BC emission rates can be expected during the NSBL conditions, since stratification of SNBL can play a role in measured black carbon concentration. This is important especially when comparing traffic and biomass burning BC sources, since their emissions have different characteristics. BC_{TR} is emitted from the sources at the ground surface, whereas biomass burning sources are usually several meters higher, at the height of the chimneys. Due to dispersion and dilution processes, the concentration gradient flattens with time. Thus, in the case of traffic related BC with higher intensity during the day, there would be enough time for the dispersion of BC_{TR} before stratification of SNBL. However, the morning emissions before the break of SNBL could be slightly underestimated in AJ, where sampling was performed at 12 m above ground. On the other hand, biomass burning BC is emitted higher above ground. For the Ljubljana basin it was shown that BC_{BB} is homogeneously distributed within the city (Ogrin et al., 2016). At AJ location, with numerous biomass burning sources over smaller area, the concentration profile could be more significant, especially in stable atmospheric conditions, which could lead to increased BC_{BB} measured for the same level of emissions. This could in turn cause slight overestimation of E_{BB} in the afternoon – early evening, before the emission plume is dispersed. However, a rough estimate of the emission inventory leads us to believe that biomass-burning is ubiquitous in AJ, not leading to significant emission gradients in the urban area.

Overall, the box model results are more reliable in stable atmospheric conditions, especially during the morning hours, after the break of stratified SNBL and before mid-afternoon advection prevails the convective mixing. To account for the uncertainty, the mid-afternoon MLH estimates were excluded from the E_{Rn} calibration procedure and weighted averaging was used to determine daily average of BC emission rates. Measurements of pollutant concentration should be conducted at background sites, to allow for their homogeneous dispersion, resulting in lower noise of the calculated emission rates.

~~1.~~

4. Conclusions

We present a method for the determination of the source specific black carbon emission rates and apply it to measurements in two different environments: an urban location in Ljubljana and a rural one in the Vipava valley (Slovenia, Europe), which differ also in their natural characteristics (geology, geomorphology, meteorology). The influence of atmospheric dynamics was quantified based on atmospheric Rn concentration and monthly resolved E_{Rn}, allowing for 1-hour time resolution MLH determination for periods of thermally driven PBL evolution. Intensity of BC sources – BC emission rate – was determined by taking into account horizontal advection term, simplified by temporal and spatial exponential decay. Whereas the choice of temporal decay constant introduces only small offset in determined BC emission rates, the spatial decay constant was shown to influence the daily pattern of calculated BC emission rates significantly. Different spatial decay rate was introduced for traffic and biomass burning emission sources depending on the area under consideration and spatial distribution of both sources. Therefore γ_{BB} for the Ljubljana basin was set to 5×10^{-5} m^{-1} which corresponds to half-distance decay of approximately 14 km. On the other hand, a smaller contributing area was chosen for BC_{TR}, with γ_{TR} set to 7×10^{-5} m^{-1} (corresponding to 10 km half-distance decay). Distribution of sources within the Vipava valley indicates smaller contribution area, with γ_{BB} and γ_{TR} set to 10^{-4} m^{-1} (7 km half-distance decay).

The rural characteristics of Vipava valley area reflect in significantly higher BC contribution from biomass burning during winter in AJ (~~62~~ 60 %) in comparison to LJ (~~31~~ 27 %). The average BC concentration in winter was 4.5 ± 5.7 and 3.4 ± 4.2 μg m^{-3} for LJ and AJ, respectively. However, during stable PBL conditions in winter, BC concentration in AJ can easily exceed concentrations in LJ, reaching average daily BC concentration of 10 – 15 μg m^{-3}. BC concentrations decrease in warmer months.

Results show the overall BC emission rates in Ljubljana in the range from ~~280~~ 210 to ~~300~~ 260 μg $m^{-2}h^{-1}$ in spring and winter, respectively. By accounting for the uncertainty introduced by estimation of radon exhalation rate, the range may be extended to 190 – 250 μg $m^{-2}h^{-1}$ and 210 – 300 μg $m^{-2}h^{-1}$ in spring and winter, respectively. ~~Only 25% lower overall~~ BC emissions ~~were found~~ in the Vipava valley were lower in spring: ~~and were in the range from 210~~150 (120 – 160) μg $m^{-2}h^{-1}$, but in the same range in winter: ~~to 240~~ 250 (200 – 300) μg $m^{-2}h^{-1}$. ~~in spring and winter, respectively~~. This shows that the emission rates are not necessarily related to the population density and sparsely populated areas do feature high black carbon emission rates. As expected, BC emissions from traffic prevails in Ljubljana city and account for ~~80~~ 73 % in wintertime. On the other hand, biomass burning in individual houses contribute more than half (~~58~~ 60 %) of the emitted BC in Vipava valley during the heating season. Due to the difference in respective daily dynamics of emission rates from biomass burning and traffic, the fraction of BC concentration from biomass burning is slightly higher than the fraction of its emission rate. Traffic emissions are occurring mostly during the daytime and are dispersed in the PBL more effectively than biomass burning emissions, with the sources active also during the night hours, thus having a stronger impact on the concentrations. Although BC concentrations from both sources decrease towards warmer months, traffic related emission rates remain constant year-round, whereas biomass burning emission rates strongly depend on the outside temperature, which drives the heating demand.

Different diurnal pattern of E_{TR} was revealed for both measurement locations, reflecting traffic dynamics characteristic for Ljubljana and Vipava valley. ~~Besides a~~A narrow peak in E_{TR} in the morning (LJ: ~~280~~ 170 – 250 μg $m^{-2}h^{-1}$ and AJ: ~~250~~ 130 – 190 μg $m^{-2}h^{-1}$) was observed at both locations. Traffic related emissions remained elevated through the whole day in Ljubljana, whereas emissions decreased substantially in the Vipava valley in the late morning hours. Mid-afternoon estimated emissions are higher, but also subjected to high uncertainties~~the highest E_{TR} was observed during the afternoon traffic peak, which is between 15:00 and 16:00 (median E_{TR} of 530 μg $m^{-2}h^{-1}$) in LJ, and between 15:00 and 17:00 in AJ (median E_{TR} of 410 μg $m^{-2}h^{-1}$)~~. Biomass burning BC emission rates, on the other hand, show weaker diurnal dynamics than traffic BC emission rates. In Ljubljana, E_{BB} slowly increases from the early morning ~~(10 μg $m^{-2}h^{-1}$)~~ to the afternoon. ~~(100 μg $m^{-2}h^{-1}$).~~ More pronounced daily dynamics of E_{BB} was observed in Vipava valley in winter, when ~~with~~ increase of ~~E~~$_{BB}$ biomass burning emissions was observed in the morning and in the afternoon~~of 150 μg $m^{-2}h^{-1}$ between 7:00 and 8:00, followed by stronger afternoon peak of 420 μg $m^{-2}h^{-1}$ at 16:00~~.

Coupling of highly time-resolved measurements of primary, inert air pollutant, such as BC, with atmospheric radon concentration measurements provides a useful tool for direct, high time resolution measurements of intensity of emission sources. This information is essential for short-term forecast of air pollution episodes, as well as for the evaluation of the efficiency of air ~~quality~~ pollution abatement measures.

Although a set of criteria has to be fulfilled to keep the level of uncertainty in the reasonable range, the presented approach may be applicable also in the complex terrain, under the condition of relatively constant radon source term.

Figures

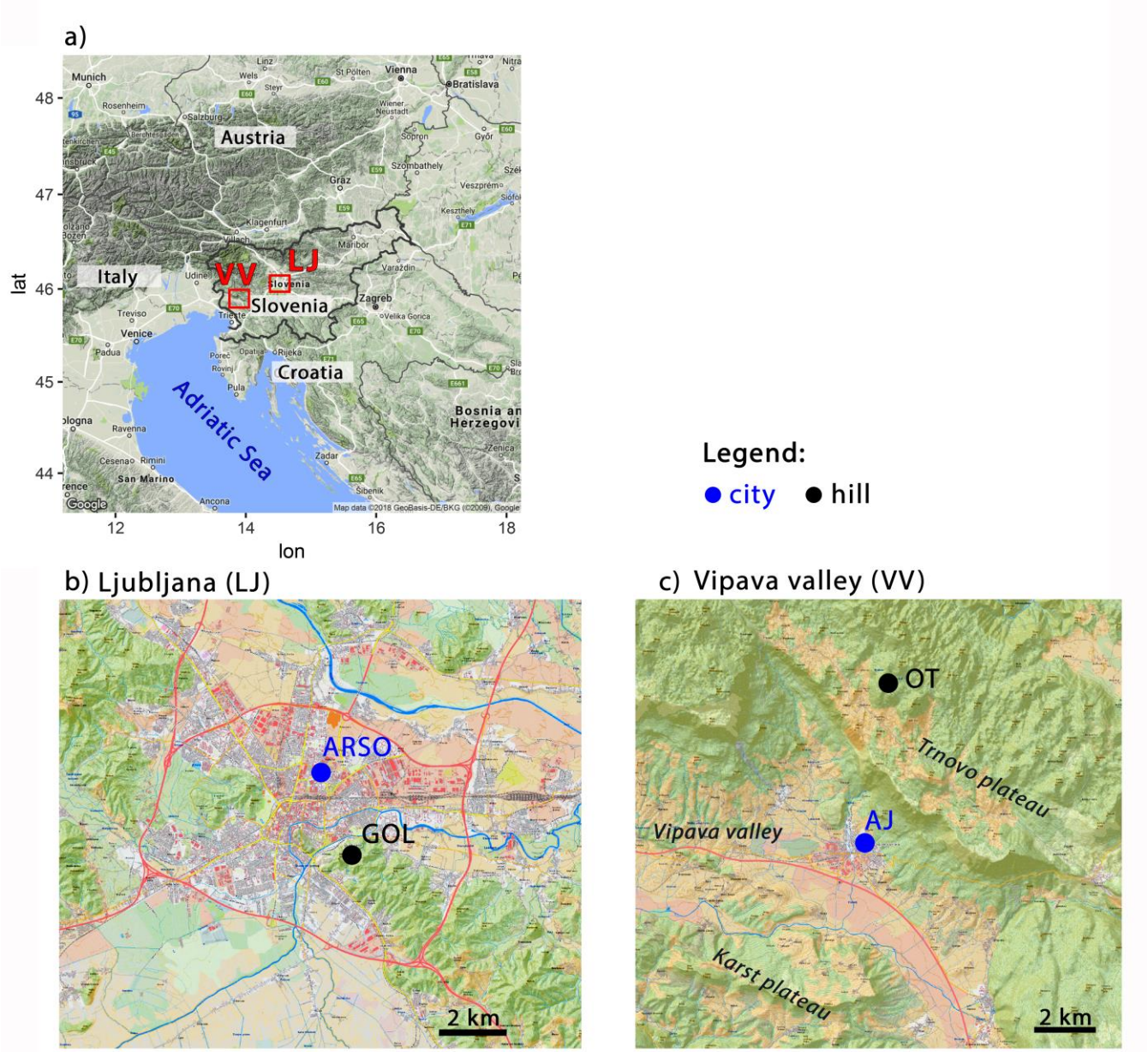

Figure 2: Map of Slovenia (a) with marked areas of measurement sites Ljubljana (LJ) and Vipava valley (VV). b) ~~area~~ The city of Ljubljana with urban background (ARSO) and hill (Golovec – GOL) measurement sites. c) Area of the Vipava valley with urban background (Ajdovščina – AJ) and hill (Otlica – OT) measurement sites (Source: Map data ©2018 GeoBasis-DE/BKG (©2009) Google and OpenStreetMap)

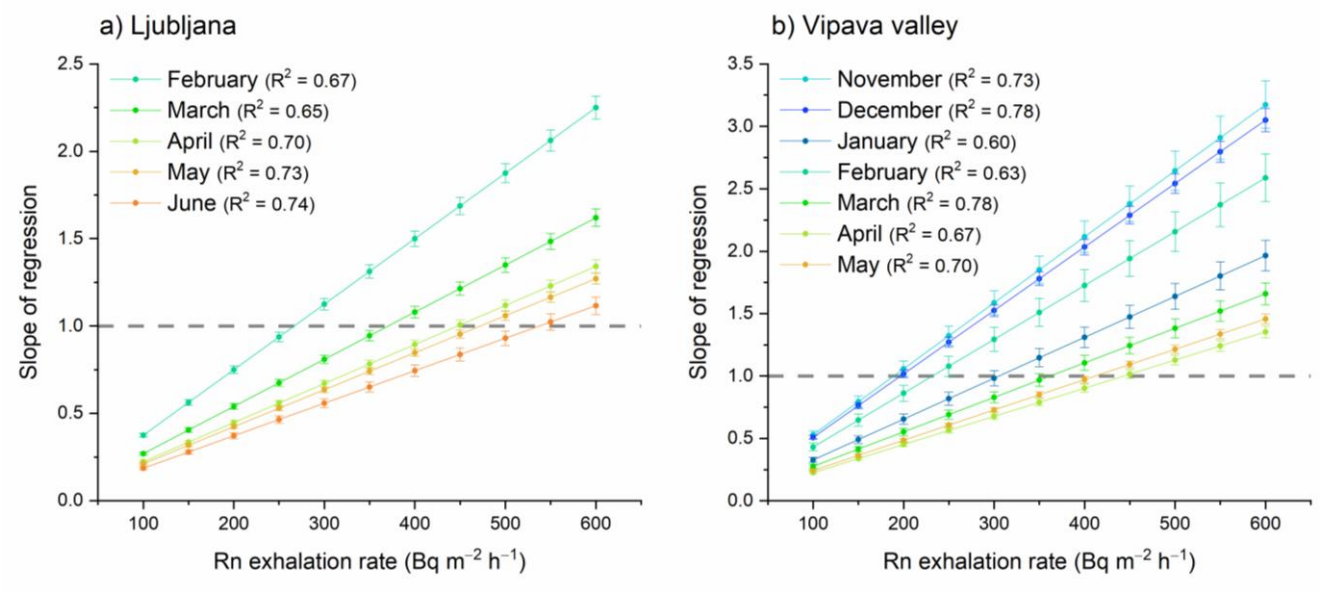

~~**Figure 2: Dependence of the slope of linear regression between calculated MLH from Rn measurements and GDAS data, on Rn exhalation rate for Ljubljana (a) and Vipava valley (b). This is used to determine the Rn exhalation rate at unity slope.**~~

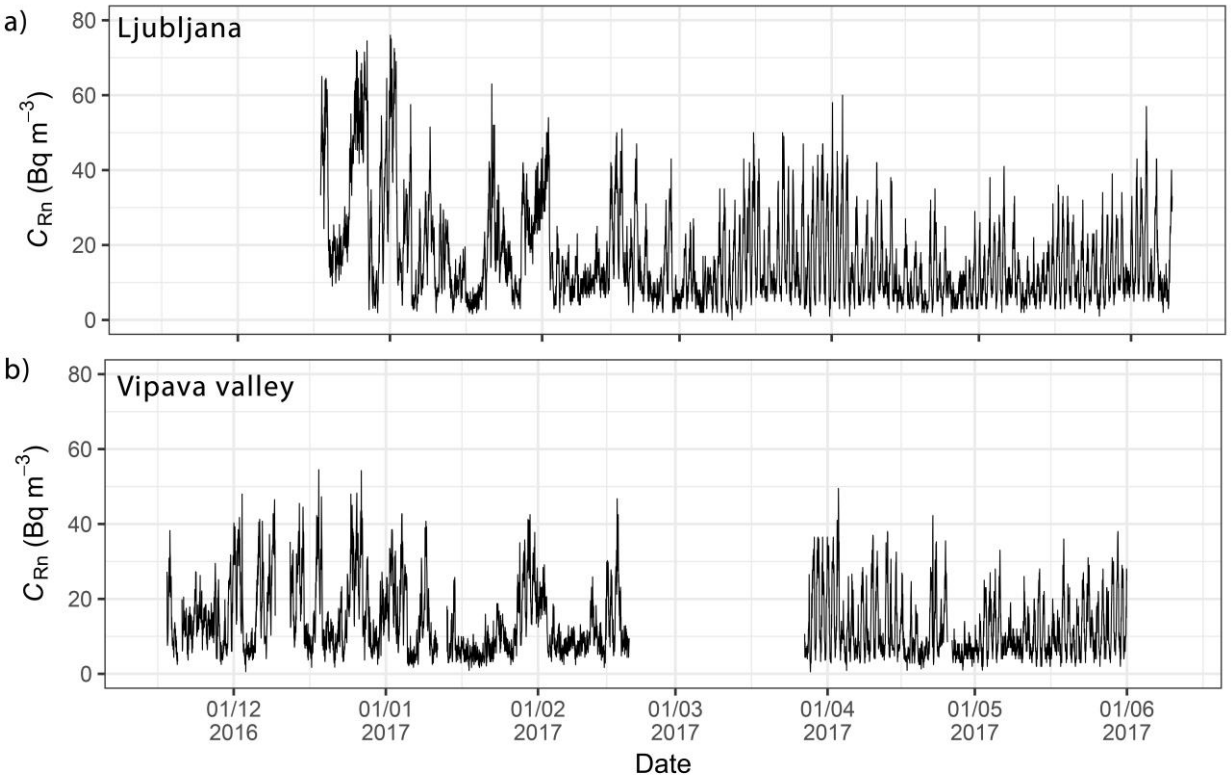

Figure 3: Time series of radon activity concentration (C_{Rn}) measured in Ljubljana and (a) and in Ajdovščina (at the floor of Vipava valley).

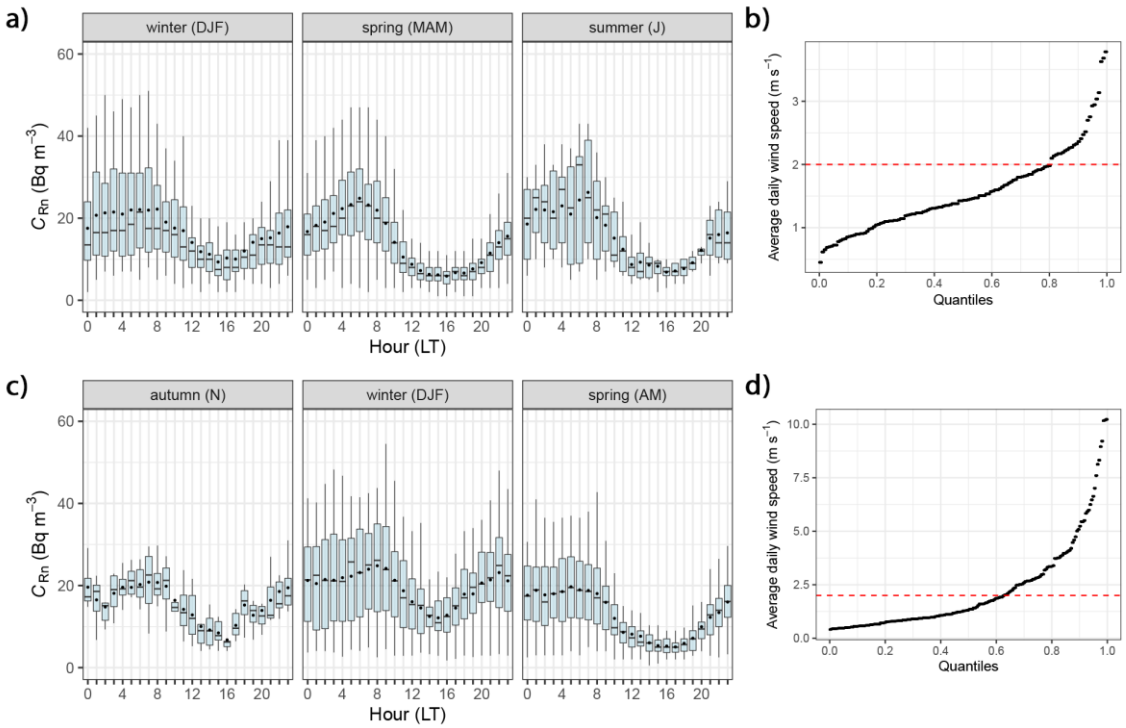

Figure 4: Diurnal variation (local time: CET/CEST) of radon concentration (C_{Rn}) in Ljubljana (a) and Vipava valley (c), grouped by season for the whole period of Rn measurements. Statistics for every hour in a day are represented by a box plot derived from 1-hour data (point: mean, horizontal line: median, grey-coloured box: 25th – 75th percentile, whiskers: 5th – 95th percentile). Only days during which daily average wind speed is below 2 m s^{-1} ~~the 80th percentile of all data (2 m s^{-1} and 2.7 m s^{-1} for Ljubljana and Vipava valley, respectively)~~ are considered. Distribution of wind speed for Ljubljana and Vipava valley is presented~~, as shown~~ on plots b) and d).

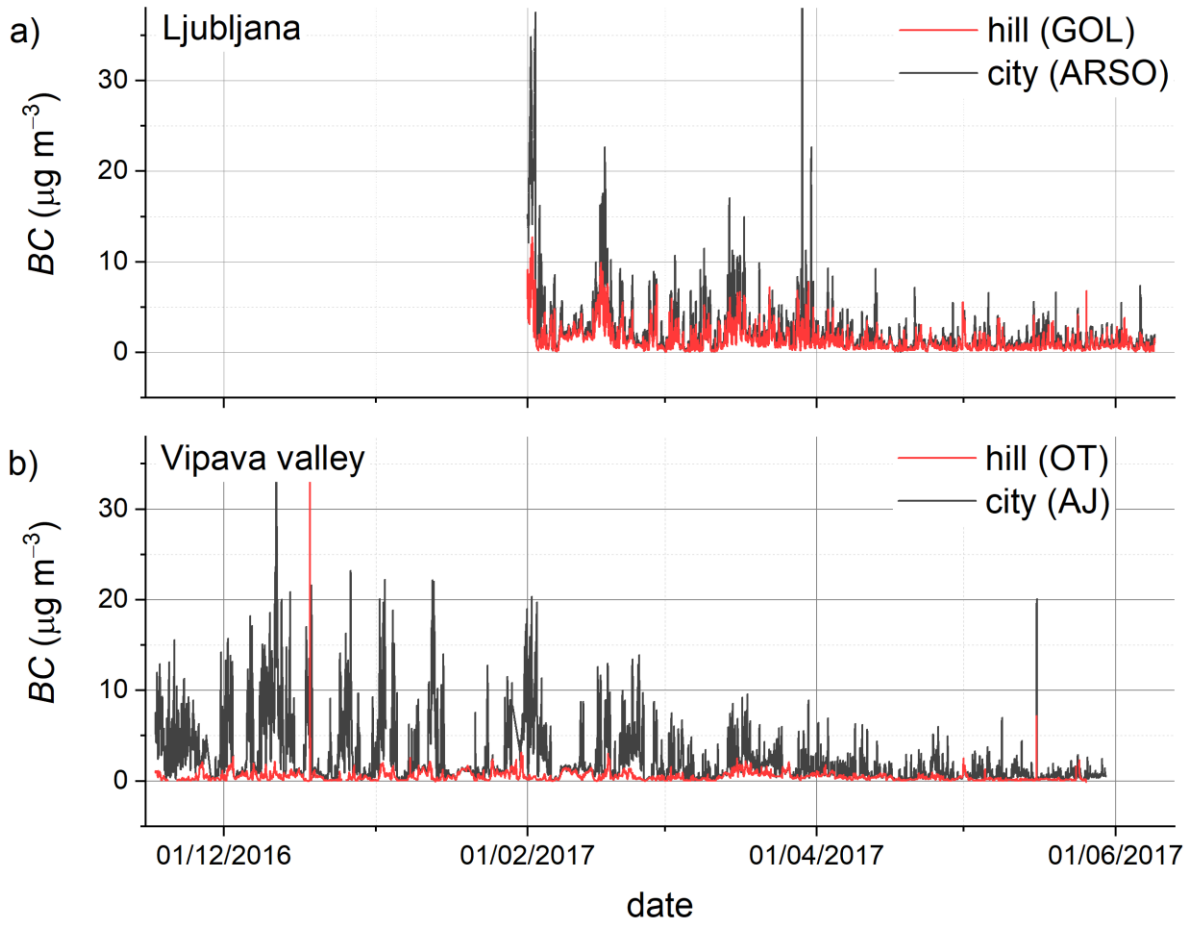

Figure 5: Time series (1-hour running average is applied to 1-minute data) of black carbon concentration (BC) measured at two measurement sites (city - black, hill - red) in Ljubljana (a) and in Vipava valley (b).

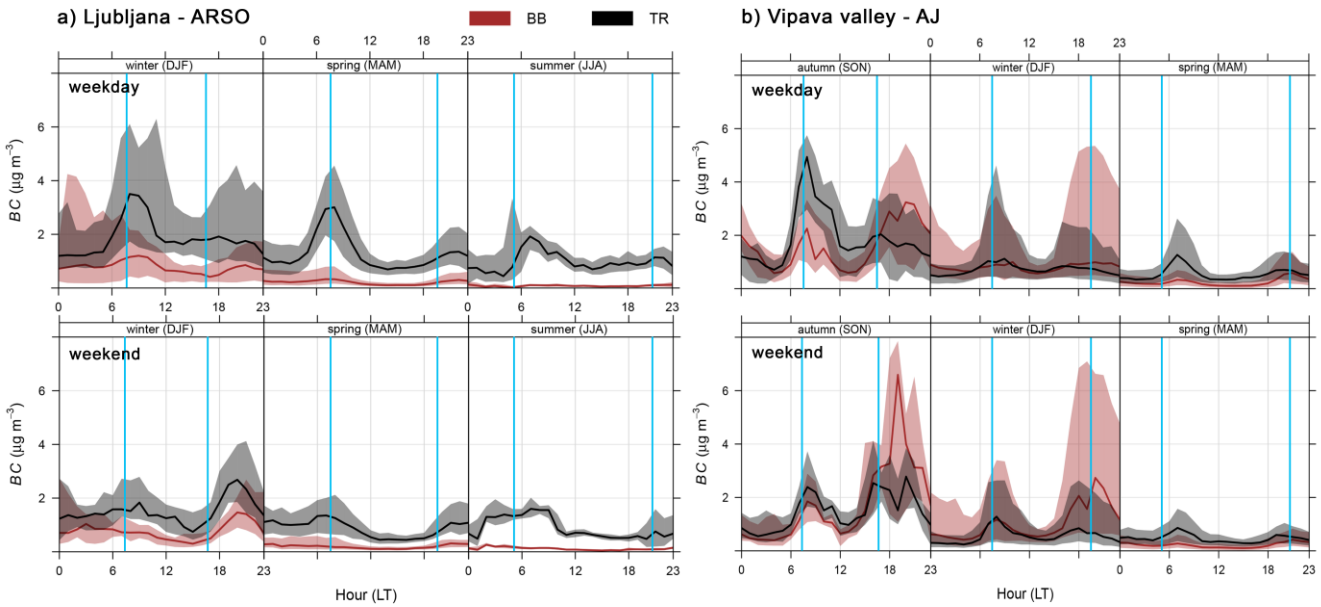

Figure 6: Diurnal variation (local time: CET/CEST) of source specific black carbon concentration (traffic – TR and biomass burning – BB) at Ljubljana urban background - ARSO (a), and Vipava valley urban background - AJ (b), grouped by season and weekday/weekend. The statistics for every hour in a day are represented by median value (line) and 25th – 75th percentile (shaded area) derived from 1-minute data. AAE_{TR} and AAE_{BB} were set to 1 and 2, respectively. Blue vertical lines mark the sunrise and sunset time.

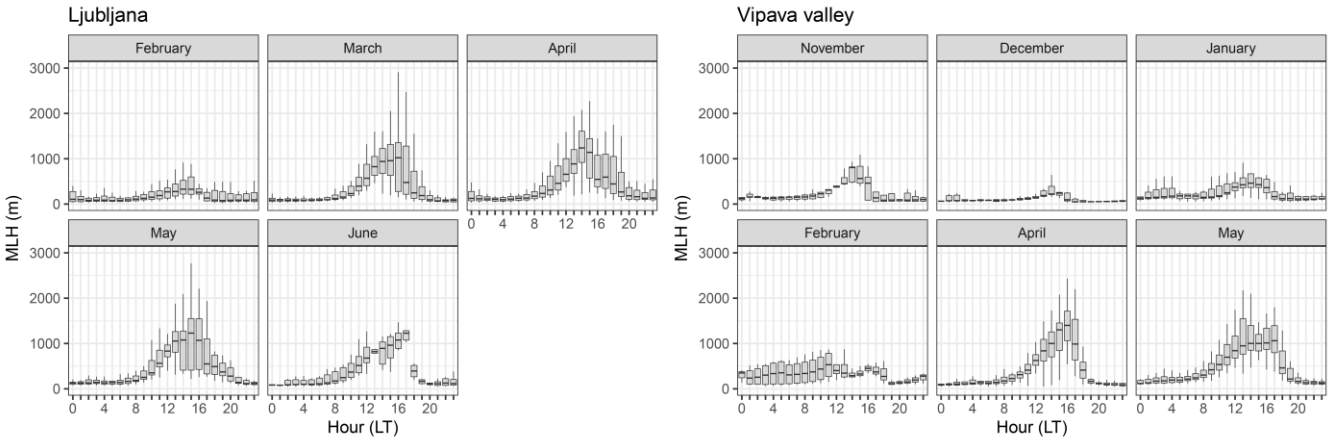

Figure 7: Diurnal variation (local time: CET/CEST) of modelled mixing layer height (MLH) grouped by months for the periods of thermally driven PBL convection, for Ljubljana and Vipava valley. Hourly statistics are represented by box plots (horizontal line: median, grey-coloured box: 25th-75th percentile, whiskers: 5th-95th percentile).

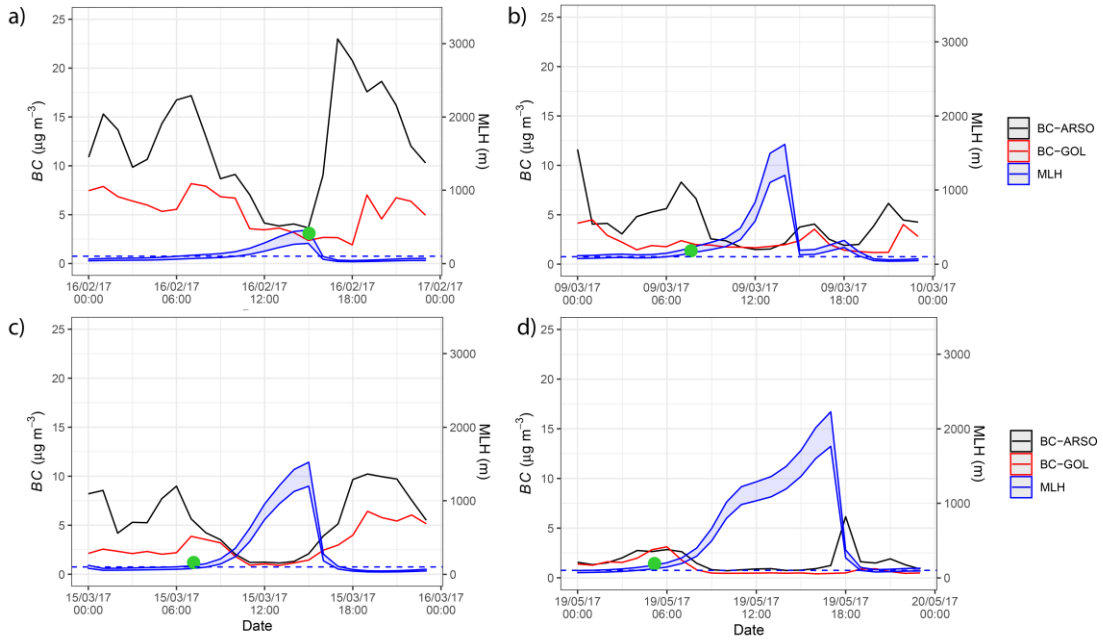

Figure 8: Time series (UTC) of BC concentration measured in Ljubljana (ARSO) and on the hill (GOL) with modelled MLH_{Rn} (based on min and max E_{Rn} estimate) in blue, and MLH_{BC} determined by flight measurements (green point) on February 16, Feb 2017 (a), March 9,2017 (b), March 15, 2017 (c) and May 19, 2017 (d).

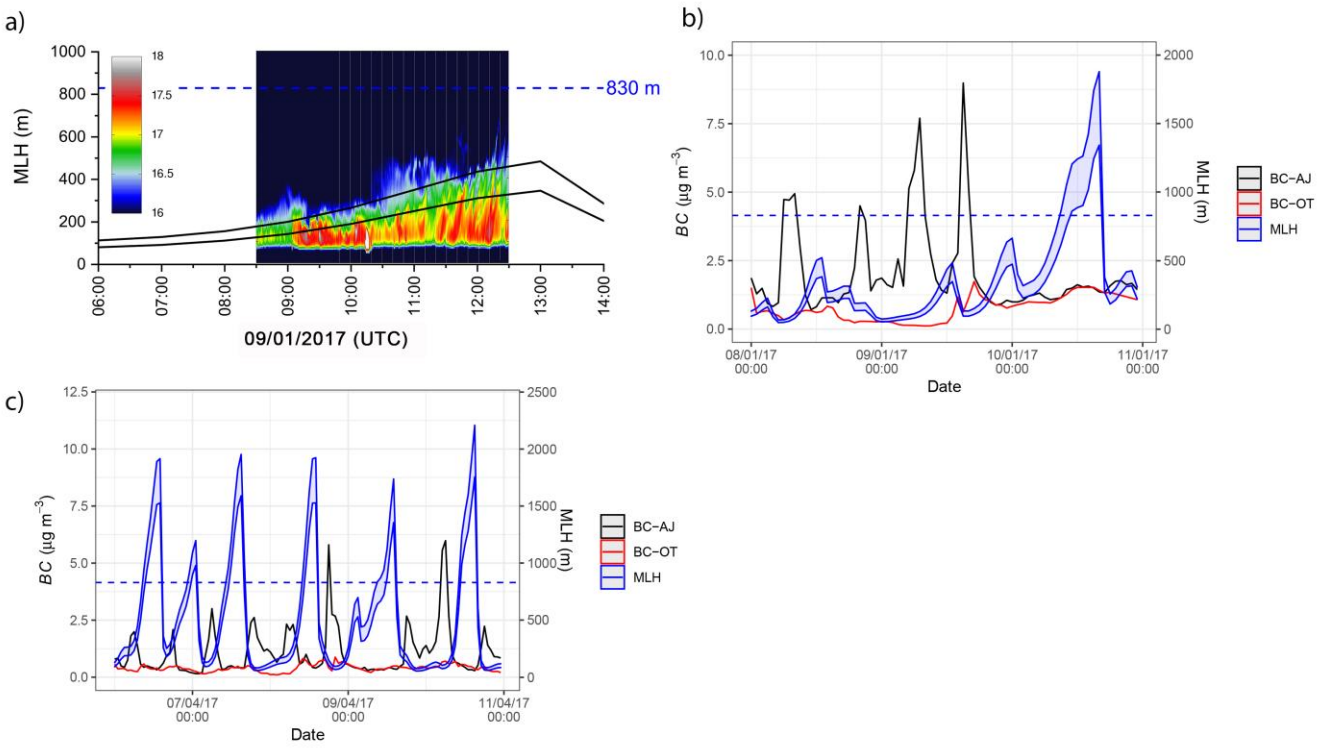

Figure 9: Comparison of modelled MLH (black line) over the Vipava valley with range-corrected lidar return signal on 09/01/2017 (a), time series (UTC) of BC concentration in the city (AJ) and on the hill (OT) with modelled MLH$_{Rn}$ (based on min and max E_{Rn} estimate) ~~in~~ in the period January 8 – 10, 2017 (b) and April 6 – 10, 2017 (c). Dashed blue line represents the altitude of OT site, 830 m a.g.l. .

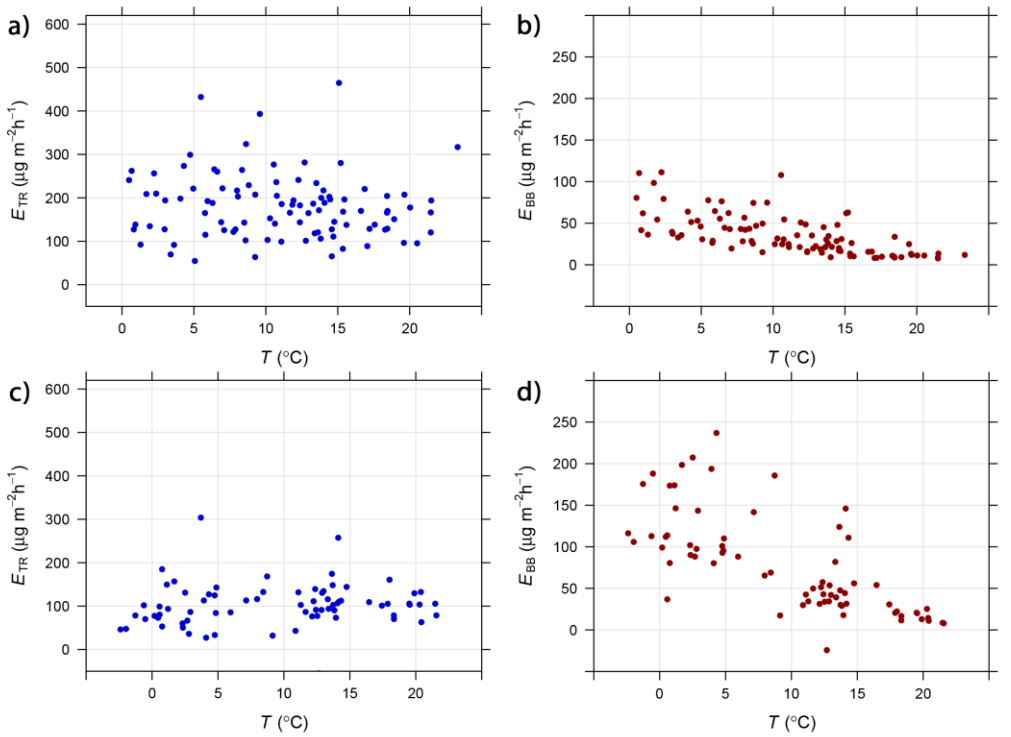

Figure 10: Dependence of source specific emission rates E_{TR} (traffic) and E_{BB} (biomass burning) on the outdoor air temperature for Ljubljana (a, b) and Vipava valley (c, d). Daily average values are shown.

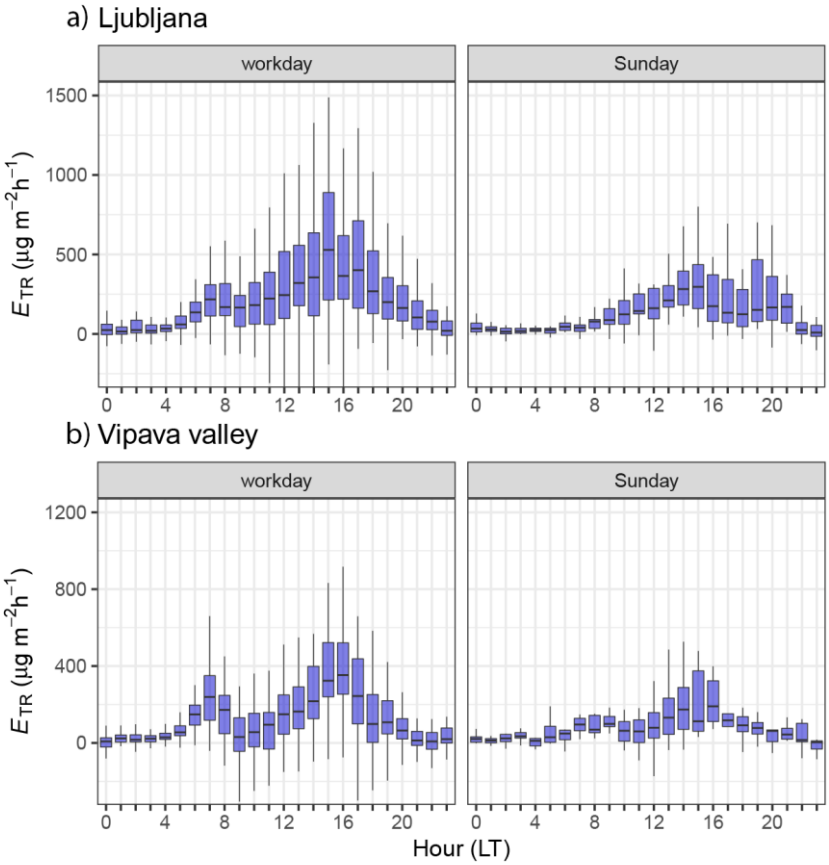

Figure 11: Diurnal variation (local time: CET/CEST) of emission rate of traffic related BC (E_{TR}) in Ljubljana (a) and Vipava valley (b), grouped by working days and Sundays. The statistics for every hour in a day are represented by a box plot (horizontal line: median, blue-coloured box: 25th-75th percentile, whiskers: 5th-95th percentile).

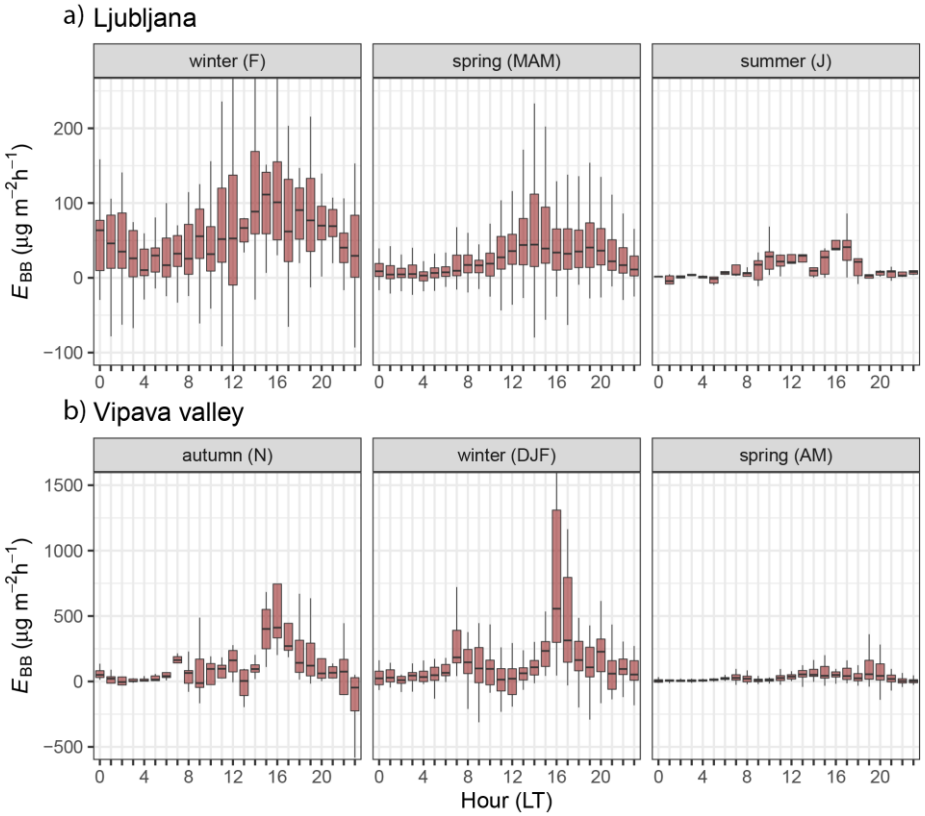

Figure 12: Diurnal variation (local time: CET/CEST) of emission rate of biomass burning related BC (E_{BB}) in Ljubljana (a) and Vipava valley (b), grouped by season (note the different scales). The statistics for every hour in a day are represented by a box plot (horizontal line: median, brown-coloured box: 25th-75th percentile, whiskers: 5th-95th percentile).

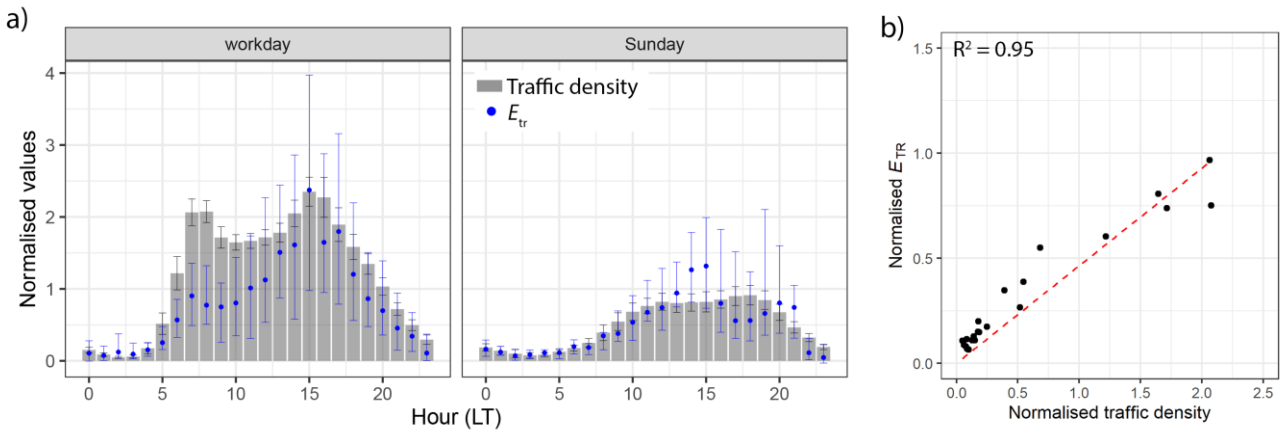

Figure 13: Comparison between diurnal profiles of traffic density and modelled E_{TR} in Ljubljana. Normalized mean hourly values are presented for traffic density, whereas E_{TR} values are presented in terms of normalized median, 25th and 75th quantile (a). Linear regression (without offset) of points from 00:00 to 10:00 that are presented on the diurnal plot results in R^2=0.95.

Tables:

Table 1: List of symbols and acronyms.

Acronym/Symbol	Definition	Units
λ'_s	temporal decay constant	h^{-1}
AAE	absorption Ångström exponent	
AAE_{BB}	biomass burning related AAE	
AAE_{TR}	traffic related AAE	
AJ	Ajdovščina location	
ARSO	Slovenian Environmental Agency	
b_{abs}	absorption coefficient	Mm^{-1}
BC	black carbon concentration	ng m^{-3}
BC_{BB}	biomass burning related black carbon concentration	ng m^{-3}
BC_{TR}	traffic related black carbon concentration	ng m^{-3}
C	multiple scattering parameter	
C_{Rn}	radon activity concentration	Bq m^{-3}
C_s	species concentration	
E_{BC}	black carbon emission rate	μg m^{-2} h^{-1}
E_{BB}	black carbon emission rate from biomass burning sources	μg m^{-2} h^{-1}
E_{TR}	black carbon emission rate from traffic sources	μg m^{-2} h^{-1}
EMEP	The European Monitoring and Evaluation Programme	
E_{Rn}	radon exhalation rate	Bq m^{-2} h^{-1}
E_s	species emission rate	
FFT	Fast Fourier transform	
GDAS	Global Data Assimilation System	
GOL	Golovec Astronomical and Geophysical Observatory	
h	effective mixing layer height	m
LJ	Ljubljana location	
ML	mixing layer	
MLH	mixing layer height	m
MLH_{BC}	mixing layer height from black carbon vertical profiles	m
MLH_{Rn}	mixing layer height from radon model	m
NOAA-ARL	NOAA Air Resources Laboratory	
OT	Otlica Meteorological observatory	
PBL	planetary boundary layer	
PM	particulate matter	
SNBL	stable nocturnal boundary layer	
T	air temperature	°C
wd	wind direction	
ws	wind speed	m s^{-1}
γ_s	spatial decay constant	m^{-1}
σ_{air}	mass absorption cross section	m^2 g^{-1}

Table 2: Selected Rn exhalation rates (E_{Rn}) and the range ($E_{Rn\text{-}min}$ – $E_{Rn\text{-}max}$) for each month for both measurement locations.

Month	E_{Rn} (Bq m^{-2} h^{-1})	
	Ljubljana	Vipava valley
November 2016	/	200 (150 – 250)
December 2016	/	200 (150 – 250)
January 2017	/	300 (250 – 350)*
February 2017	~~250~~150 (100 – 200)	~~250~~300 (250 – 350)*
March 2017	~~350~~250 (200 – 300)	~~350~~300 (250 – 350)*
April 2017	~~450~~250 (200 – 300)*	~~450~~300 (250 – 350)
May 2017	~~450~~300 (250 – 350)	~~400~~350 (300 – 400)
June 2017	~~550~~300 (250 – 350)	/

* High uncertainty

Table 3: Summary of temporal and spatial decay constants selected for Ljubljana and Vipava valley modelled area.

Measurement location	λ (h^{-1})		γ (m^{-1})	
	TR	BB	TR	BB
Ljubljana	0.006	0.006	7×10^{-5}	5×10^{-5}
Vipava valley	0.006	0.006	10^{-4}	10^{-4}

Table 4: Summary statistics (mean ± standard deviation) of measured Rn concentration (Bq m^{-3}), BC (µg m^{-3}) concentration apportioned to traffic and biomass burning for urban background sites in Ljubljana (ARSO)and Vipava valley (AJ) and BC (µg m^{-3}) concentration at the hill sites (GOL and OT).

season	Ljubljana						Vipava valley					
	C_{Rn}	BC_{city}	$BC_{TR\text{-}city}$	$BC_{BB\text{-}city}$	*BB %*	BC_{hill}	C_{Rn}	BC_{city}	$BC_{TR\text{-}city}$	$BC_{BB\text{-}city}$	*BB %*	BC_{hill}
Autumn 2016	/	/	/	/	/	/	14 ± 7	3.2 ± 2.4	1.6 ± 1.4	1.6 ± 1.4	50	0.4 ± 0.5
Winter 2016/17	15 ± 11	4.5 ± 5.7	3.1 ± 4.1	1.4 ± 1.8	31	2.2 ± 2.0	14 ± 10	3.4 ± 4.2	1.3 ± 1.6	2.1 ± 2.8	62	0.6 ± 0.8
Spring 2017	13 ± 9	1.9 ± 1.9	1.5 ± 1.6	0.4 ± 0.5	21	1.1 ± 1.0	12 ± 8	1.1 ± 1.2	0.8 ± 0.9	0.4 ± 0.5	36	0.4 ± 0.4
Summer 2017	16 ± 11	1.3 ± 0.9	1.2 ± 0.9	0.1 ± 0.1	8	0.8 ± 0.5	/	/	/	/	/	/

Table 5: BC emission rates (E_{BC}) (weighted mean ± standard deviation derived from daily mean values) and range of E_{BC} for lower and upper MLH_{Rn} estimate ($E_{BC\text{-}min} - E_{BC\text{-}max}$). ~~for~~ TR (traffic) and BB (biomass burning) emissions are reported separately for each season (all days, mornings of working days and Sundays) and location, expressed in µg $m^{-2}h^{-1}$. ~~and contribution of E_{BB} to overall BC emissions.~~

season	Part of day	Ljubljana				Vipava valley			
		E_{TR}	E_{BB}	E_{BB}/E (%)	# days	E_{TR}	E_{BB}	E_{BB}/E (%)	# days
Autumn 2016	**all**	/	/	/	/	**70 ± 50** (50 – 80)	**70 ± 50** (50 – 80)	**50**	6
	Working days 6:00 – 8:00	/	/	/	/	220 ± 110 (170 – 280)	100 ± 20 (80 – 130)	31	4
	Sunday 6:00 – 8:00	/	/	/	/	50 ± / (40 – 60)	30 ± / (20 – 40)	38	1
Winter 2016/17	**all**	**190 ± 90** (150 – 230)	**70 ± 30** (60 – 70)	**27**	22	**100 ± 60** (80 – 120)	**150 ± 110** (120 – 180)	**60**	37
	Working days 6:00 – 8:00	240 ± 110 (190 – 290)	60 ± 70 (50 – 70)	20	15	260 ± 130 (210 – 310)	200 ± 160 (170 – 240)	43	23
	Sunday 6:00 – 8:00	30 ± 20 (30 – 40)	0 ± 20 (0 – 0)	0	4	90 ± 20 (70 – 100)	140 ± 20 (110 – 170)	61	7
Spring 2017	**all**	**180 ± 100** (160 – 210)	**30 ± 20** (30 – 40)	**14**	69	**110 ± 40** (90 – 120)	**40 ± 30** (30 – 40)	**27**	54
	Working days 6:00 – 8:00	210 ± 160 (170 – 240)	20 ± 18 (17 – 24)	9	50	170 ± 90 (140 – 190)	50 ± 50 (40 – 50)	23	42
	Sunday 6:00 – 8:00	60 ± 20 (50 – 70)	6 ± 4 (5 – 7)	9	12	70 ± 30 (60 – 80)	20 ± 20 (10 – 20)	22	6
Summer 2017	**all**	**170 ± 70** (160 – 210)	**13 ± 9** (12 – 15)	**7**	7	/	/	/	/
	Working days 6:00 – 8:00	200 ± 240 (180 – 230)	15 ± 17 (14 – 18)	7	6	/	/	/	/
	Sunday 6:00 – 8:00	/	/	/	/	/	/	/	/

Acknowledgement

This work was supported by TRL 6-9/4300-1/2016-60 grant from the Ministry of Economic Development and Technology of Republic of Slovenia and by research programmes I0-0033, P1-0385, ~~and~~ P1-0099 and P1-0143 of the Slovenian Research Agency.

Code/Data availability

The data used in this publication is available upon request to the corresponding author (asta.gregoric@aerosol.eu).

Author contribution

AG, LD, IJ and GM designed the study, JV and AG performed and analysed radon measurements, ML, DG, LD and GM performed and analysed measurements by ultralight aircraft, LW, MM and SS performed lidar measurements. Model development and paper preparation were performed by AG, LD and GM. All authors contributed to the scientific discussion.

Conflicts of interest

At the time of the research, A. Gregorič, G. Močnik and L. Drinovec were also employed by the manufacturer of the Aethalometer instruments, used to measure black carbon. Other authors declare no conflict of interest. The funding sponsors had no role in the design of the study; in the collection, analyses, or interpretation of data; in the writing of the manuscript, and in the decision to publish the results.

References

LRTAP 2018: European Union emission inventory report 1990-2016 under the UNECE Convention on Long-range Transboundary Air Pollution, European Environment Agency, Luxemburg, 150, 2018.

Allegrini, I., Febo, A., Pasini, A., and Schiarini, S.: Monitoring of the nocturnal mixed layer by means of participate radon progeny measurement, J. Geophys. Res. - Atmos., 99, 18765-18777, doi:10.1029/94JD00783, 1994.

Athanasopoulou, E., Speyer, O., Brunner, D., Vogel, H., Vogel, B., Mihalopoulos, N., and Gerasopoulos, E.: Changes in domestic heating fuel use in Greece: effects on atmospheric chemistry and radiation, Atmos. Chem. Phys., 17, 10597-10618, 10.5194/acp-17-10597-2017, 2017.

Aurela, M., Saarikoski, S., Timonen, H., Aalto, P., Keronen, P., Saarnio, K., Teinilä, K., Kulmala, M., and Hillamo, R.: Carbonaceous aerosol at a forested and an urban background sites in Southern Finland, Atmos. Environ., 45, 1394-1401, https://doi.org/10.1016/j.atmosenv.2010.12.039, 2011.

Blanco-Alegre, C., Calvo, A. I., Coz, E., Castro, A., Oduber, F., Prevot, A. S. H., Mocnik, G., and Fraile, R.: Quantification of source specific black carbon scavenging using an aethalometer and a disdrometer, Environ Pollut, 246, 336-345, 10.1016/j.envpol.2018.11.102, 2019.

Bond, T. C., Bhardwaj, E., Dong, R., Jogani, R., Jung, S., Roden, C., Streets, D. G., and Trautmann, N. M.: Historical emissions of black and organic carbon aerosol from energy-related combustion, 1850–2000, Global Biogeochemical Cycles, 21, 1944-9224, 10.1029/2006GB002840, 2007.

Bond, T. C., Doherty, S. J., Fahey, D. W., Forster, P. M., Berntsen, T., DeAngelo, B. J., Flanner, M. G., Ghan, S., Kärcher, B., Koch, D., Kinne, S., Kondo, Y., Quinn, P. K., Sarofim, M. C., Schultz, M. G., Schulz, M., Venkataraman, C., Zhang, H., Zhang, S., Bellouin, N., Guttikunda, S. K., Hopke, P. K., Jacobson, M. Z., Kaiser, J. W., Klimont, Z., Lohmann, U., Schwarz, J. P., Shindell, D., Storelvmo, T., Warren, S. G., and Zender, C. S.: Bounding the role of black carbon in the climate system: A scientific assessment, J. Geophys. Res. - Atmos., 118, 5380-5552, 10.1002/jgrd.50171, 2013.

Brioude, J., Angevine, W. M., Ahmadov, R., Kim, S. W., Evan, S., McKeen, S. A., Hsie, E. Y., Frost, G. J., Neuman, J. A., Pollack, I. B., Peischl, J., Ryerson, T. B., Holloway, J., Brown, S. S., Nowak, J. B., Roberts, J. M., Wofsy, S. C., Santoni, G. W., Oda, T., and Trainer, M.: Top-down estimate of surface flux in the Los Angeles Basin using a mesoscale inverse modeling technique: assessing anthropogenic emissions of CO, NO_x and CO_2 and their impacts, Atmos. Chem. Phys., 13, 3661-3677, 10.5194/acp-13-3661-2013, 2013.

Cape, J. N., Coyle, M., and Dumitrean, P.: The atmospheric lifetime of black carbon, Atmos. Environ., 59, 256-263, 10.1016/j.atmosenv.2012.05.030, 2012.

Carslaw, D. C., and Ropkins, K.: openair — An R package for air quality data analysis, Environmental Modelling & Software, 27–28, 52-61, http://dx.doi.org/10.1016/j.envsoft.2011.09.008, 2012.

Chambers, S. D., Wang, F., Williams, A. G., Xiaodong, D., Zhang, H., Lonati, G., Crawford, J., Griffiths, A. D., Ianniello, A., and Allegrini, I.: Quantifying the influences of atmospheric stability on air pollution in Lanzhou, China, using a radon-based stability monitor, Atmos. Environ., 107, 233-243, http://dx.doi.org/10.1016/j.atmosenv.2015.02.016, 2015a.

Chambers, S. D., Williams, A. G., Crawford, J., and Griffiths, A. D.: On the use of radon for quantifying the effects of atmospheric stability on urban emissions, Atmos. Chem. Phys., 15, 1175-1190, 10.5194/acp-15-1175-2015, 2015b.

Chambers, S. D., Podstawczyńska, A., Williams, A. G., and Pawlak, W.: Characterising the influence of atmospheric mixing state on Urban Heat Island Intensity using Radon-222, Atmos. Environ., 147, 355-368, http://dx.doi.org/10.1016/j.atmosenv.2016.10.026, 2016.

Chambers, S. D., Podstawczyńska, A., Pawlak, W., Fortuniak, K., Williams, A. G., and Griffiths, A. D.: Characterizing the state of the Urban Surface Layer using Radon-222, J. Geophys. Res. - Atmos., doi:10.1029/2018JD029507, 2019.

Crawford, J., Chambers, S., Cohen, D. D., Dyer, L., Wang, T., and Zahorowski, W.: Receptor modelling using Positive Matrix Factorisation, back trajectories and Radon-222, Atmos. Environ., 41, 6823-6837, https://doi.org/10.1016/j.atmosenv.2007.04.048, 2007.

Crawford, J., Chambers, S., Cohen, D., Williams, A., Griffiths, A., and Stelcer, E.: Assessing the impact of atmospheric stability on locally and remotely sourced aerosols at Richmond, Australia, using Radon-222, Atmos. Environ., 127, 107-117, http://dx.doi.org/10.1016/j.atmosenv.2015.12.034, 2016.

Crilley, L. R., Bloss, W. J., Yin, J., Beddows, D. C. S., Harrison, R. M., Allan, J. D., Young, D. E., Flynn, M., Williams, P., Zotter, P., Prevot, A. S. H., Heal, M. R., Barlow, J. F., Halios, C. H., Lee, J. D., Szidat, S., and Mohr, C.: Sources

and contributions of wood smoke during winter in London: assessing local and regional influences, Atmos. Chem. Phys., 15, 3149-3171, 10.5194/acp-15-3149-2015, 2015.

Crippa, M., DeCarlo, P. F., Slowik, J. G., Mohr, C., Heringa, M. F., Chirico, R., Poulain, L., Freutel, F., Sciare, J., Cozic, J., Di Marco, C. F., Elsasser, M., Nicolas, J. B., Marchand, N., Abidi, E., Wiedensohler, A., Drewnick, F., Schneider, J., Borrmann, S., Nemitz, E., Zimmermann, R., Jaffrezo, J. L., Prévôt, A. S. H., and Baltensperger, U.: Wintertime aerosol chemical composition and source apportionment of the organic fraction in the metropolitan area of Paris, Atmos. Chem. Phys., 13, 961-981, 10.5194/acp-13-961-2013, 2013.

Denier van der Gon, H. A. C., Bergström, R., Fountoukis, C., Johansson, C., Pandis, S. N., Simpson, D., and Visschedijk, A. J. H.: Particulate emissions from residential wood combustion in Europe – revised estimates and an evaluation, Atmos. Chem. Phys., 15, 6503-6519, 10.5194/acp-15-6503-2015, 2015.

Drinovec, L., Močnik, G., Zotter, P., Prévôt, A. S. H., Ruckstuhl, C., Coz, E., Rupakheti, M., Sciare, J., Müller, T., Wiedensohler, A., and Hansen, A. D. A.: The "dual-spot" Aethalometer: an improved measurement of aerosol black carbon with real-time loading compensation, Atmos. Meas. Tech., 8, 1965-1979, 10.5194/amt-8-1965-2015, 2015.

Etiope, G., and Martinelli, G.: Migration of carrier and trace gases in the geosphere: an overview, Phys. Earth Planet. In., 129, 185-204, http://dx.doi.org/10.1016/S0031-9201(01)00292-8, 2002.

Favez, O., Cachier, H., Sciare, J., Sarda-Estève, R., and Martinon, L.: Evidence for a significant contribution of wood burning aerosols to PM2.5 during the winter season in Paris, France, Atmos. Environ., 43, 3640-3644, http://dx.doi.org/10.1016/j.atmosenv.2009.04.035, 2009.

Favez, O., El Haddad, I., Piot, C., Boréave, A., Abidi, E., Marchand, N., Jaffrezo, J. L., Besombes, J. L., Personnaz, M. B., Sciare, J., Wortham, H., George, C., and D'Anna, B.: Inter-comparison of source apportionment models for the estimation of wood burning aerosols during wintertime in an Alpine city (Grenoble, France), Atmos. Chem. Phys., 10, 5295-5314, 10.5194/acp-10-5295-2010, 2010.

Ferrero, L., Mocnik, G., Ferrini, B. S., Perrone, M. G., Sangiorgi, G., and Bolzacchini, E.: Vertical profiles of aerosol absorption coefficient from micro-Aethalometer data and Mie calculation over Milan, Sci. Total. Environ., 409, 2824-2837, http://dx.doi.org/10.1016/j.scitotenv.2011.04.022, 2011.

Ferrero, L., Castelli, M., Ferrini, B. S., Moscatelli, M., Perrone, M. G., Sangiorgi, G., D'Angelo, L., Rovelli, G., Moroni, B., Scardazza, F., Močnik, G., Bolzacchini, E., Petitta, M., and Cappelletti, D.: Impact of black carbon aerosol over Italian basin valleys: high-resolution measurements along vertical profiles, radiative forcing and heating rate, Atmos. Chem. Phys., 14, 9641-9664, 10.5194/acp-14-9641-2014, 2014.

Fuller, G. W., Tremper, A. H., Baker, T. D., Yttri, K. E., and Butterfield, D.: Contribution of wood burning to PM10 in London, Atmos. Environ., 87, 87-94, http://dx.doi.org/10.1016/j.atmosenv.2013.12.037, 2014.

Gjerek, M., Koleša, T., Logar, M., Matavž, L., Murovec, M., Rus, M., and Žabkar, R.: Kakovost zraka v Sloveniji v letu 2017 (Air quality in Slovenia in 2017), Agencija Republike Slovenije za Okolje (Slovenian Environment Agency), Ljubljana, 130, 2018.

Griffiths, A. D., Parkes, S. D., Chambers, S. D., McCabe, M. F., and Williams, A. G.: Improved mixing height monitoring through a combination of lidar and radon measurements, Atmos. Meas. Tech., 6, 207-218, 10.5194/amt-6-207-2013, 2013.

Guerrette, J. J., and Henze, D. K.: Four-dimensional variational inversion of black carbon emissions during ARCTAS-CARB with WRFDA-Chem, Atmos. Chem. Phys., 17, 7605-7633, 10.5194/acp-17-7605-2017, 2017.

Hansen, A. D. A., Artz, R. S., Pszenny, A. A. P., and Larson, R. E.: Aerosol black carbon and radon as tracers for air mass origin over the North Atlantic ocean, Global biogeochemical cycles, 4, 189-199, 1990.

He, T.-Y., Gao, F., Stanič, S., Veberič, D., Bergant, K., Dolžan, A., and Song, X.-Q.: Scanning mobile lidar for aerosol tracking and biological aerosol identification, SPIE Remote Sensing, SPIE, 2010.

Helin, A., Niemi, J. V., Virkkula, A., Pirjola, L., Teinilä, K., Backman, J., Aurela, M., Saarikoski, S., Rönkkö, T., Asmi, E., and Timonen, H.: Characteristics and source apportionment of black carbon in the Helsinki metropolitan area, Finland, Atmos. Environ., 190, 87-98, 10.1016/j.atmosenv.2018.07.022, 2018.

Herich, H., Gianini, M. F. D., Piot, C., Močnik, G., Jaffrezo, J. L., Besombes, J. L., Prévôt, A. S. H., and Hueglin, C.: Overview of the impact of wood burning emissions on carbonaceous aerosols and PM in large parts of the Alpine region, Atmos. Environ., 89, 64-75, http://dx.doi.org/10.1016/j.atmosenv.2014.02.008, 2014.

Hovorka, J., Pokorná, P., Hopke, P. K., Křůmal, K., Mikuška, P., and Píšová, M.: Wood combustion, a dominant source of winter aerosol in residential district in proximity to a large automobile factory in Central Europe, Atmos. Environ., 113, 98-107, https://doi.org/10.1016/j.atmosenv.2015.04.068, 2015.

IPCC: Contribution of Working Group I to the Fifth Assessment Report of the Intergovernmental Panel on Climate Change, in: Climate Change 2013: the Physical Science Basis, edited by: Stocker, T. F., Qin, D., Plattner, G.-K., Tignor, M., Allen, S. K., Boschung, J., Nauels, A., Xia, Y., Bex, V., and Midgley, P. M., Cambridge University Press, Cmbridge, United Kingdom and New York, USA, 1533, 2013.

Janssen, N. A., Hoek, G., Simic-Lawson, M., Fischer, P., van Bree, L., ten Brink, H., Keuken, M., Atkinson, R. W., Anderson, H. R., Brunekreef, B., and Cassee, F. R.: Black carbon as an additional indicator of the adverse health effects of airborne particles compared with PM10 and PM2.5, Environ. Health Persp., 119, 1691-1699, 10.1289/ehp.1003369, 2011.

Janža, M., Lapanje, A., Šram, D., Rajver, D., and Novak, M.: Research of the geological and geothermal conditions for the assessment of the shallow geothermal potential in the area of Ljubljana, Slovenia, Geologija, 60, 309-327, 10.5474/geologija.2017.022, 2017.

Jež, J.: Reasons and mechanism for soil sliding processes in the Rebrnice area, Vipava valley, SW Slovenia, Geologija, 50, 55-63, 10.5474/geologija.2007.005, 2007.

Ježek, I., Blond, N., Skupinski, G., and Močnik, G.: The traffic emission-dispersion model for a Central-European city agrees with measured black carbon apportioned to traffic, Atmos. Environ., 184, 177-190, https://doi.org/10.1016/j.atmosenv.2018.04.028, 2018.

Kardos, R., Gregorič, A., Jónás, J., Vaupotič, J., Kovács, T., and Ishimori, Y.: Dependence of radon emanation of soil on lithology, J. Radioanal. Nucl. Chem., 304, 1321 - 1327, 10.1007/s10967-015-3954-3, 2015.

Karstens, U., Schwingshackl, C., Schmithüsen, D., and Levin, I.: A process-based 222radon flux map for Europe and its comparison to long-term observations, Atmos. Chem. Phys., 15, 12845-12865, 10.5194/acp-15-12845-2015, 2015.

Kikaj, D., Vaupotič, J., and Chambers, S. D.: Identifying persistent temperature inversion events in a subalpine basin using radon-222, Atmos. Meas. Tech., 12, 4455-4477, 10.5194/amt-12-4455-2019, 2019.

Klimont, Z., Kupiainen, K., Heyes, C., Purohit, P., Cofala, J., Rafaj, P., Borken-Kleefeld, J., and Schöpp, W.: Global anthropogenic emissions of particulate matter including black carbon, Atmos. Chem. Phys., 17, 8681-8723, 10.5194/acp-17-8681-2017, 2017.

Leukauf, D., Gohm, A., and Rotach, M. W.: Quantifying horizontal and vertical tracer mass fluxes in an idealized valley during daytime, Atmos. Chem. Phys., 16, 13049-13066, 10.5194/acp-16-13049-2016, 2016.

McGrath-Spangler, E. L., Molod, A., Ott, L. E., and Pawson, S.: Impact of planetary boundary layer turbulence on model climate and tracer transport, Atmos. Chem. Phys., 15, 7269-7286, 10.5194/acp-15-7269-2015, 2015.

Mole, M., Wang, L., Stanič, S., Bergant, K., Eichinger, W. E., Ocaña, F., Strajnar, B., Škraba, P., Vučković, M., and Willis, W. B.: Lidar measurements of Bora wind effects on aerosol loading, Journal of Quantitative Spectroscopy and Radiative Transfer, 188, 39-45, https://doi.org/10.1016/j.jqsrt.2016.05.020, 2017.

Mues, A., Rupakheti, M., Münkel, C., Lauer, A., Bozem, H., Hoor, P., Butler, T., and Lawrence, M. G.: Investigation of the mixing layer height derived from ceilometer measurements in the Kathmandu Valley and implications for local air quality, Atmos. Chem. Phys., 17, 8157-8176, 10.5194/acp-17-8157-2017, 2017.

Ogrin, M., Vintar Mally, K., Planinšek, A., Gregorič, A., Drinovec, L., and Močnik, G.: Nitrogen dioxide and black carbon concentrations in Ljubljana, GeograFF, Ljubljana University Press, Faculty of Arts, Ljubljana, 118 pp., 2016.

Pakkanen, T. A., Kerminen, V.-M., Ojanen, C. H., Hillamo, R. E., Aarnio, P., and Koskentalo, T.: Atmospheric black carbon in Helsinki, Atmos. Environ., 34, 1497-1506, https://doi.org/10.1016/S1352-2310(99)00344-1, 2000.

Pal, S., Lopez, M., Schmidt, M., Ramonet, M., Gibert, F., Xueref-Remy, I., and Ciais, P.: Investigation of the atmospheric boundary layer depth variability and its impact on the 222Rn concentration at a rural site in France, J. Geophys. Res. - Atmos., 120, 623-643, 10.1002/2014JD022322, 2015.

Pearson, J. E., and Jones, G. E.: Emanation of radon 222 from soils and its use as a tracer, Journal of Geophysical Research, 70, 5279-5290, 10.1029/JZ070i020p05279, 1965.

Perrino, C., Pietrodangelo, A., and Febo, A.: An atmospheric stability index based on radon progeny measurements for the evaluation of primary urban pollution, Atmos. Environ., 35, 5235-5244, https://doi.org/10.1016/S1352-2310(01)00349-1, 2001.

Podstawczyńska, A.: Differences of near-ground atmospheric Rn-222 concentration between urban and rural area with reference to microclimate diversity, Atmos. Environ., 126, 225-234, https://doi.org/10.1016/j.atmosenv.2015.11.037, 2016.

Pöschl, U.: Atmospheric aerosols: composition, transformation, climate and health effects, Angewandte Chemie - International Edition, 44, 7520-7540, 10.1002/anie.200501122, 2005.

Quan, J., Gao, Y., Zhang, Q., Tie, X., Cao, J., Han, S., Meng, J., Chen, P., and Zhao, D.: Evolution of planetary boundary layer under different weather conditions, and its impact on aerosol concentrations, Particuology, 11, 34-40, http://dx.doi.org/10.1016/j.partic.2012.04.005, 2013.

R Core Team: R: A language and environment for statistical computing, R Foundation for Statistical Computing, Vienna, Austria, 2018.

Reche, C., Querol, X., Alastuey, A., Viana, M., Pey, J., Moreno, T., Rodríguez, S., González, Y., Fernández-Camacho, R., de la Rosa, J., Dall'Osto, M., Prévôt, A. S. H., Hueglin, C., Harrison, R. M., and Quincey, P.: New considerations for PM, Black Carbon and particle number concentration for air quality monitoring across different European cities, Atmos. Chem. Phys., 11, 6207-6227, 10.5194/acp-11-6207-2011, 2011.

Ricard, V., Jaffrezo, J. L., Kerminen, V. M., Hillamo, R. E., Sillanpaa, M., Ruellan, S., Liousse, C., and Cachier, H.: Two years of continuous aerosol measurements in northern Finland, J. Geophys. Res. - Atmos., 107, ACH 10-11-ACH 10-17, 10.1029/2001jd000952, 2002.

Rolph, G., Stein, A., and Stunder, B.: Real-time Environmental Applications and Display sYstem: READY, Environmental Modelling & Software, 95, 210-228, https://doi.org/10.1016/j.envsoft.2017.06.025, 2017.

Salzano, R., Pasini, A., Casasanta, G., Cacciani, M., and Perrino, C.: Quantitative Interpretation of Air Radon Progeny Fluctuations in Terms of Stability Conditions in the Atmospheric Boundary Layer, Boundary-Layer Meteorol, 160, 529-550, 10.1007/s10546-016-0149-6, 2016.

Sandradewi, J., Prévôt, A. S. H., Szidat, S., Perron, N., Alfarra, M. R., Lanz, V. A., Weingartner, E., and Baltensperger, U.: Using aerosol light absorption measurements for the quantitative determination of wood burning and traffic emission contributions to particulate matter, Environ. Sci. Technol., 42, 3316-3323, 10.1021/es702253m, 2008a.

Sandradewi, J., Prévôt, A. S. H., Weingartner, E., Schmidhauser, R., Gysel, M., and Baltensperger, U.: A study of wood burning and traffic aerosols in an Alpine valley using a multi-wavelength Aethalometer, Atmos. Environ., 42, 101-112, http://dx.doi.org/10.1016/j.atmosenv.2007.09.034, 2008b.

Seibert, P., Beyrich, F., Gryning, S.-E., Joffre, S., Rasmussen, A., and Tercier, P.: Review and intercomparison of operational methods for the determination of the mixing height, Atmos. Environ., 34, 1001-1027, https://doi.org/10.1016/S1352-2310(99)00349-0, 2000.

Seinfeld, J. H., and Pandis, S. N.: Atmospheric chemistry and physics, from air pollution to climate change, 3rd ed., John Wiley & Sons, Hoboken, New Jersey, 2016.

Sesana, L., Caprioli, E., and Marcazzan, G. M.: Long period study of outdoor radon concentration in Milan and correlation between its temporal variations and dispersion properties of atmosphere, Journal of Environmental Radioactivity, 65, 147-160, 10.1016/s0265-931x(02)00093-0, 2003.

Stull, R. B.: An introduction to Boundary Layer Meteorology, Kluwer Academics Press, Dordrecht, The Netherlands, 670 pp., 1988.

Sun, T., Liu, L., Flanner, M. G., Kirchstetter, T. W., Jiao, C., Preble, C. V., Chang, W. L., and Bond, T. C.: Constraining a Historical Black Carbon Emission Inventory of the United States for 1960–2000, J. Geophys. Res. - Atmos., 124, 4004-4025, 10.1029/2018jd030201, 2019.

Tang, G., Zhang, J., Zhu, X., Song, T., Münkel, C., Hu, B., Schäfer, K., Liu, Z., Zhang, J., Wang, L., Xin, J., Suppan, P., and Wang, Y.: Mixing layer height and its implications for air pollution over Beijing, China, Atmos. Chem. Phys., 16, 2459-2475, 10.5194/acp-16-2459-2016, 2016.

Titos, G., Lyamani, H., Drinovec, L., Olmo, F. J., Močnik, G., and Alados-Arboledas, L.: Evaluation of the impact of transportation changes on air quality, Atmos. Environ., 114, 19-31, http://dx.doi.org/10.1016/j.atmosenv.2015.05.027, 2015.

UNSCEAR: Sources and effects of ionizing radiation, 2000.

Vaupotič, J., Žvab, P., Gregorič, A., Dujmovič, P., Kocman, D., Kobal, I., Kozak, K., Mazur, J., Kochowska, E., and Haber, R.: Soil gas radon potential on radon prone areas, Jozef Stefan InstituteIJS-DP-9694, 2007.

Vaupotič, J., Gregorič, A., Kobal, I., Žvab, P., Kozak, K., Mazur, J., Kochowska, E., and Grządziel, D.: Radon concentration in soil gas and radon exhalation rate at the Ravne Fault in NW Slovenia, Nat. Hazard. Earth Sys., 10, 895-899, 10.5194/nhess-10-895-2010, 2010.

Vecchi, R., Piziali, F. A., Valli, G., Favaron, M., and Bernardoni, V.: Radon-based estimates of equivalent mixing layer heights: A long-term assessment, Atmos. Environ., 197, 150-158, 10.1016/j.atmosenv.2018.10.020, 2018.

Wang, F., Chambers, S. D., Zhang, Z., Williams, A. G., Deng, X., Zhang, H., Lonati, G., Crawford, J., Griffiths, A. D., Ianniello, A., and Allegrini, I.: Quantifying stability influences on air pollution in Lanzhou, China, using a radon-based "stability monitor": Seasonality and extreme events, Atmos. Environ., 145, 376-391, http://dx.doi.org/10.1016/j.atmosenv.2016.09.014, 2016a.

Wang, L., Stanič, S., Bergant, K., Eichinger, W., Močnik, G., Drinovec, L., Vaupotič, J., Miler, M., Gosar, M., and Gregorič, A.: Retrieval of Vertical Mass Concentration Distributions—Vipava Valley Case Study, Remote Sensing, 11, 106, 10.3390/rs11020106, 2019.

Wang, P., Wang, H., Wang, Y. Q., Zhang, X. Y., Gong, S. L., Xue, M., Zhou, C. H., Liu, H. L., An, X. Q., Niu, T., and Cheng, Y. L.: Inverse modeling of black carbon emissions over China using ensemble data assimilation, Atmos. Chem. Phys., 16, 989-1002, 10.5194/acp-16-989-2016, 2016b.

WHO: Health effects of Black Carbon, The WHO European Centre for Environment and Health, Bonn, 86, 2012.

Wickham, H.: ggplot2: Elegant Graphics for Data Analysis, Springer-Verlag, New York, 2009.

Williams, A. G., Zahorowski, W., Chambers, S., Griffiths, A., Hacker, J. M., Element, A., and Werczynski, S.: The Vertical Distribution of Radon in Clear and Cloudy Daytime Terrestrial Boundary Layers, Journal of the Atmospheric Sciences, 68, 155-174, 10.1175/2010jas3576.1, 2011.

Williams, A. G., Chambers, S., and Griffiths, A.: Bulk Mixing and Decoupling of the Nocturnal Stable Boundary Layer Characterized Using a Ubiquitous Natural Tracer, Boundary-Layer Meteorol, 149, 381-402, 10.1007/s10546-013-9849-3, 2013.

Williams, A. G., Chambers, S. D., Conen, F., Reimann, S., Hill, M., Griffiths, A. D., and Crawford, J.: Radon as a tracer of atmospheric influences on traffic-related air pollution in a small inland city, Tellus B, 68, 10.3402/tellusb.v68.30967, 2016.

Zhang, Y., Favez, O., Petit, J. E., Canonaco, F., Truong, F., Bonnaire, N., Crenn, V., Amodeo, T., Prévôt, A. S. H., Sciare, J., Gros, V., and Albinet, A.: Six-year source apportionment of submicron organic aerosols from near-continuous measurements at SIRTA (Paris area, France), Atmos. Chem. Phys. Discuss., 2019, 1-41, 10.5194/acp-2019-515, 2019.

The determination of highly time resolved and source separated black carbon emission rates using radon as a tracer of atmospheric dynamics (Supplement)

Asta Gregorič[1,2], Luka Drinovec[1,2,3], Irena Ježek[1], Janja Vaupotič[4], Matevž Lenarčič[5], Domen Grauf[5], Longlong Wang[2], Maruška Mole[2,6], Samo Stanič[2], Griša Močnik[1,2,3]

[1]Aerosol d.o.o., Ljubljana, SI-1000, Slovenia
[2]Centre for Atmospheric Research, University of Nova Gorica, Nova Gorica, SI-5000, Slovenia
[3]Department of Condensed Matter Physics, Jozef Stefan Institute, Ljubljana, SI-1000, Slovenia
[4]Department of Environmental Sciences, Jozef Stefan Institute, Ljubljana, SI-1000, Slovenia
[5]Aerovizija d.o.o., Ljubljana, SI-1000, Slovenia
[6]Quasar Science Resources S.L., ES-28232 Madrid, Spain

Correspondence to: Asta Gregorič (asta.gregoric@aerosol.eu)

1. Source apportionment of BC: Estimation of the site specific AAE_{TR} and AAE_{BB}:

The Aethalometer model (Sandradewi et al., 2008) uses an a priori assumed pair of absorption Ångström exponents (AAE) for traffic (AAE_{TR}) and biomass burning (AAE_{BB}) to determine the contribution of both sources. A narrow range of AAE_{TR} (0.8 – 1.1) values is reported in the literature, whereas larger AAE_{BB} values (from about 1.5 up to 3.5) in the wider range are characteristic for biomass burning sources (Kirchstetter, 2004; Saleh et al., 2013; Garg et al., 2016; Zotter et al., 2017). Higher values of AAE_{BB} result from enhanced light absorption in the near-UV and blue part of the spectrum caused by organic carbon species, present in biomass-smoke. Source specific AAE can be independently determined using auxiliary measurements of OC/EC. and ^{14}C (Sandradewi et al., 2008; Zotter et al., 2017), or biomass burning tracers like levoglucosan (Favez et al., 2010; Herich et al., 2014; Hellén et al., 2017; Helin et al., 2018). Since independent measurements allowing the determination of the AAE pair representative for our measurement locations were not available, the most suitable AAE pair was estimated according to the commonly used AAE values published in the literature, by considering overall distribution of AAE (Figure S1) for each measurement location and the corresponding diurnal variation of traffic (BC_{TR}) and biomass burning related BC (BC_{BB}) (Figure S2). AAE was calculated using the Eq. 1 for 470 nm and 950 nm wavelengths, where b_{abs} stands for the absorption coefficient at 470 nm and 950 nm.

$$AAE = \frac{\ln\left(\frac{b_{abs(470)}}{b_{abs(950)}}\right)}{\ln(950/470)} \quad (1)$$

By taking into account equations provided by Sandradewi et al. (2008), the BC_{BB} and BC_{TR} were finally calculated using the Eq. 2 and 3, respectively.

$$BC_{BB} = \frac{\frac{b_{abs(470)}}{b_{abs(950)}} - \left(\frac{950}{470}\right)^{AAE_{TR}}}{\left(\frac{950}{470}\right)^{AAE_{BB}} - \left(\frac{950}{470}\right)^{AAE_{TR}}} \times BC \quad (2)$$

$$BC_{TR} = BC - BC_{BB} \quad (3)$$

A histogram of absorption Ångström exponent (AAE) derived by Eq. 1 from AE33 measurements for both measurement locations is shown on Fig. S1. For direct comparison, only the time period with available measurements at both locations simultaneously was considered and covers the period from February to May 2017. Winter AAE median values of 1.36 and 1.60 and spring median values of 1.22 and 1.36 are characteristic for Ljubljana (LJ)and Ajdovščina (AJ) location, respectively. Lower AAE values measured in LJ correspond well to the urban nature of LJ measurement site, where stronger influence of traffic on BC concentrations is expected.

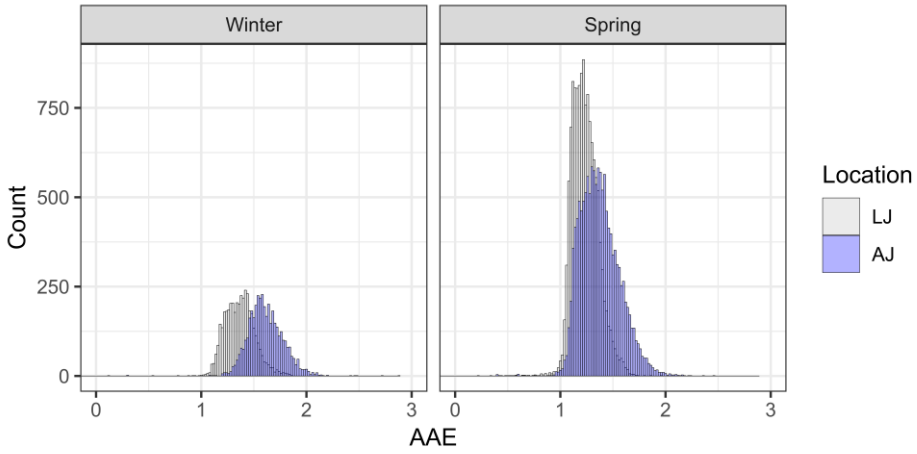

Figure S1: Absorption Ångström exponent (AAE) frequency distributions of 10-minute averages for Ajdovščina (AJ) and Ljubljana (LJ) for the period from February – May 2017 (winter: February, March; spring: April, May).

The same AAE_{TR} – AAE_{BB} pair of 1.0 and 2.0 was chosen for both measurement locations, based on the evaluation of AAE distribution (Fig. S1). Source apportioned BC concentration (Sandradewi et al., 2008; Zotter et al., 2017) diurnal variation is shown on Fig. S2 for two limiting AAE_{BB} values: 1.7 and 2.0 and fixed AAE_{TR} = 1.0. The AAE pair of 1.0 and 1.7 results in BC_{TR} and BC_{BB} concentrations presented by blue line, whereas the AAE pair of 1.0 and 2.0 results are presented by red line. Shaded area shows the range of source apportioned concentration between the limiting AAE_{BB} values.

The lower limit of 1.7 for AAE_{BB} is apparently not suitable for AJ location, since overall AAE distribution of aerosol mixture in winter ~~frequently~~ often exceeds 2.0 (Fig. S1). The source specific AAE values used for source apportionment are representative for the location and type of combustion, they can be interpreted as "average" values at the specific receptor site. The choice of AAE_{BB} needs to fall just below the maximum values seen at this site (a case of exclusive contribution of biomass burning, allowing still some variation of "real" AAE_{BB}, which may vary with time to a certain degree, depending on the primary emissions of combustion and the formation of light absorbing secondary organic aerosol (Kumar et al., 2018)). Moreover, an increase of BC_{BB} causes simultaneous decrease of BC_{TR}. This effect can be clearly observed in the Ajdovščina winter diurnal profile after 21:00, when BC_{TR} unrealistically drops to almost zero (Fig. S2c). On the other hand, AAE_{BB} = 2 results in reasonable diurnal variation of source apportioned BC. In winter, BC_{TR} and BC_{BB} concentrations start to increase around 5:00 and exhibit the morning peak between 7:00 and 8:00, when BC is dominated by traffic sources. After daytime dilution in the rising PBL, both BC_{TR} and BC_{BB} start to increase between 16:00 and 17:00 due to decreased mixing in the PBL. BC_{TR} exhibits the afternoon peak around 19:00, whereas BC_{BB} further increases until 21:00.

AAE distribution at LJ location is clearly shifted to lower values, as compared to AJ location, which can be assigned to stronger contribution of traffic sources. However, by considering only the AAE distribution and the diurnal variation of source apportioned BC, without any other independent measurements, it is not possible to define a reliable source specific AAE pair used for source apportionment. Therefore, a suitable AAE pair for source apportionment was evaluated also by re-evaluation

of subsequently modelled BC emission rate (discussed in Section 3.4). Average BC biomass burning fraction resulting from source apportionment using two different values of AAE_{BB} (1.7 or 2.0) is presented in Table S1.

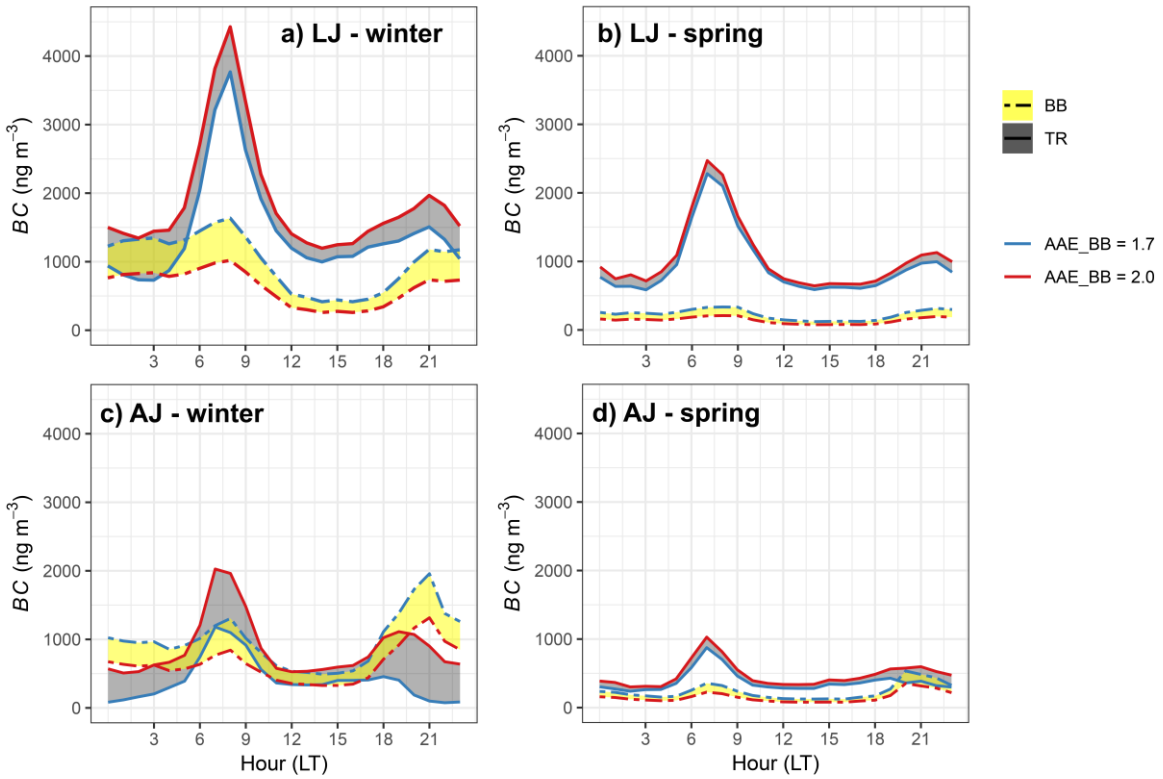

Figure S2: Diurnal variation (local time: CET/CEST) of contribution of traffic (BC_{TR}) and biomass burning (BC_{BB}) to total *BC* concentration in winter (January – February) and spring (March – April) period for Ljubljana (LJ) and Ajdovščina (AJ) measurement site, by considering different pairs of absorption Ångström exponents (AAE). AAE_{TR} was fixed to 1.0, AAE_{BB} was set to 1.7 (blue line) and 2 (red line). The shaded area represents a range of BC_{TR} (grey) and BC_{BB} (yellow) concentrations calculated between both extreme values of AAE_{BB}. Diurnal variation is derived from 1-minute data by considering median of concentration for specific hour.

Table S1: Average BC biomass burning fraction (BB%) based on source apportionment using fixed AAE_{TR} = 1.0 and limit values of 1.7 and 2.0 for AAE_{BB}.

Measurement location	Winter BB% (AAE_{BB} = 1.7)	Winter BB% (AAE_{BB} = 2.0)	Spring BB% (AAE_{BB} = 1.7)	Spring BB% (AAE_{BB} = 2.0)
LJ	51	32	31	20
AJ	85	60	53	35

2. BC vertical profile measurements by ultralight aircraft over Ljubljana

Black carbon vertical profiles (Figure S3) were measured in the Ljubljana basin using an ultralight airplane (Aerospool Dynamic WT9; see GLWF, 2019). The air was sampled using an isokinetic inlet and a modified version of the Aethalometer AE33 with 1 second time resolution (Drinovec et al., 2015). The location of the inlet prevented self-pollution from the airplane exhaust and the inlet was designed to be iso-kinetic at the airplane airspeed. The inlet is a conical diffusor, mounted on the holder of the Pitot tube under the wing, and designed for airspeed 240 km/h. The plane followed the helical path between 400 m and 1100 m ~~ASL~~ a.s.l. (100 – 800 m ~~AGL~~a.g.l.). The BC concentration was used as a parameter quantifying the influence of ground sources on the primary air pollution in the mixing layer and the mixing layer height was estimated from BC vertical profiles (MLH_{BC}). The measured data was fitted using a Boltzmann function:

$$y = \frac{A_1 - A_2}{1 + e^{(x - x_0)/dx}} + A_2 \ ,$$

where x_0 represents the mixing layer height (MLH_{BC}). Comparison of MLH_{BC} determined by plane measurements and Rn-model (MLH_{Rn}) are presented in Table S2. The uncertainty of derived MLH_{BC} is estimated to be 50 m.

The lower and upper ranges of MLH_{Rn} fall within the uncertainty range of MLH_{BC}.

Table S2: Summary of MLH determined from BC vertical profile measured by plane (MLH_{BC}) and MLH determined by Rn box model (MLH_{Rn}) (data for the closest hour is reported).

Date & time (UTC)	~~BC vertical profile~~ MLH_{BC} ~~(m a.s.l) /~~ (m a.g.l.)	~~Radon model~~ MLH_{Rn} (min – max) (m a.g.l.)
16/02/2017 15:03	~~712 ± 3 / 412~~ 410 ~~± 3~~	~~453~~370 (270 – 460)
09/03/2017 7:40	~~481 ± 1 /~~ 180~~1 ± 1~~	~~264~~200 (160 – 240)
15/03/2017 7:10	~~460 ± 2 /~~ 160 ~~± 2~~	~~127~~100 (80 – 110)
19/05/2019 5:10	~~490 ± 3 /~~ 190 ~~± 3~~	~~196~~140 (120 – 160)

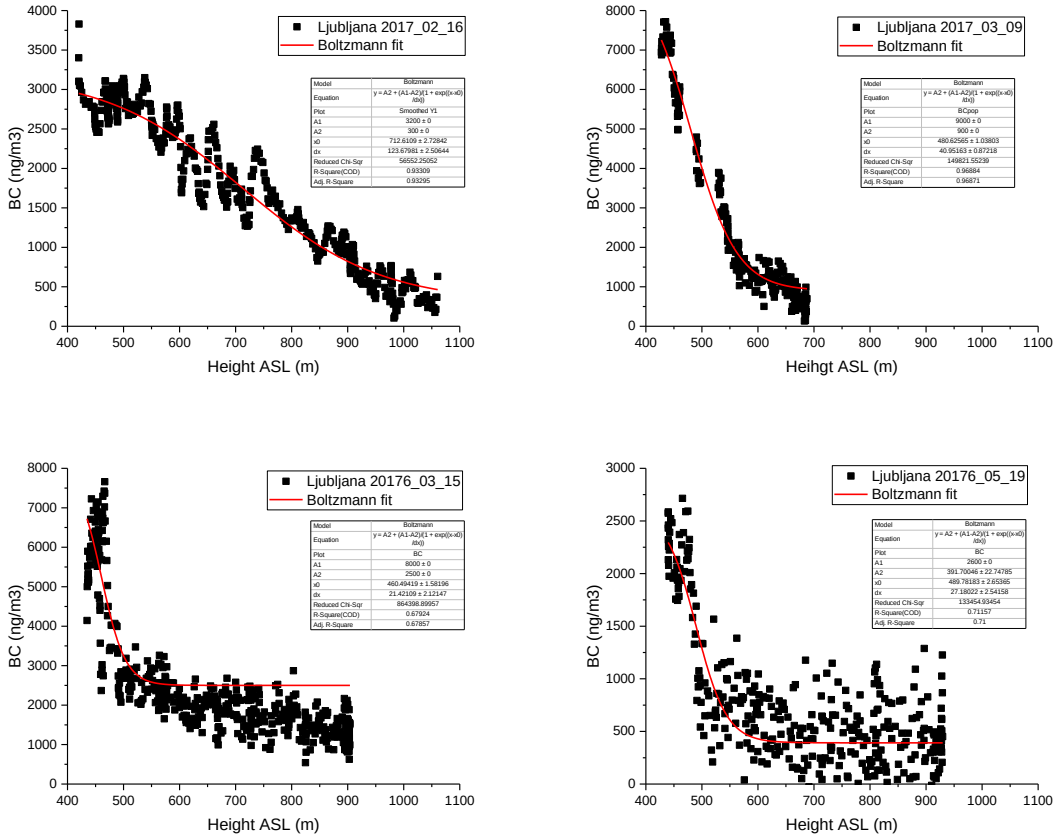

Figure S3: Black carbon vertical profiles above Ljubljana (300 m a.s.l.) at different conditions of atmospheric stability.

3. Local wind conditions

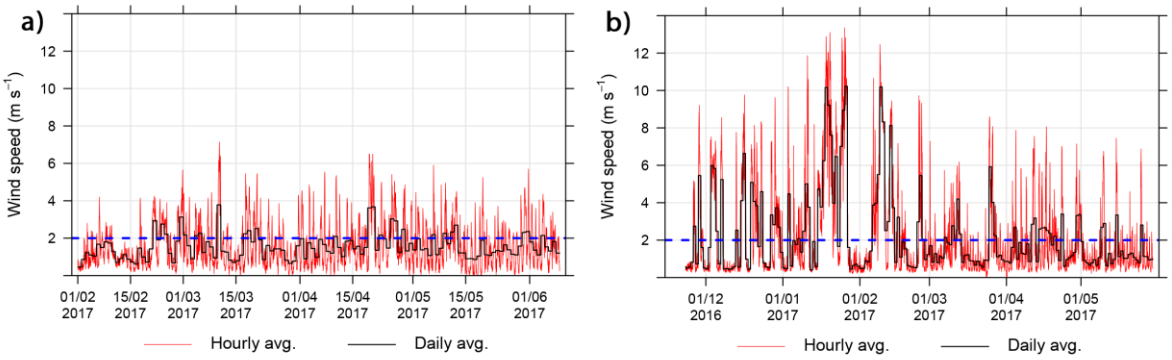

Figure S4: Time series of hourly and daily average wind speeds (ws) for Ljubljana (a) and Ajdovščina (Vipava valley) (b). Dashed blue line represent daily average wind speed of 2 m s^{-1} ~~at 80th percentile of all data distribution~~. Days, when daily average ws exceeds the limit value of 2 m s^{-1} ~~and 2.7 m s^{-1} for Ljubljana and Ajdovščina, respectively,~~ are not considered in the analyses.

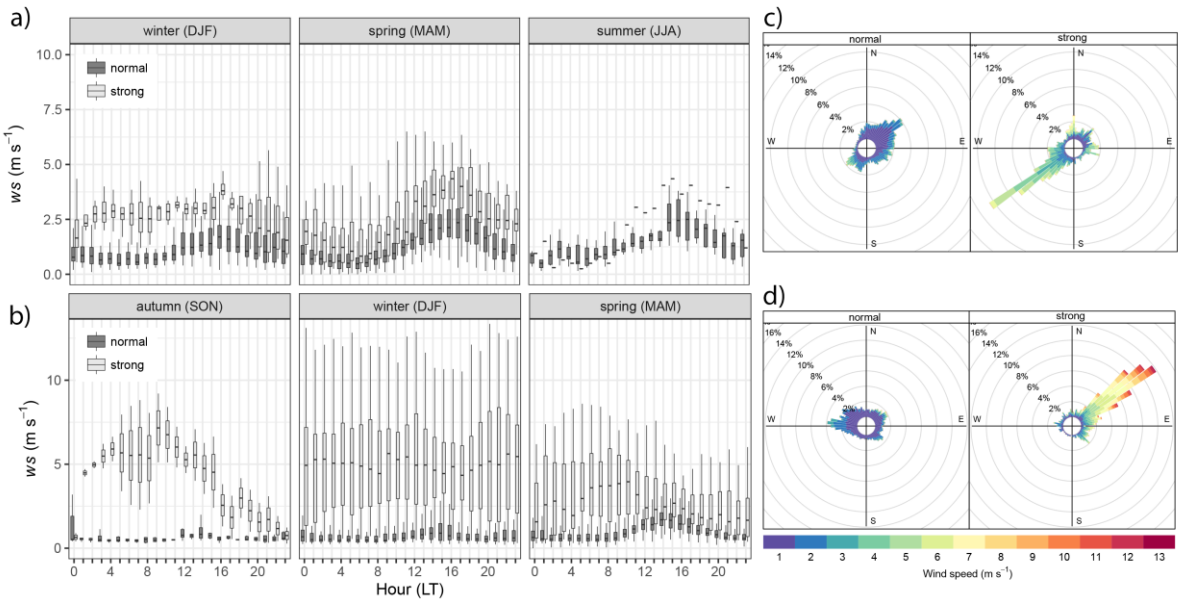

Figure S5: Diurnal variation of wind speed (ws) for normal and strong wind conditions for Ljubljana (a) and Vipava valley (b), grouped by season, and corresponding wind roses for Ljubljana (c) and Vipava valley (d).

4. Smoothing of Rn concentration (C_{Rn}) measurements

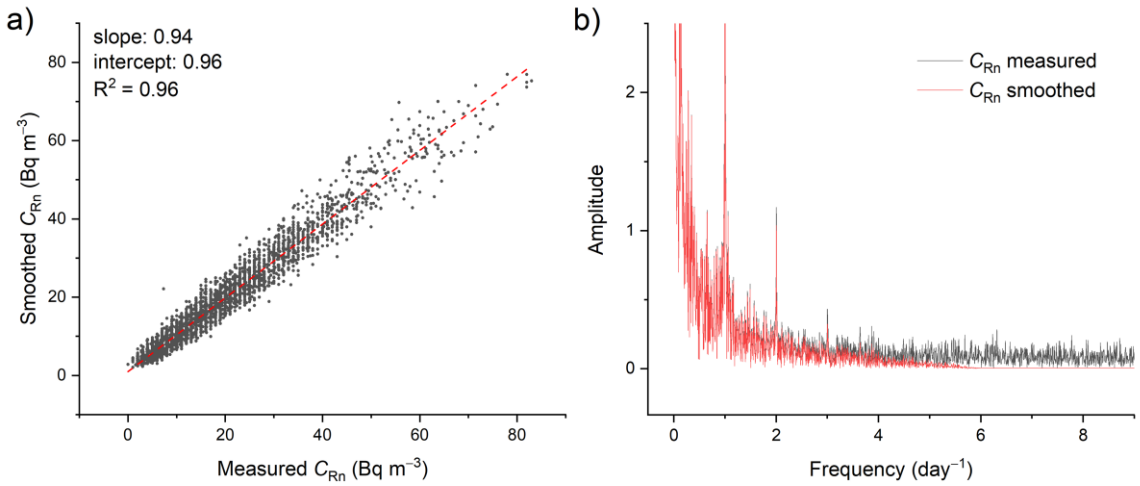

Fig. S6: a) Linear regression between measured C_{Rn} and smoothed C_{Rn} data for Ljubljana. b) FFT filter with cut-off frequency of 0.25 h^{-1} was applied to raw data.

5. Estimation of the radon exhalation rate

5.1 Calibration of E_{Rn} with the NOAA mixing layer height

The following procedure was used to compare radon derived MLH and MLH from the NOAA database. This was the first step for the estimation of appropriate monthly resolved E_{Rn}.

1. A subset of the dataset with daily average wind speed below 2 m/s limited to the period without rain was used for comparison.
2. In order to avoid the period of day, when both models have the highest uncertainty, only 9 hours from 4:00 – 13:00 were considered. Due to 3 hour time resolution of NOAA database, 4 points per day were included in the analyses, namely at 4:00, 7:00, 10:00, 13:00 (CET). A daily average (and standard deviation) of both MLH estimates was used for further analyses (Fig. S7 a).
3. Deming regression (Cornbleet and Gochman, 1979) was applied to obtain the regression slope between MLH from radon data and NOAA MLH data (Z_i) (regression was forced through zero) (Fig. S7 b). Deming regression minimizes the sum of distances in both the x and y direction. Standard deviation in x and y were used with the confidence level of 95%. Consequently, days with more stable atmospheric conditions have higher influence on the slope of regression.
4. The E_{Rn} which resulted in the slope of unity was considered as the most appropriate E_{Rn} estimate. E_{Rn} was rounded to 50 Bq $m^{-2}h^{-1}$ with 100 Bq $m^{-2}h^{-1}$ acceptable range.

a)

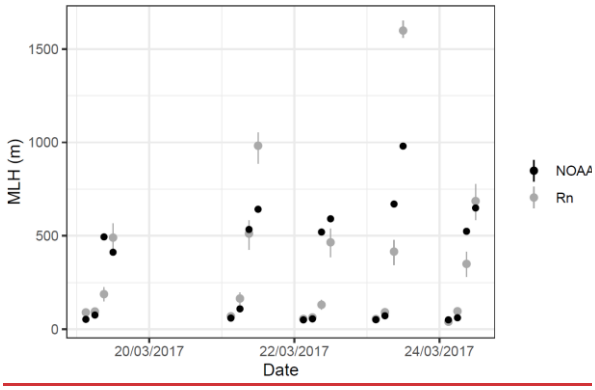

b)

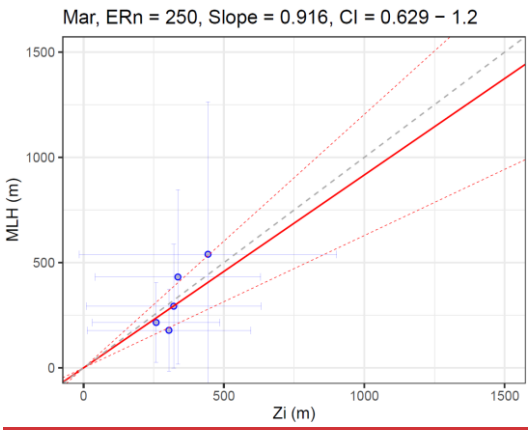

Fig. S7 Example of a subset of data for Ljubljana from 19 – 24 March, 2017. Data points for 4:00, 7:00, 10:00 and 13:00 (CET) (matching the 3 hour time resolution of NOAA dataset) were considered. MLH obtained from the radon model is presented by a point and range calculated for 100 Bq m^2 h^{-1} range (200, 250 and 300 Bq m^2 h^{-1} are used in the selected case). Data for March 20 are omitted from the comparison due to average daily wind speed exceeding the value of 2 m s^{-1}. b) Deming regression is fitted through daily averages (and standard deviation) of MLH. Red dotted line represents the lower and upper 95% confidence interval, dashed grey line represents 1:1 line.

5.2 Monthly estimates of radon exhalation rate

Appropriate E_{Rn} was determined based on combination of three different approaches, as explained in Section 2.5 of the main text. Selected cases are presented for each month for LJ and AJ location.

1. The slope of unity between radon based MLH and NOAA MLH data obtained by the procedure explained in the section Supplement 5.1, represents the first best estimate of E_{Rn} (Fig. S8). In the case of high uncertainty (low number of data points, wide confidence interval range, unrealistic values of E_{Rn} estimate), the second approach was used to confirm the previously obtained E_{Rn} estimates or to obtain a suitable range of E_{Rn}.
2. In the second phase estimated E_{Rn} was evaluated by comparison of black carbon concentration measured at different elevation (city – hill). Strong vertical gradient in concentration indicates period when MLH is below the upper measurement site (hill).
3. Lastly, radon based MLH was compared to the MLH estimated from the vertical BC profile measured by light aircraft in LJ and with lidar measurement for AJ location. When the data were available, the third approach was used superior to the approach 1 and 2.

a)

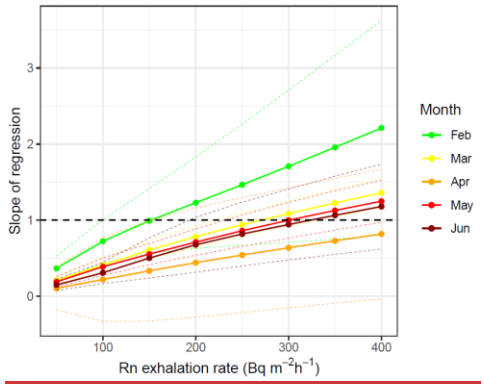

b)

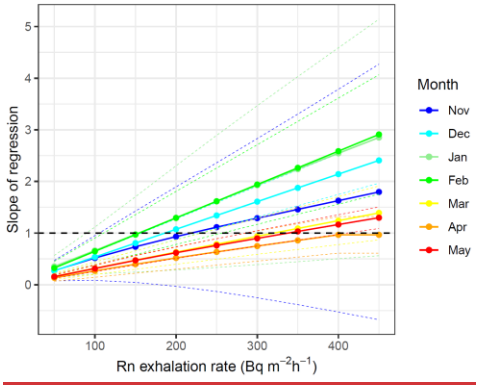

Fig S8: Dependence of the slope of the Deming regression between calculated MLH from Rn measurements and NOAA data, on Rn exhalation rate for Ljubljana (a) and Vipava valley (b). This is used to determine the Rn exhalation rate at unity slope in the first phase. Points are connected with line for visualization purposes only. Dotted lines represent the envelope of 95% confidence interval.

Ljubljana

Month	~~2.~~1. Comparison with NOAA	~~3.~~2. BC – city/hill	~~4.~~3. BC vertical profiles
February (150-250)**	**a** 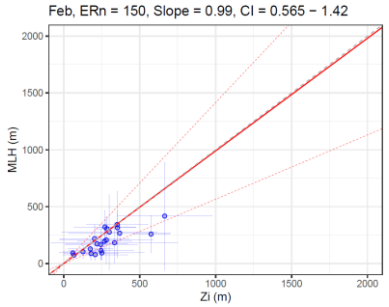	**b** 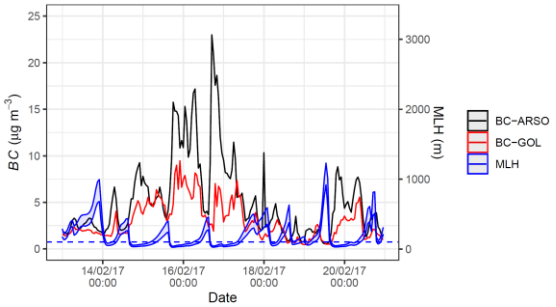	**c** 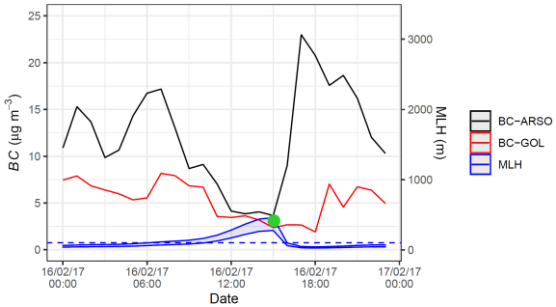
March (200-300)	**d** 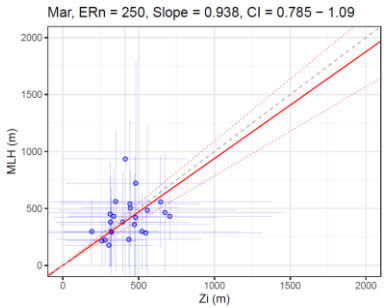	**e** 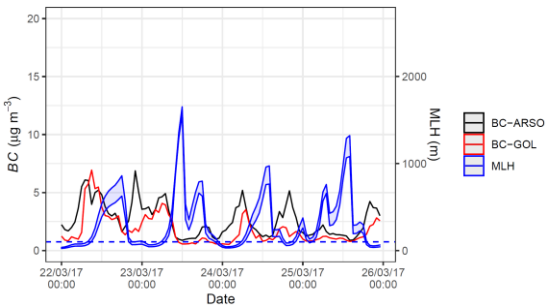	**f** 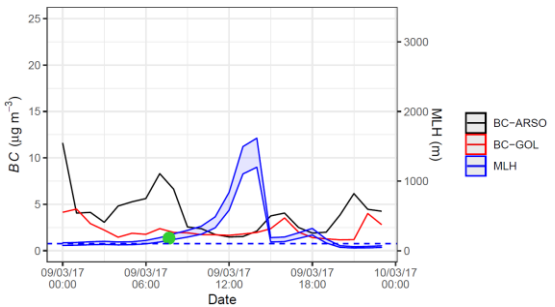 **g** 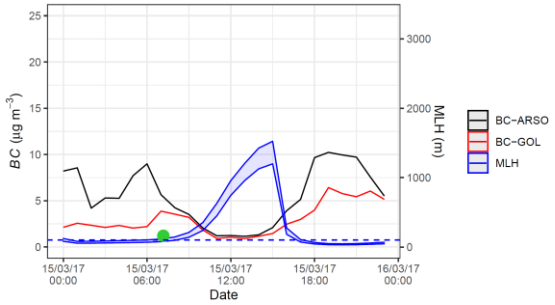

April* **(200-300)**	**h** 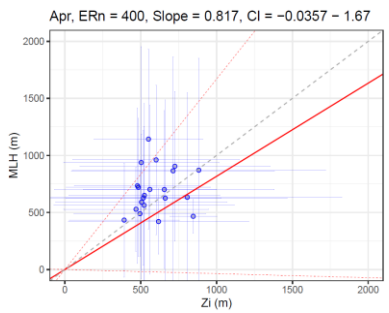	**i** 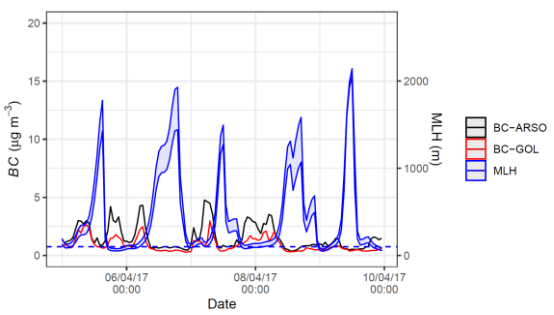	**j**
May **(250-350)**	**k** 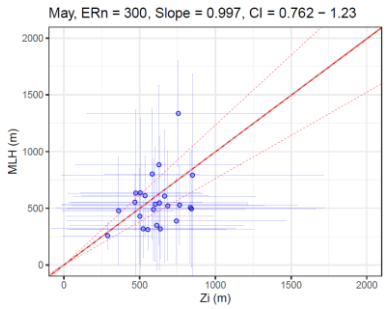	**l** 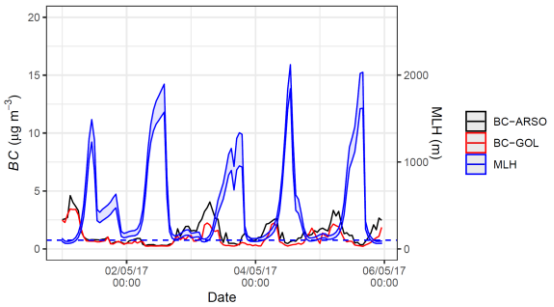	**m** 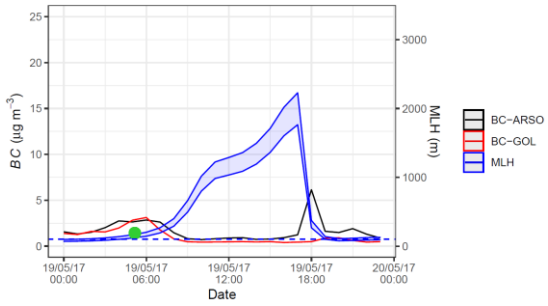
June **(250-350)**	**n** 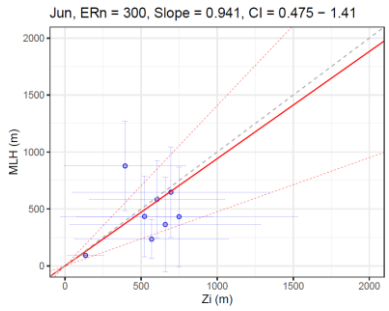	**o** 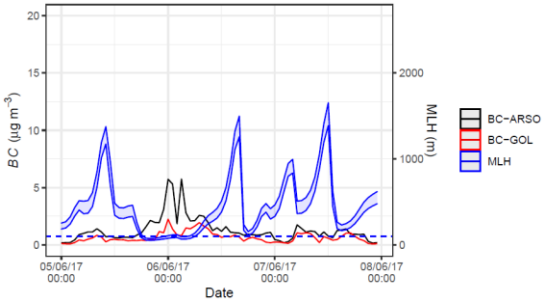	

Fig. S9: Estimation of appropriate E_{Rn}. Phase 1 (a, d, h, k, n) – Deming regression of radon based MLH vs. NOAA MLH data for the selected E_{Rn} where the slope is closest to unity. Dotted red line represents lower and upper confidence interval. Phase 2 (b, e, i, l, o): Comparison of the range of radon based MLH (blue lines) and black carbon concentration measured at two elevations (BC-ARSO: city, BC-GOL: (hill)), dashed blue line represents the elevation of the hill site. Phase 3 (c, f, g, m): same as phase 2 plots, green dot represents MLH determined from BC vertical profiles based on aircraft measurements. * - E_{Rn} was estimated based on phase 2, ** - E_{Rn} was estimated based on phase 3.

Vipava valley

Month	1. Comparison with NOAA	2. BC – city/hill	3. Lidar
November (150-250)	**a** 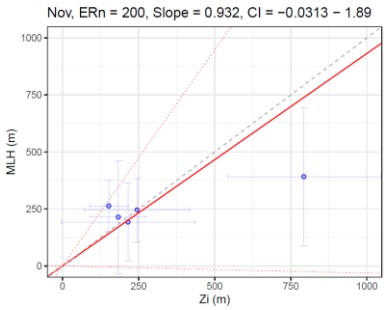	**b** 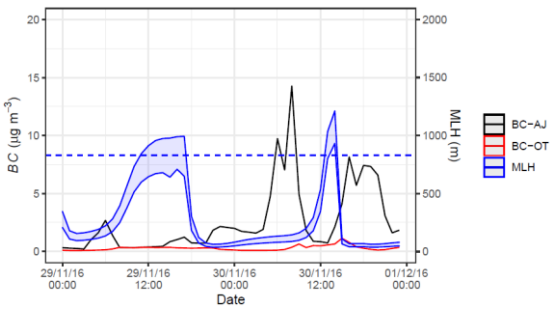	
December (150-250)	**c** 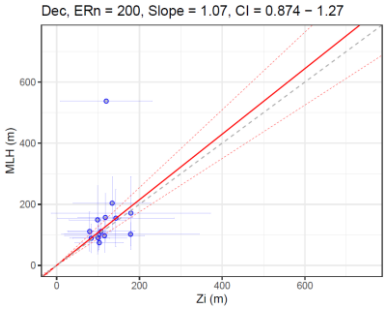	**d** 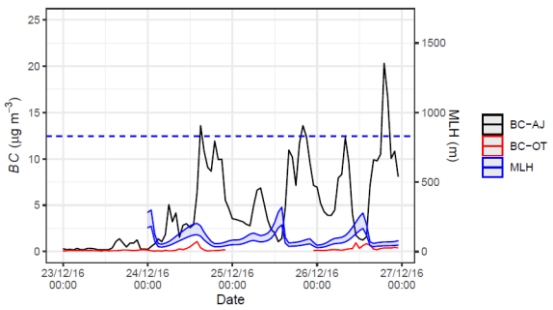	
January (250-350)**	**e** 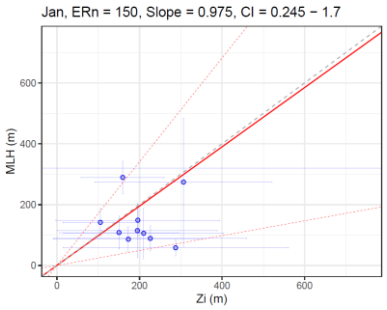	**f** 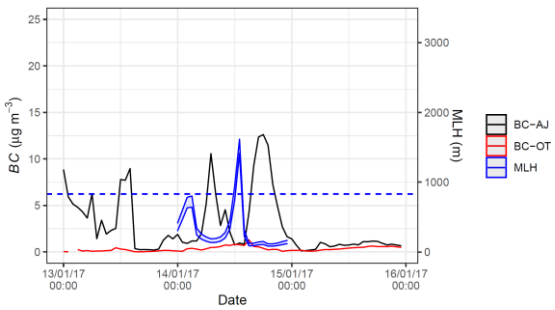	**g** 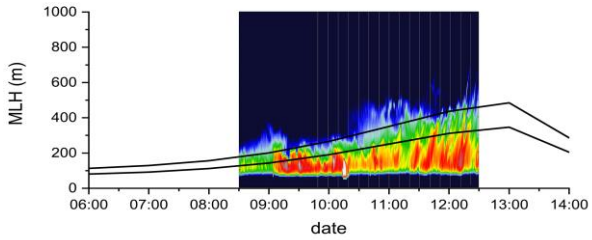

February* **(250-350)**	**h** 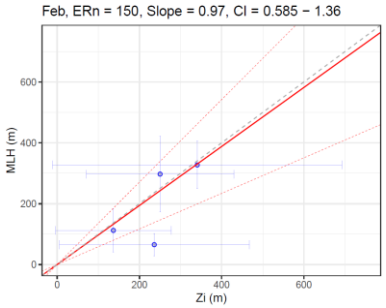	**i** 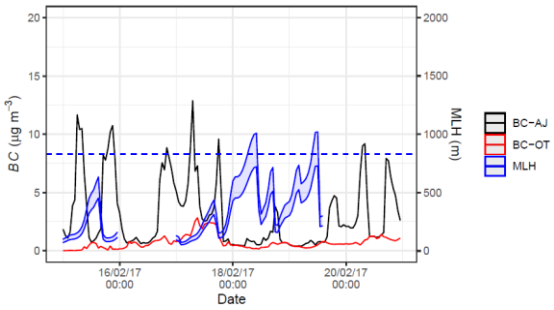	
March **(250-350)**	**j** 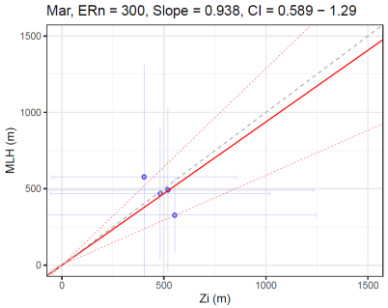	**k** 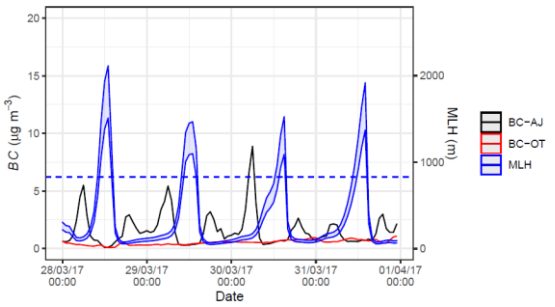	
April* **(250-350)**	**l** 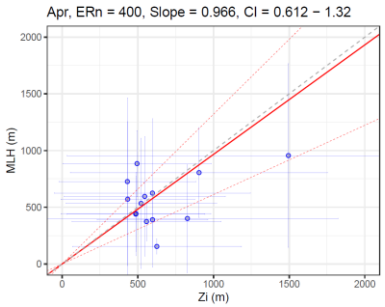	**m** 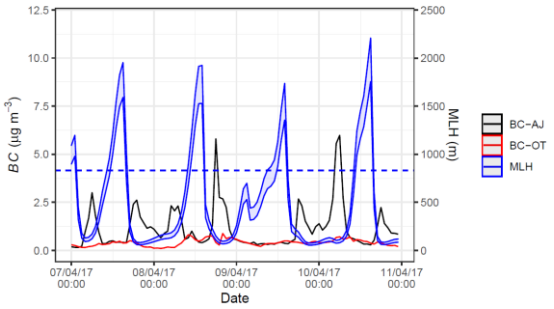	

May (300-400)	**n** 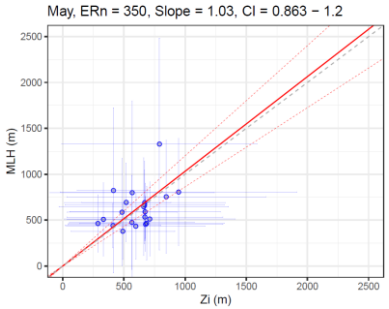	**o** 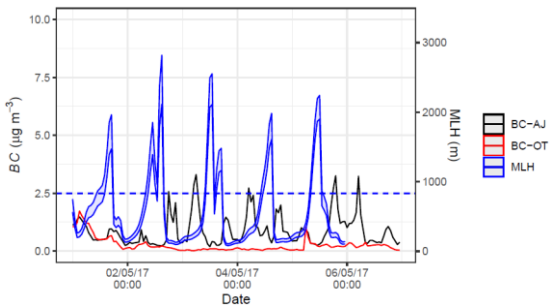	

Fig. S10: Estimation of appropriate E_{Rn}. Phase 1 (a, c, e, h, j, l, n) – Deming regression of radon based MLH vs. NOAA MLH data for the selected E_{Rn} where the slope is closest to unity. Dotted red line represents lower and upper confidence interval. Phase 2 (b, d, f, I, k, m, o): Comparison of the range of radon based MLH (blue lines) and black carbon concentration measured at two elevations (BC-ARSO: city, BC-GOL: (hill)), dashed blue line represents the elevation of the hill site. Phase 3 (g): Comparison of the range of modelled MLH (black lines) over the Vipava valley with range-corrected lidar return signal on 09/01/2017. * - E_{Rn} was estimated based on phase 2, - E_{Rn} was estimated based on phase 3.**

6. Sensitivity analyses of spatial decay constant

Sensitivity analyses of modelled E_{TR} for different γ_{TR} values were performed based on comparison with measured traffic density at representative street section, which connects two of Ljubljana arteries leading from the ring to the city center (Figure S117). Traffic during working days in Ljubljana is characterized by two significant peaks, morning peak between 7:00 and 9:00 and afternoon peak between 15:00 and 17:00. The fraction of freight vehicles is higher in morning hours, whereas mainly car traffic is characteristic for afternoon hours. After 17:00 traffic density decreases towards midnight and is the lowest between midnight and 4:00. Sunday diurnal pattern significantly differs from working days by about 50 % smaller traffic density and the missing morning peak.

Linear regression (presented as R^2) between normalized traffic density (normalized by mean) diurnal profile and normalized E_{TR} diurnal profile (normalized by median values) for different choice of spatial decay constant (γ_{TR}) is presented on Figure S128 and S129 b. Linear regression was forced through zero for the time period 00:00 – 10:00, when the uncertainty of the model is expected to be the lowest. The strength of correlation is the highest for γ_{TR} selection between 45 $\times 10^{-5}$ m^{-1} and 97 $\times 10^{-5}$ m^{-1} (points marked with "A" to "F"~~"B", "C" and "D"~~ on Figure S129 b). As shown by diurnal evolution (in terms of median E_{TR}) on Figure S129 c, the reason for weaker correlation with traffic density for point "G" is the overestimation of E_{TR} in the afternoon hours, which is caused by stronger wind speeds in afternoon hours and higher uncertainty of the MLH estimates. Decreasing γ_{TR} from "D" to "B" would cause ~~23~~26% lower median E_{TR} calculated for the afternoon peak emissions at 15:00, ~~where~~ when the highest model uncertainty is expected. On the other hand, increasing γ_{TR} from "D" to "G" would result in 3~~6~~% higher E_{TR} for the same time period.

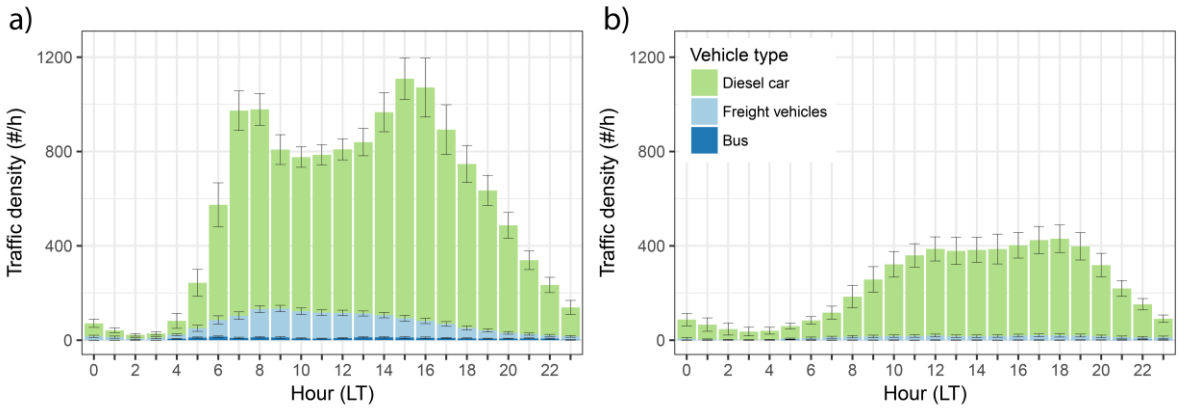

Figure S117: Mean traffic density (and standard deviation) for working days (a) and Sundays (b) for diesel cars, freight vehicles and buses. The ratio between gasoline and diesel cars in Slovenia is 55 (gasoline):45(diesel) (Si-Stat, 2019).

~~a)~~ ~~b)~~

~~**Figure S8: Comparison between diurnal profiles of traffic density and modelled E_{TR} in Ljubljana. Normalized mean hourly values are presented for traffic density, whereas E_{TR} values are presented in terms of normalized median, 25th and 75th quantile (a). Linear regression of points that are presented on the diurnal plot results in R^2=0.75.**~~

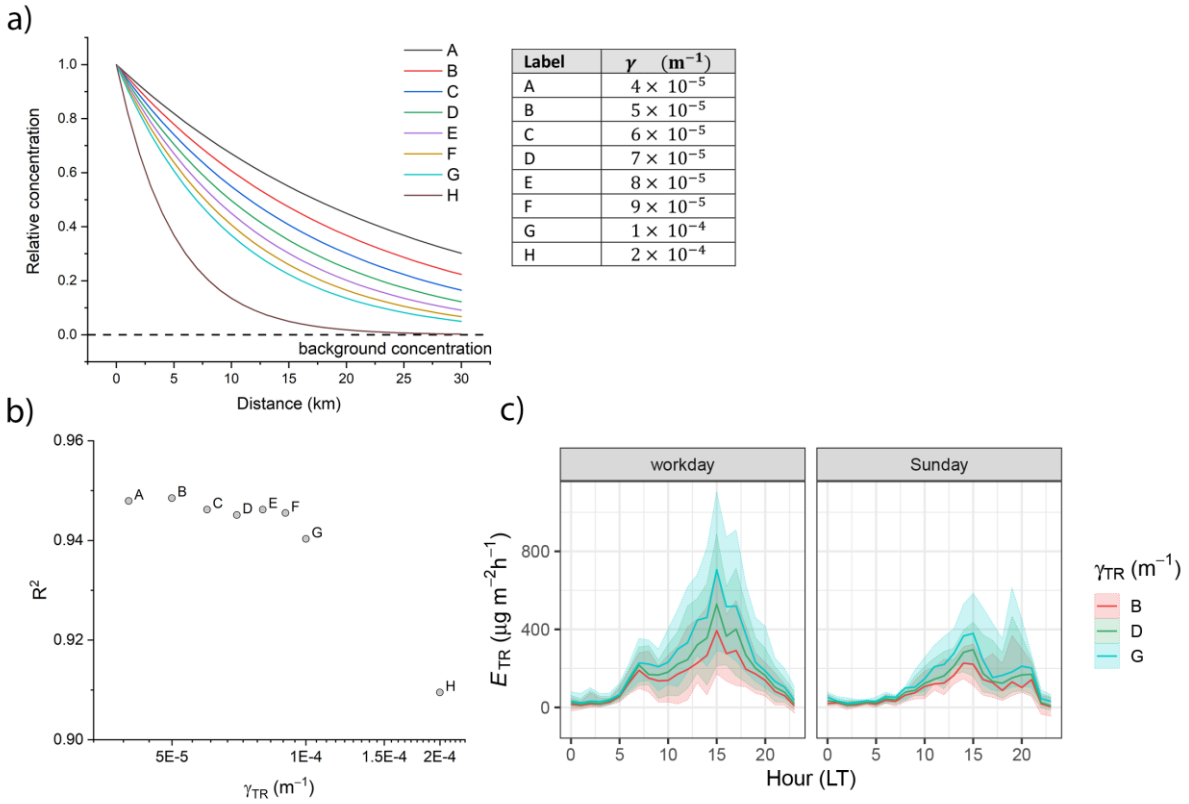

Label	γ (m^{-1})
A	4×10^{-5}
B	5×10^{-5}
C	6×10^{-5}
D	7×10^{-5}
E	8×10^{-5}
F	9×10^{-5}
G	1×10^{-4}
H	2×10^{-4}

Figure S129: Dependence of modelled E_{TR} on the choice of horizontal advection term. a) Spatial decrease of BC concentration from the source by different γ. Labels are explained in the table. b) Dependence of R^2 for correlation between normalized diurnal profile of traffic density and normalized diurnal profile (in terms of median hourly values) of modelled E_{TR} for Ljubljana from midnight to 10:00. c) Diurnal profile of modelled E_{TR} for selected cases of γ_{TR} for Ljubljana: line – median, shaded area – 25th to 75th quantile.

6.7. References

Cornbleet, P. J., and Gochman, N.: Incorrect least-squares regression coefficients in method-comparison analysis, Clinical chemistry, 25, 432–438, 1979.

Drinovec, L., Močnik, G., Zotter, P., Prévôt, A. S. H., Ruckstuhl, C., Coz, E., Rupakheti, M., Sciare, J., Müller, T., Wiedensohler, A., and Hansen, A. D. A.: The "dual-spot" Aethalometer: an improved measurement of aerosol black carbon with real-time loading compensation, Atmos. Meas. Tech., 8, 1965-1979, 10.5194/amt-8-1965-2015, 2015.

Favez, O., El Haddad, I., Piot, C., Boréave, A., Abidi, E., Marchand, N., Jaffrezo, J. L., Besombes, J. L., Personnaz, M. B., Sciare, J., Wortham, H., George, C., and D'Anna, B.: Inter-comparison of source apportionment models for the estimation of wood burning aerosols during wintertime in an Alpine city (Grenoble, France), Atmos. Chem. Phys., 10, 5295-5314, 10.5194/acp-10-5295-2010, 2010.

Garg, S., Chandra, B. P., Sinha, V., Sarda-Esteve, R., Gros, V., and Sinha, B.: Limitation of the Use of the Absorption Angstrom Exponent for Source Apportionment of Equivalent Black Carbon: a Case Study from the North West Indo-Gangetic Plain, Environmental science & technology, 50, 814-824, 10.1021/acs.est.5b03868, 2016.

GLWF: https://www.worldgreenflight.com/, access: May 27, 2019.

Helin, A., Niemi, J. V., Virkkula, A., Pirjola, L., Teinilä, K., Backman, J., Aurela, M., Saarikoski, S., Rönkkö, T., Asmi, E., and Timonen, H.: Characteristics and source apportionment of black carbon in the Helsinki metropolitan area, Finland, Atmos. Environ., 190, 87-98, 10.1016/j.atmosenv.2018.07.022, 2018.

Hellén, H., Kangas, L., Kousa, A., Vestenius, M., Teinilä, K., Karppinen, A., Kukkonen, J., and Niemi, J. V.: Evaluation of the impact of wood combustion on benzo[a]pyrene (BaP) concentrations; ambient measurements and dispersion modeling in Helsinki, Finland, Atmos. Chem. Phys., 17, 3475-3487, 10.5194/acp-17-3475-2017, 2017.

Herich, H., Gianini, M. F. D., Piot, C., Močnik, G., Jaffrezo, J. L., Besombes, J. L., Prévôt, A. S. H., and Hueglin, C.: Overview of the impact of wood burning emissions on carbonaceous aerosols and PM in large parts of the Alpine region, Atmos. Environ., 89, 64-75, http://dx.doi.org/10.1016/j.atmosenv.2014.02.008, 2014.

Kirchstetter, T. W.: Evidence that the spectral dependence of light absorption by aerosols is affected by organic carbon, Journal of Geophysical Research, 109, 10.1029/2004jd004999, 2004.

Kumar, N. K., Corbin, J. C., Bruns, E. A., Massabó, D., Slowik, J. G., Drinovec, L., Močnik, G., Prati, P., Vlachou, A., Baltensperger, U., Gysel, M., El-Haddad, I., and Prévôt, A. S. H.: Production of particulate brown carbon during atmospheric aging of wood-burning emissions, Atmos. Chem. Phys., 18, 17843-17861, 10.5194/acp-18-17843-2018, 2018.

Saleh, R., Hennigan, C. J., McMeeking, G. R., Chuang, W. K., Robinson, E. S., Coe, H., Donahue, N. M., and Robinson, A. L.: Absorptivity of brown carbon in fresh and photo-chemically aged biomass-burning emissions, Atmos. Chem. Phys., 13, 7683-7693, 10.5194/acp-13-7683-2013, 2013.

Sandradewi, J., Prévôt, A. S. H., Szidat, S., Perron, N., Alfarra, M. R., Lanz, V. A., Weingartner, E., and Baltensperger, U.: Using aerosol light absorption measurements for the quantitative determination of wood burning and traffic emission contributions to particulate matter, Environ. Sci. Technol., 42, 3316-3323, 10.1021/es702253m, 2008.

Statistical Office of Republic of Slovenia (Si-Stat): https://pxweb.stat.si/SiStat, access: June 24, 2019, 2019.

Zotter, P., Herich, H., Gysel, M., El-Haddad, I., Zhang, Y., Močnik, G., Hüglin, C., Baltensperger, U., Szidat, S., and Prévôt, A. S. H.: Evaluation of the absorption Ångström exponents for traffic and wood burning in the Aethalometer-based source apportionment using radiocarbon measurements of ambient aerosol, Atmos. Chem. Phys., 17, 4229-4249, 10.5194/acp-17-4229-2017, 2017.